VISUAL PIGMENTS AND LIGHT DETECTION IN THE EYE

by

Wendy Wing Sze Yue

A dissertation submitted to The Johns Hopkins University in conformity with the requirements for the degree of Doctor of Philosophy

Baltimore, Maryland

December, 2015

Abstract

Most forms of animal vision begin with light absorption by visual pigments in the eye. A typical visual pigment consists of a G protein-coupled receptor protein – opsin – covalently conjugated to a chromophore. Sub-families of opsins show distinctive physicochemical properties and cellular expressions, often attuned to the specific visual functions that they serve. Here, we examined a number of molecular and functional features of three sub-families of opsins. We found that:

(1) an active molecule of **rhodopsin** (a ciliary opsin expressed in rod photoreceptors for dim-light vision) amplifies the light signal by activating about 20-30 transducin molecules at the peak of the current response to single photon-absorption.

(2) the thermal activation of native and some mutant **rhodopsin and cone pigments** (ciliary opsins in cone photoreceptors for color vision) in the dark is indeed an isomerization event, the rate of which can be quantitatively predicted by multi-vibrational-mode statistical mechanics.

(3) **melanopsin**, a rhabdomeric opsin that underlies the intrinsic photosensitivity of a subgroup of retinal ganglion cells and is responsible for diverse non-image-forming visual functions in mammals, is also expressed in some thick, myelinated neuronal processes in the rat iris that possibly originate from the trigeminal ganglia.

(4) **neuropsin (OPN5)**, a previous orphan opsin, mediates the photoentrainment of the local circadian rhythm in the mammalian retina and cornea.

Ph.D. DISSERTATION REFEREES FOR WENDY WING SZE YUE

King-Wai Yau, Ph.D.,
Professor, Departments of Neuroscience and Ophthalmology (faculty sponsor)

Michael Caterina, M.D., Ph.D.,
Professor, Departments of Neurosurgery, Neuroscience and Biological Chemistry (reader)

Acknowledgments

I arrived at Hopkins with eager naivety about the profession that I was entering. It was really my great fortune to have received so much intellectual inspiration, technical advice and spiritual support from colleagues, friends and family over the years that, in many ways, have accelerated my growth. I would like to take this opportunity to thank all the individuals who have especially contributed to this thesis work.

I would like to express my sincere gratitude to my advisor, Dr. King-Wai Yau. King is celebrated for his diligence and rigor towards science, but I particularly admire his vision and creativity. He has repeatedly emphasized, and personally demonstrated to us, the importance of exercising good judgements in identifying research directions as well as in developing unique perspectives towards questions. It was also for his receptiveness to new ideas that I had the freedom to chase after serendipitous findings that might not be very relevant to my originally-proposed thesis work. I also want to thank King for being generous with providing career advice and opportunities, which, I believe, will remain to be my important assets for future academic pursuit.

I would like to extend my appreciation to my thesis committee: Dr. Michael Caterina, Dr. Paul Fuchs, Dr. Daniel Raben and, in particular, Dr. Xinzhong Dong and Dr. Jeremy Nathans, with whom I have done my research rotations. Their presence has made my thesis meetings such invaluable occasions for learning–from five different sets of

mind, characters and experiences all at once. I have enjoyed all the lively discussions and their helpful comments and suggestions, especially in areas out of my research expertise.

I am grateful to everyone who has given help, in one form or another, to the development of my thesis projects. In particular, I would like to thank: Drs. Carter Cornwall and Rikard Frederiksen (Boston University) for performing microspectrophotometry on photoreceptors; the laboratory of Stephen Tsang (Columbia University) for histological evaluation of retinal degeneration; Drs. Nick Marsh-Armstrong and Elizabeth Mills (Johns Hopkins) for help with frog transgenesis; Drs. Dwight Bergles and Shin Kang (Johns Hopkins) for help with the generation of BAC transgenic mice; Dr. Mary Ann Wilson, Dr. Mary Blue, Karen Smith-Connor and Patrice Carr (Kennedy Krieger Institute) for advice and technical support on preparing microtome-slices of the brainstem and the trigeminal ganglia; Drs. Asaf Keller (University of Maryland), David Bereiter (University of Minnesota) and Kenneth Muller (University of Miami) for help with recordings on trigeminal ganglion neurons and in trigeminal nuclei of the brainstem; Drs. Russell Van Gelder and Ethan Buhr (University of Washington, Seattle) for introducing me to the field of retinal circadian photoentrainment and for performing the associated experiments; the laboratory of Dr. Richard Lang (University of Cincinnati Medical Center) for providing the *Opn5*$^{flox/flox}$ mouse line plus intellectual and experimental input to the OPN5 project; Drs. Jeannie Chen (University of Southern California), Marie Burns (University of California, Davis), Yoshinori Shichida (Kyoto University), Joseph Takahashi (University of Texas Southwestern Medical School) as well as Jay and Maureen Neitz (University of

Washington, Seattle) for their generous provision of various mouse lines; Drs. Jeremy Nathans (Johns Hopkins), Jason Chen (Baylor College of Medicine), Robert Molday (University of British Columbia), Stephen Massey (University of Texas), Yoshitaka Fukada, Daisuke Kojima (University of Tokyo), Yoshinori Shichida (Kyoto University), Hideyo Ohuchi (Okayama University) for antibodies; Drs. Michael Do, Ryan Adams (Harvard Medical School), Elizabeth Nance and Elizabeth Glowatzki (Johns Hopkins) for sharing monkey, rabbit and rat tissues or animals; and finally, Drs. Fred Rieke (University of Washington), David Berson (Brown University), Reha Erzurumlu (University of Maryland), Randall Reed, Alex Kolodkin, David Ginty, Solange Brown and Roger Reeves (Johns Hopkins) among others for discussions.

I felt blessed to have worked with an elite group of people in the lab. I have received a lot of positive influence from Dong-Gen Luo, who has not only started me on electrophysiology and the pigment-noise problem, but has also been a great source of advice on numerous other research questions because of his vast knowledge base. His intense persistence has won my full respect. I have also benefited amply from discussions with Michael Do and Tian Xue, who have always offered sharp criticisms and constructive suggestions. I want to give special thanks to Zheng Jiang for taking time to help with so many exploratory electrical-recording and calcium-imaging experiments, and most importantly, for entertaining my random thoughts and sharing my passion in science through philosophical discussions. Thanks also to Xiaozhi Ren, who has been the go-to person in the lab for molecular-biology questions. It was certainly a pressure and a pleasure to be with a group of talented fellow students – Chih-Chun Lin, Chang Liu, Qian

Wang, Yanghui Sheng, Daniel Silverman and Lujing Chen; their friendships have made my lab-life outside of the dark room more colorful. I would also like to thank Lihui Cao, Rongchang Li and Yair Ben Chiam for together providing a stimulating lab environment for me to mature; Terry Shelly for tailor-making many experimental apparatuses and for blending me into the American culture; and not in the least, the Neuroscience and BCMB program, especially our BCMB program director, Dr. Carolyn Machamer, for coordinating everything it took to facilitate my learning experience here.

I owe my deepest gratitude to my family, especially to my parents and my sister. It is purely comforting to know that someone will value me as much no matter how far I go, how high I can achieve, and even when I lose faith in my own self and have nothing to offer in return. It is in them that I find unconditional love. For that, I am forever in their debt.

Dedicated to my Father, Mother and Sister

Table of Contents

List of Figures

List of Tables

Chapter 1 Introduction

1.1 Light and organisms

Light has immense impacts on the physiology and behaviors of organisms. Even life-forms as simple as the unicellular cyanobacteria, which harvest energy directly from sunlight via photosynthesis, possess light-dependent gene-regulatory mechanisms to orchestrate different metabolic activities in a circadian manner (see Ref. 1, 2 for reviews). For example, many strains of *Synechococcus* carry out nitrogen-fixation, a process of converting atmospheric nitrogen to ammonia for use by symbiotic plants, maximally at night in order to avoid inhibition of the reaction by oxygen produced during photosynthesis at daytime[1,2]. Intriguingly, bacterial strains with a circadian period similar to that of the external light/dark cycle were found to have enhanced reproductive fitness under competition[3], suggesting that light could act as a selective pressure in the course of evolution.

Some organisms respond to light stimuli of a yet more complex nature than just a gradual, global change in ambient intensity. The green alga *Chlamydomonas reinhardtii* use light-activated ion channels called Channelrhodopsins in their eyespots to control flagellar motion and steer according to the direction of light[4]. Several species of mollusks and arthropods have been reported[5] to shut their valves rapidly in response to a sudden decrease in light intensity, which might indicate the approach of a predator. This closing response could not be triggered by a slow intensity-reduction, nor does it last, suggesting the presence of some adaptive mechanisms[5].

Perhaps the most sophisticated visual ability in existing organisms is the ability to form an image-representation of the external world. Such a feat allows organisms to navigate across various landscapes and interact with other living things more effectively. By geometrically arranging photosensitive cells and recruiting pigment cells to provide directional shielding, some invertebrate eyes, such as insects' compound eyes, have already acquired certain basic image-forming functions (see, for examples, Ref. 4, 6–8). However, because most of these eyes have limited number of photoreceptors, the images formed tend to be very coarse. The great majority of vertebrates (except for, for example, hagfish) have developed, instead, camera-type eyes (see Ref. 6, 9 for reviews and Chapter 1.2) that are capable of providing more superior focusing and resolving power.

1.2 Structure and function of the human eye

Although variable in shape and size, the eyes of all jawed vertebrates and one of the only two extant jawless fish – lamprey – are actually very similar in structure (see Ref. 6, 9 for reviews). For the sake of relevance, I shall describe here only the human eye (Fig. 1-1), which represents a reasonable example of the single refractive system (vs. the multiple optical system in compound eyes) commonly employed in most vertebrate eyes, including those of animals used in experiments described in this Dissertation. I shall also focus only on ocular structures pertinent to later chapters. More detailed descriptions can be found in Ref. 8, 10, for examples.

Light enters the eye through the cornea – a transparent tissue at the eye's anterior that serves as its principal refractive element. The cornea is made of three major layers (Fig. 1-2; from anterior to posterior): (1) an epithelial layer composed of highly-packed

cells with tight junctions and interdigitating processes that help to occlude water movement and thus maintain cornea's transparency, (2) a stromal layer with parallel lamina of collagen fibrils, the regular ordering of which contributes to transparency, and (3) an endothelial layer that also helps to keep osmotic balance by pumping ions. The corneal epithelium is continuously being renewed by repeated cell division and apoptosis, perhaps under some circadian control[11–14]. It also has a rich supply of nerve innervation linked to reflexive blinking and lacrimation.

Light passes from the anterior chamber to the posterior chamber through the pupil, which is a circular hole at the center of a usually-pigmented tissue called the iris. In addition to the border, stromal and epithelial layers (Fig. 1-3a), the iris has an important muscle layer for controlling the pupil size. This muscle layer consists of two antagonistic types of muscles (Fig. 1-3b): the circumferential sphincter muscles that immediately surround the pupil and the dilator muscles that run radially between the outer margin of the sphincter ring and that of the iris. Bright light triggers the release of acetylcholine from parasympathetic ciliary ganglion neurons onto sphincter muscles via a bilateral multi-synaptic brain circuit involving the optic nerve, thereby activating muscarinic acetylcholine receptors on the muscle cells. The resulting G protein-mediated contraction of sphincter muscles leads to pupil constriction. Dilator muscles, on the other hand, are regulated by norepinephrine released by superior cervical ganglion neurons of the sympathetic system. Norepinephrine concentrates in darkness[15] and stimulates the contraction of dilator muscles via G protein-mediated signaling from α-adrenergic receptors, thus dilating the pupil. By adjusting the amount of illumination on the retina,

this pupil reflex is critical for allowing our eyes to function over an extended range of intensities.

Light is focused by the lens onto the retina, where it is detected and converted into electrical signals. The mammalian retina is organized into three nuclear and two synaptic layers in an inverted manner (Fig. 1-4). Light absorption occurs primarily in the outer segments of rod- and cone-photoreceptors, the nuclei of which constitute the most posterior or outer nuclear layer (ONL). Photoactivation of visual pigments in rods and cones elicits a G protein-mediated phototransduction cascade (see Chapter 1.3) that causes a decrease in neurotransmitter (glutamate) release at the outer plexiform layer (OPL), where photoreceptors synapse onto bipolar cells' dendrites. Also in the inner nuclear layer (INL) with the bipolar cells' somata are interneurons called horizontal cells and amacrine cells, which integrate and modulate various aspects of the light responses, although some amacrine cells have their cell bodies displaced to the ganglion cell layer (GCL). Bipolar cells relay light signals to retinal ganglion cells (RGCs), which arborize their dendrites in the inner plexiform layer (IPL) but have their cell bodies located in the INL or the GCL. The signals are eventually carried to the brain as nerve impulses via RGCs' axons, which together bundle into the commonly-known "optic nerve".

Light uncaptured by the retina is absorbed by the melanin-rich retinal pigment epithelium (RPE) that lies posterior to the outer segment of photoreceptors. The RPE provides metabolic, immune and various other kinds of support to the retina, especially to the photoreceptors. Above all, it is the center for the visual cycle – the RPE takes up chromophores released from light-activated visual pigments in photoreceptors, regenerates them through a series of biochemical reactions, and finally returns them to

photoreceptors for reconstituting light sensitivity. A similar function of chromophore regeneration is served by Müller glia in the retina, although they operate with a distinct biochemical pathway[16].

1.3 Opsins and phototransduction

Organisms have evolved many photo-sensory proteins, for examples, microbial opsins (including the aforementioned Channelrhodopsin) in prokaryotes, as well as cryptochromes and phytochromes in plants[4]. Most forms of animal vision rely on animal opsins[4,6,9] (also known as Type 2 opsins for differentiation from microbial or Type 1 opsins; for brevity, I shall refer to them simply as opsins henceforth) – a family of homologous seven-transmembrane proteins that typically associate covalently with vitamin A-based chromophores like 11-cis-retinal.

Nearly all opsins share a number of critical functional motifs, for instance, a lysine residue for conjugating the chromophore, a glutamate residue (counterion) for stabilizing the conjugation, a cytoplasmic (D/ERY) and a transmembrane (NPXXY) motif important for G protein activation[4,6,9,17], etc. Based on amino-acid-sequence alignment, opsins can be broadly classified into five sub-families[6,9,17,18] (Fig. 1-5): (1) vertebrate ciliary opsins, (2) G_s-coupled ciliary opsins, (3) rhabdomeric opsins, (4) G_o-coupled opsins, as well as (5) RGR-opsin and neuropsin. The first four groups are visual opsins that generally act as G protein-coupled receptors (GPCRs) to directly signal light absorption. RGR-opsin was believed to be a photoisomerase, responsible for light-dependent conversion of chromophore from all-trans to 11-cis configuration; there is, however, recent evidence for a signaling function[19–23]. Comparatively, the role of

neuropsin is less well-characterized (see Chapter 4 for more details). Within each opsin sub-family, variations in amino acid sequences exist to create differences in molecular properties, such as in absorption spectra, and the thermostabilities of photo-intermediates. In such ways, the sequence-differences are fundamental to our sense of colors and visual temporal resolution, among other crucial qualities of vision.

Below, I shall expand on two best-studied opsin sub-families: ciliary opsins and rhabdomeric opsins.

Vertebrate ciliary opsins are found in ciliary photoreceptors, which feature a modified cilium made up of membrane invaginations or vesicles. Vertebrate rod- and cone-opsins, highly-packed in membranous discs or plasma-membrane evaginations in the outer segment of rod- and cone-photoreceptors, respectively, are typical examples of ciliary opsins. Absorption of a photon by a rhodopsin or cone-pigment molecule leads to the isomerization of its chromophore, 11-cis-retinal, into the all-trans form (Fig. 1-6). The activated pigment binds to the G protein, transducin, and catalyzes the exchange of GDP for GTP in its α subunit (i.e., $G_{t\alpha}$). $G_{t\alpha}$ relieves the inhibition on phosphodiesterase (PDE) by PDE's γ subunit, thereby enhancing its hydrolysis of cGMP into GMP. Consequent to a drop in intracellular cGMP concentration, the plasma-membrane cyclic-nucleotide-gated (CNG) channels, which produce the standing current in darkness, close and hyperpolarize the cell. The final outcome of this phototransduction cascade is a reduction in glutamate release at the synaptic terminal. Interestingly, all ciliary photoreceptors examined so far uniformly use a slightly modified but overall similar cyclic-nucleotide motif for phototransduction[4,6,17,18,24].

Rhabdomeric opsins (e.g. insect rhodopsins) are normally present in rhabdomeric photoreceptors characterized by microvilli that are formed by membrane evagination at the apical cell surface. Melanopsin, responsible for the intrinsic photosensitivity of a population of mammalian RGCs (see Chapter 3 for more details), represents a special type of rhabdomeric opsins. Regardless, it adopts a phospholipase C (PLC)-phototransduction motif[18,25,26] common to other rhabdomeric opsins (Fig. 1-7). Melanopsin couples to G protein(s) of the G_q-family, which stimulates PLC of the β4 isoform (PLCβ4)[26] to catalyze the conversion of phosphatidylinositol 4, 5-bisphosphate (PIP_2) into inositol 1,4,5-trisphosphate (IP_3) and diacylglycerol (DAG), ultimately resulting in the opening of transient receptor potential channels (TRPC6 and 7)[26] on the plasma membrane and, hence, cell depolarization.

1.4 Objectives of the studies

In the work reported in this Dissertation, I sought to understand certain molecular and functional attributes of several opsins of different sub-families as a doorway to understanding how light impacts on the physiology and behavior of animals. In Chapter 2, I shall look into how different native and mutant rod- and cone-opsins vary in their rate of spontaneous activation in the dark, a phenomenon that adds noise to the visual system. In Chapter 3, I shall describe an unexpected finding of melanopsin expression in neuronal processes in the iris that may originate from the trigeminal ganglia. Chapter 4 is devoted to a collaborative study suggesting a function for the orphan opsin, neuropsin, in regulating the circadian rhythms in mammalian retina and cornea.

1.5 Figures

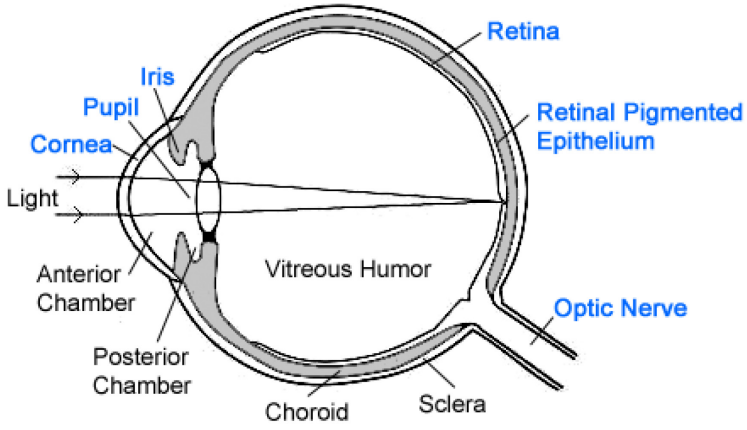

Fig. 1-1 **Structure of the human eye.** See text for description of structures indicated in blue. Arrows indicate the direction of light path.

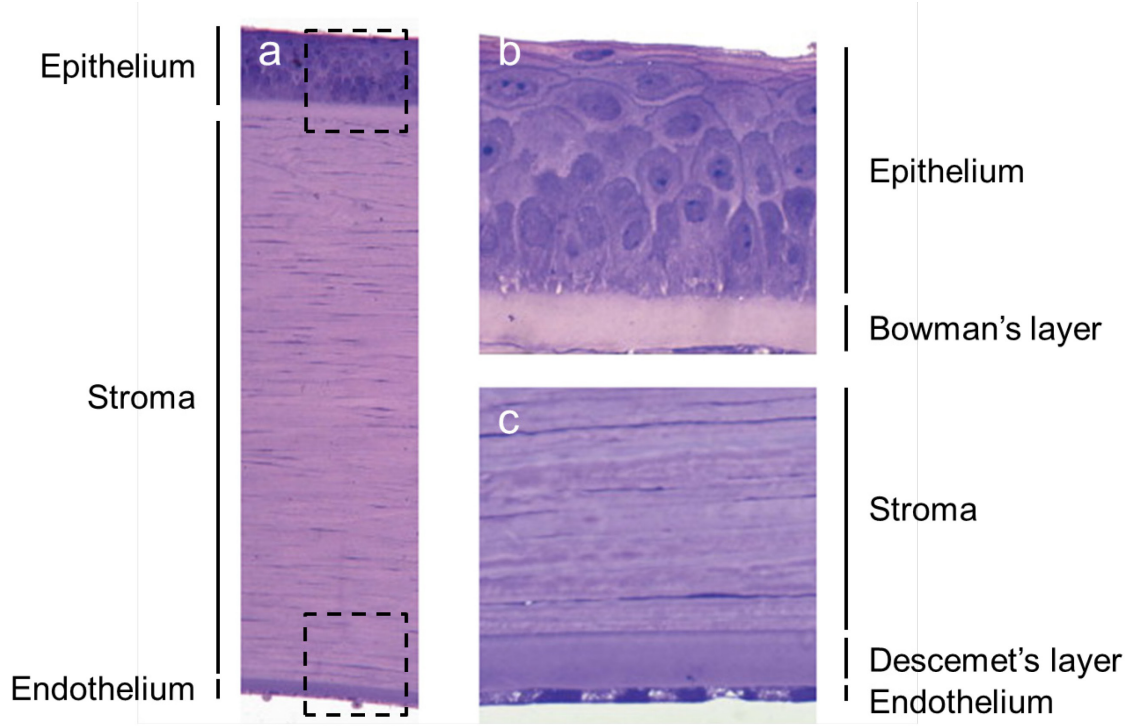

Fig. 1-2 **Microscopic structure of the cornea. a,** Cross-section of the cornea at low magnification, showing three major layers– epithelium, stroma and endothelium. The cornea is about 520 μm thick at its center and 670 μm close to its junction with the sclera. Light comes from top in this image-orientation. **b,** High-magnification of boxed areas in **a.** The anterior limiting Bowman's layer is rich in collagen as in the stroma but lacks fibroblasts. The posterior limiting Descemet's layer serves as the basement membrane of the endothelium. Image modified from Ref. 27. Scale bars not available in original images.

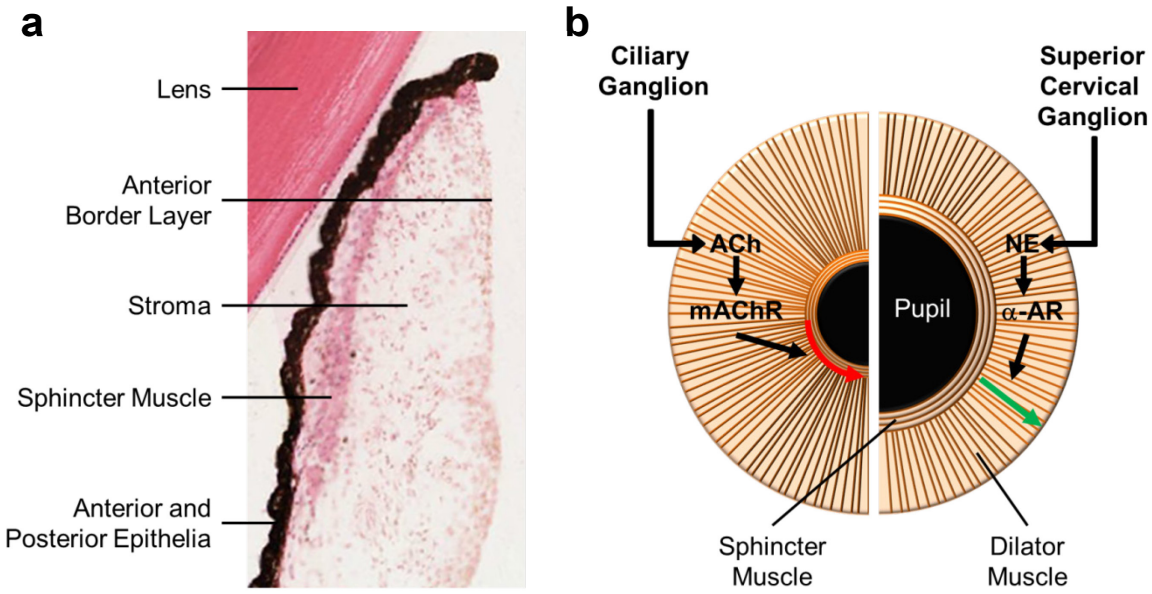

Fig. 1-3 Microscopic structure of the iris and mechanism of pupillary light reflex. a, Cross-section of the iris. The dilator muscle layer is outside of the plane of view. Light comes from right. Image modified from Ref. 28. **b,** Neural mechanism of pupillary reflex to light. Pupil constriction (left) is driven by contraction of the sphincter muscle (red arrow) in response to acetylcholine. Pupil dilation (right) results from norepinephrine-stimulated contraction of the dilator muscle (green arrow).

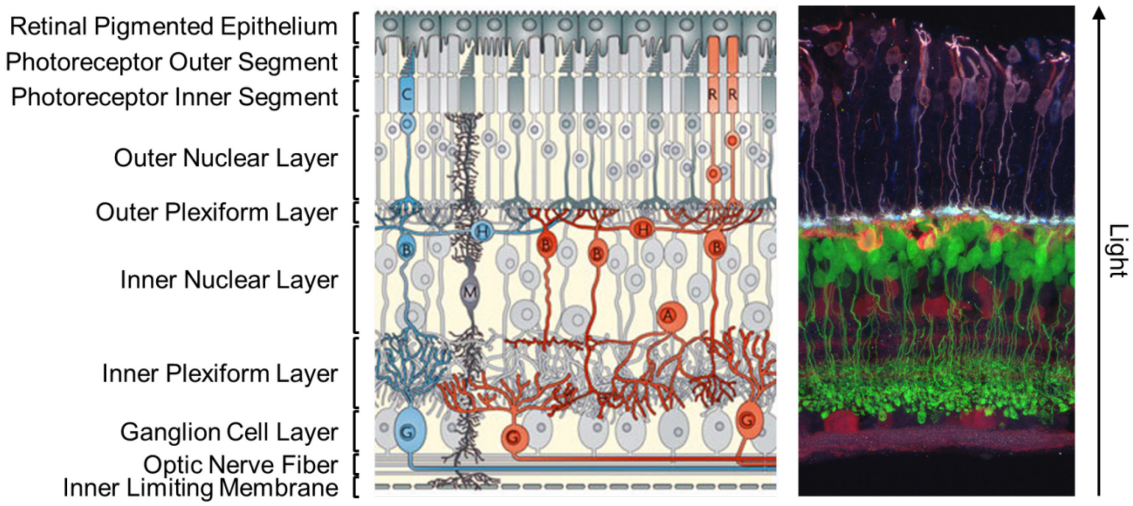

Fig. 1-4 **Structure of the retina.** Nuclear and synaptic layers indicated on left. R: rod, C: cone, B: bipolar cell, H: horizontal cell, A: amacrine cell, G: ganglion cell, M: Müller glial cell. The inner limiting membrane is formed by the end-feet of Müller glia. Cells indicated in red or blue participate in the typical rod or cone pathway, respectively. Image on left is adapted by permission from Macmillan Publishers Ltd: Nature Reviews Neuroscience (Ref. 29), copyright (2010). Image on right is taken from a mouse retina[10]. Purple: cones, Orange: horizontal cells, Green: bipolar cells, Magenta: amacrine and ganglion cells. Arrow indicates the direction of light.

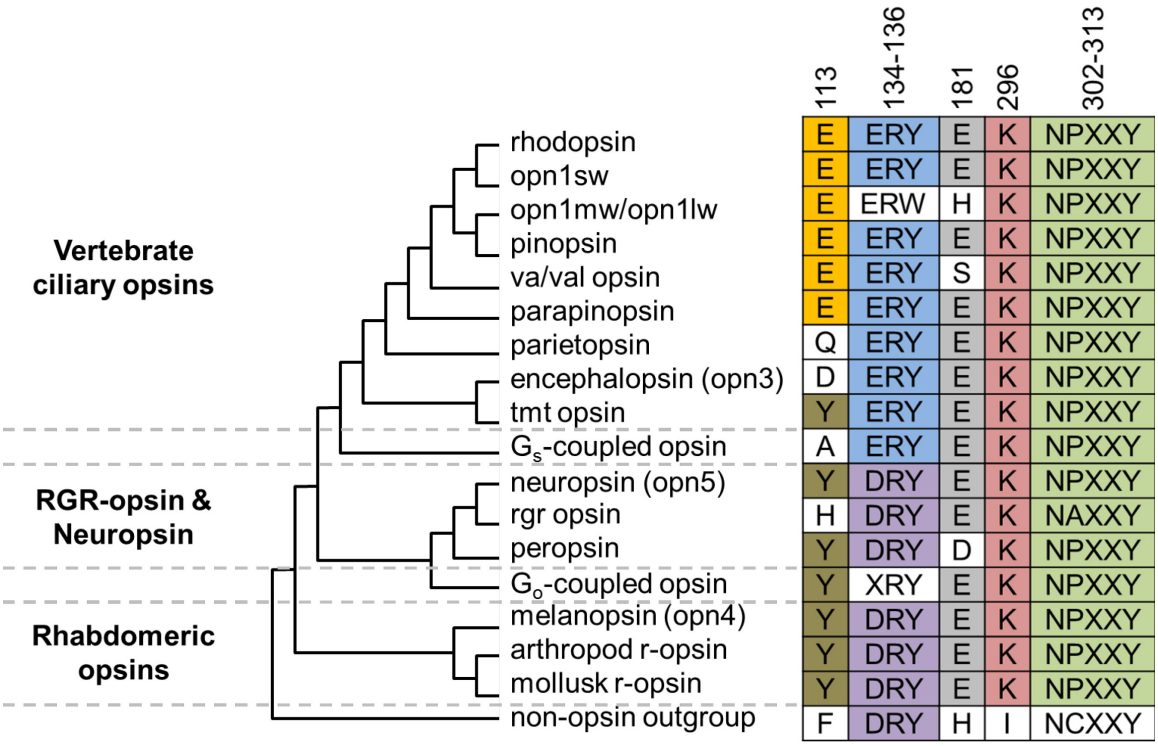

Fig. 1-5 **Phylogeny of opsins. Left,** Phylogeny of a subset of opsins from different sub-families (bold). Length of lines does not reflect evolutionary distance. **Right,** Amino acid sequences of the selected opsins at important functional motifs. Chromophore is conjugated to opsins at Lysine 296. Glutamate at position 113 or 181 serves as a counterion for stabilizing the chromophore-conjugation. D/ERY triad and NPXXY (X represents any amino acid) motif are crucial for G-protein binding and activation. Residue number is referenced to that of bovine rhodopsin. Image modified from Ref. 6.

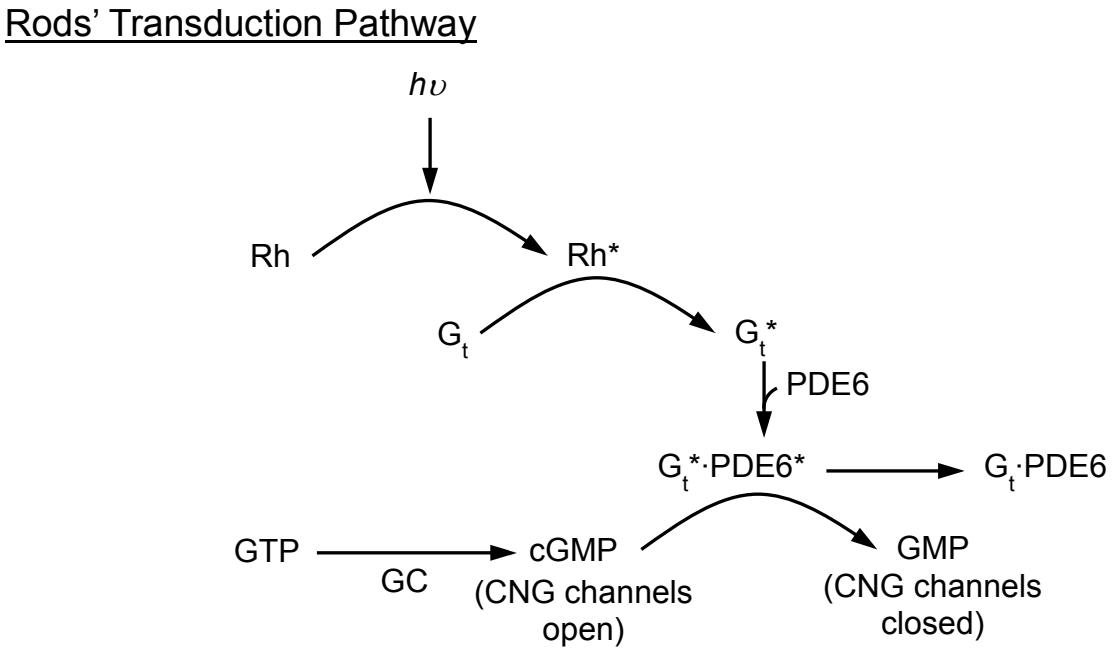

Fig. 1-6 Phototransduction pathway in rods. Light ($h\upsilon$)-activation of rhodopsin (Rh) causes the activation of the downstream G protein, transducin (G_t), and subsequently, phosphodiesterase (PDE6). PDE6 catalyzes the degradation of cGMP to GMP, resulting in the closure of cyclic-nucleotide-gated (CNG) channels on the plasma membrane. The reduction in inward current leads to the hyperpolarization of the rod cell, and thus a decrease in its synaptic release. Guanylate cyclase (GC) catalyzes the synthesis of cGMP from GTP to restore the cGMP level in the dark. Asterisks indicate the active forms of proteins.

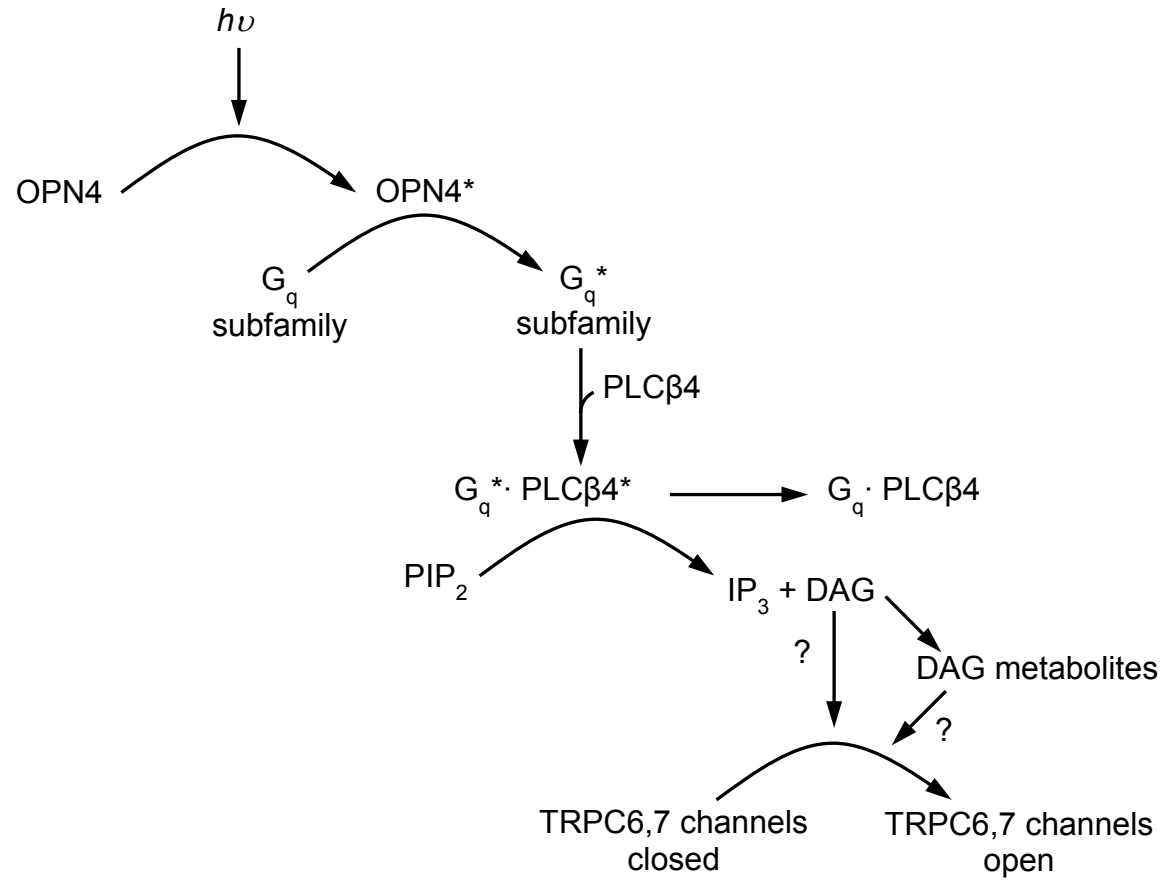

Fig. 1-7 Phototransduction pathway in melanopsin-expressing, intrinsically-photosensitive retinal ganglion cells (ipRGCs). Light ($h\upsilon$)-activation of melanopsin (OPN4) causes the activation of downstream G protein(s) of the G_q family, and subsequently, phospholipase C (PLCβ4). PLCβ4 catalyzes the degradation of PIP_2 to IP_3 and DAG, ultimately resulting in the opening of transient receptor potential channels (TRPC6 and 7) on the plasma membrane. The rise in inward current leads to the depolarization of the ipRGC, and thus an increase in its synaptic release. The exact gating mechanism for TRPC6 and 7 is unknown (question marks). Asterisks indicate the active forms of proteins.

1.6 References

1. Williams, S. B. in *Advances in Microbial Physiology* **52,** 229–296 (2006).

2. Johnson, C. H., Mori, T. & Xu, Y. A Cyanobacterial Circadian Clockwork. *Curr. Biol.* **18,** 816–825 (2008).

3. Ouyang, Y., Andersson, C. R., Kondo, T., Golden, S. S. & Hirschie, C. Resonating circadian clocks enhance fitness in cyanobacteria. **95,** 8660–8664 (2009).

4. Gehring, W. J. The evolution of vision. *Wiley Interdiscip. Rev. Dev. Biol.* **3,** 1–40 (2014).

5. Mast, S. O. *Light and the behavior of organisms*. (John Wiley and Sons, 1911).

6. Lamb, T. D. Evolution of phototransduction, vertebrate photoreceptors and retina. *Prog. Retin. Eye Res.* **36,** 52–119 (2013).

7. Nilsson, D.-E. The evolution of eyes and visually guided behaviour. *Philos. Trans. R. Soc. Lond. B. Biol. Sci.* **364,** 2833–2847 (2009).

8. Oyster, C. W. *The human eye: structure and function*. (Sinauer Associates, Inc., 1999).

9. Lamb, T. D., Collin, S. P. & Pugh, E. N. Evolution of the vertebrate eye: opsins, photoreceptors, retina and eye cup. *Nat. Rev. Neurosci.* **8,** 960–976 (2007).

10. *Webvision: the organization of the retina and visual system*. at <http://webvision.med.utah.edu/>

11. Håskjold, E., Refsum, S. B. & Bjerknes, R. Circadian variations in the DNA synthesis of the rat corneal epithelium. *Virchows Arch. B Cell Pathol. Incl. Mol. Pathol.* **58,** 229–234 (1989).

12. Håskjold, E., Refsum, S. B. & Bjerknes, R. Circadian variation in the mitotic rate of the rat corneal epithelium. Cell divisions and migration are analyzed by a mathematical model. *Virchows Arch. B. Cell Pathol. Incl. Mol. Pathol.* **58,** 123–127 (1989).

13. Fogle, J. a, Yoza, B. K. & Neufeld, a H. Diurnal rhythm of mitosis in rabbit corneal epithelium. *Albrecht Von Graefes Arch. Klin. Exp. Ophthalmol.* **213,** 143–148 (1980).

14. Scheving, E. Circadian influence on the wave form of the frequency of labeled mitosis in mouse corneal epithelium. 61–66 (1975).

15. Owman, C., Edvinsson, L., Lindvall, M. & Sjöberg, N. O. Influence of external light conditions on norepinephrine levels in organs innervated by sympathetic nerves from different levels. *Brain Res. Bull.* **9,** 777–779 (1982).

16. Wang, J. S. & Kefalov, V. J. The Cone-specific visual cycle. *Prog. Retin. Eye Res.* **30,** 115–128 (2011).

17. Shichida, Y. & Matsuyama, T. Evolution of opsins and phototransduction. *Philos. Trans. R. Soc. Lond. B. Biol. Sci.* **364,** 2881–2895 (2009).

18. Yau, K. W. & Hardie, R. C. Phototransduction Motifs and Variations. *Cell* **139,** 246–264 (2009).

19. Wenzel, A. *et al.* The retinal G protein-coupled receptor (RGR) enhances isomerohydrolase activity independent of light. *J. Biol. Chem.* **280,** 29874–29884 (2005).

20. Maeda, T. *et al.* Evaluation of the role of the retinal G protein-coupled receptor (RGR) in the vertebrate retina in vivo. *J. Neurochem.* **85,** 944–956 (2003).

21. Radu, R. a. *et al.* Retinal pigment epithelium-retinal G protein receptor-opsin mediates light-dependent translocation of all-trans-retinyl esters for synthesis of visual chromophore in retinal pigment epithelial cells. *J. Biol. Chem.* **283,** 19730–19738 (2008).

22. Chen, P., Lee, T. D. & Fong, H. K. W. Interaction of 11-cis-Retinol Dehydrogenase with the Chromophore of Retinal G Protein-coupled Receptor Opsin. *J. Biol. Chem.* **276,** 21098–21104 (2001).

23. Chen, P. *et al.* A photic visual cycle of rhodopsin regeneration is dependent on Rgr. *Nat. Genet.* **28,** 256–260 (2001).

24. Fain, G. L., Hardie, R. & Laughlin, S. B. Phototransduction and the Evolution of Photoreceptors. *Curr. Biol.* **20,** R114–R124 (2010).

25. Graham, D. M. *et al.* Melanopsin ganglion cells use a membrane-associated rhabdomeric phototransduction cascade. *J. Neurophysiol.* **99,** 2522–2532 (2008).

26. Xue, T. *et al.* Melanopsin signalling in mammalian iris and retina. *Nature* **479,** 67–73 (2011).

27. *Gray's Anatomy: The Anatomical Basis of Clinical Practice*. (Elsevier Health Sciences, 2015).

28. WebScope6. at <http://141.214.65.171/Histology/Central Nervous System/EYE-2_HISTO_20X.svs/view.apml?x=-0.3664978570&y=0.1487488520&zoom=100.0000000000&transform=>

29. Swaroop, A., Kim, D. & Forrest, D. Transcriptional regulation of photoreceptor development and homeostasis in the mammalian retina. *Nat. Rev. Neurosci.* **11,** 563–576 (2010).

Chapter 2 Signal Amplification and Noise Associated with Rod and Cone Pigments

2.1 Introduction

Our visual system operates with an extreme sensitivity that approaches the physical limit of light. In a classic psychophysical experiment, Hecht, Shlaer and Pirenne[1] showed that dark-adapted human subjects can consciously detect the absorption of only 5 to 8 photons, the elementary particle of light. Because these few photons were delivered to a substantial retinal area (comprising of ~500 rods), and thus the probability of a single rod photoreceptor absorbing more than one photon was low, it follows that a dark-adapted rod can signal the absorption of a single photon[1]. With the advent of the suction-pipette-recording technique[2] (see Methods), the electrical response of a rod to a single photon has in fact been observed in various species (see, for example, Ref. 3).

One prerequisite for the remarkable sensitivity of rods is a large signal-to-noise ratio accomplished in phototransduction (see Chapter 1.3). Signal (absorption of a photon by a rhodopsin molecule) is amplified in three steps along the phototransduction cascade[4–6]: (1) a single photoexcited rhodopsin molecule (R*) activates multiple transducin molecules in its lifetime, (2) each photodiesterase (PDE) molecule, as a downstream effector of transducin, hydrolyzes many cGMP molecules during its activation, and (3) a small decrease in cGMP concentration causes a 3-fold larger reduction in photocurrent due to the cooperative gating of the cyclic-nucleotide-gated (CNG) channels by cGMP. Meanwhile, rods are able to keep their intrinsic noise low

because of the very thermally-stable nature of their pigment, rhodopsin[7], and the presence of various regulatory mechanisms[8].

In this chapter, we shall present work that addresses two fundamental questions regarding the signal-amplification and noise originating from rod and/or cone pigments, namely: (1) how many transducin molecules are activated by a single rhodopsin molecule during its active lifetime in a single-photon response, and (2) how is the thermal noise rate of a visual pigment quantitatively related to the pigment's peak absorption wavelength (λ_{max})? More detailed descriptions of these problems will follow.

2.2 Signal-amplification by rhodopsin

The activation of transducin by photoexcited rhodopsin has long been thought to enjoy high amplification. Nevertheless, the degree of such amplification has been a subject of continuous debate. The controversy rests upon the widely different measures of the rate of transducin activation per R* and of the lifetime of R*, which, by multiplication, give the number of transducin molecules activated over the course of a single-photon response.

The rate of transducin activation per R* could be deduced from biochemical binding assays (reviewed in Ref. 4). In these experiments, preparations of rod outer segment (ROS) membranes, disrupted either by electropermeabilization, mechanical shearing or sonication, were incubated with radiolabeled guanosine 5'-triphosphate (GTP) or its nonhydrolyzable analogs, guanosine 5'-[β,γ-imido]triphosphate (pNHppG) or guanosine 5'-[γ-thio]triphosphate (GTPγS). Upon light stimulation, these nucleotides were incorporated into transducin as R* catalyzed the GDP-to-GTP exchange on

transducin. The rate of transducin activation per R* was then derived from the amount of nucleotides bound over a certain period of reaction time, together with the amount of R* produced by the given intensity of light. Table 2-1 summarizes the results from calculations done by Pugh and Lamb[4] based on four nucleotide-binding studies and those from a separate study by Leskov *et al*.[9]. As shown, the estimated rate varies by up to 10 fold. This variation in part stems from several limitations/shortcomings of binding assays[4,5]. First, these binding experiments are fairly insensitive; thus, accurate measurements are difficult to be made at intensities low enough for producing a linear relationship with reaction rate. Second, owing to limited sampling, binding experiments offer very poor time resolution and are often allowed to last for a duration (minutes) much longer than that of a typical rod photoresponse (seconds). Results may thus be complicated by rhodopsin inactivation. Third, ROS membrane preparations are usually heavily disrupted in binding experiments, leading potentially to a loss or dilution of some critical soluble factors. In fact, preparations that were more gently treated by using electropermeabilization gave a higher transducin-activation rate[10]. Lastly, in most binding experiments, the concentrations of the reaction components as well as other reaction conditions are quite arbitrarily assigned. It is now known that the transducin-activation rate actually depends on, for examples, the concentration of GTP and Mg^{2+} in the reaction[4,5,9].

Estimates of the rate of transducin activation per R* have also come from light-scattering studies (see Table 2-1; reviewed in Ref. 4,5,11). In these experiments, ROS membrane preparations, suspensions of dissociated rods or intact retinas were probed by near-infrared light pulses. Signals scattered from these probe-pulses were believed to

reflect structural changes due to molecular movements resulting from the activation of the phototransduction cascade by a separate light beam. Light-scattering experiments support higher sensitivity and time resolution, and demand a milder treatment of rod preparations compared to nucleotide-binding assays[4,5,11]. These factors partly explain why light-scattering studies generally yield 10- to 100-fold higher estimates for transducin-activation rates. Nonetheless, it has been arguable as to what molecular processes the light-scattering signals really correspond to[5,11]. Some signals have been taken to reflect the binding of transducin to R*; some were thought to arise from transducin partitioning between the membrane-bound and soluble forms; some others were believed to originate from the contraction of ROS disks in association with transducin activation. It is not clear whether these different signals are actually one and the same, and whether some of them are simply physiologically-irrelevant artefacts. In estimating the transducin-activation rate, such ill-defined readouts are prone to create errors. As an example, the transducin-activation rate could have been overestimated if a signal for R*-transducin binding was used without appropriate corrections because it is unlikely that every R*-transducin binding event would lead to effective activation of the transducin molecule[4].

As for the length of R* lifetime, there is likewise not yet a consensus. Rieke and Baylor (1998)[12] studied the time-dependent rhodopsin activity by manipulating the concentration of GTP in truncated toad ROS (thus altering the gain in the R*-to-transducin step) at specific time of a photoresponse. They concluded that rhodopsin activity declined over time with a time constant of 2 – 2.5 sec. Subsequently, Burns and colleagues[13] pointed out that manipulations that lengthens the lifetime of R* or transducin

(such as the truncated rod experiments above) would not help in identifying whether the shut-off of R* or transducin is the rate-limiting step in the decay of a light response, simply because a non-limiting step may artificially be made limiting by such manipulations. Instead, these authors overexpress in mouse rods the GTPase-activating complex (GAP complex, consisting of RGS9-1, Gβ5 and R9AP proteins) that promotes the hydrolysis of GTP in transducin, and hence its deactivation. Based on the accelerated decay of light responses of these rods, the authors contended that transducin deactivation is the true rate-limiting step whereas the lifetime of R* is < 80 msec. With a similar mouse line overexpressing the GAP complex but to a different extent, Chen *et al*.[14] arrived at a R* lifetime of < 54 msec. Surprisingly, Rieke and colleagues[15] reported also an acceleration of the decay of saturated photoresponses in rods lacking arrestin ($Arr1^{-/-}$), which, by binding to phosphorylated rhodopsin, is involved in the shut-off of R*. Based on this and other evidence regarding the variability of single-photon responses, the authors maintained that rhodopsin should have a lifetime (~0.4 sec) two times longer than that of transducin (~0.2 sec). In contradiction, Gross and Burns[16] found no change in response kinetics in $Arr1^{-/-}$ rods, and refined their estimate for the lifetime of R* by computational modeling first to < 53 msec[17] and then to ~36 msec[18]. An earlier modeling study[19], however, gave ~1.3 sec, although acknowledging that R* is not the rate-limiting reaction in the decay of the photoresponse.

In short, there are still uncertainties surrounding the estimates of the transducin-activation rate and the lifetime of R*, two of the important factors determining the degree of amplification in rod phototransduction. To circumvent these uncertainties, we have devised a method to directly provide an estimate of the number of transducin molecules

activated over the course of a single-photon response from simple electrophysiological measurements on genetically-engineered mouse rods.

Table 2-1 Experimental measurements of transducin-activation rate

Species	Temperature (°C)	Labeled nucleotide	Conc. of GTP or analog (μM)	Fraction of rhodopsin isomerized	Transducin-activation rate (G* s^{-1} per R*)	Reference(s)
Nucleotide-binding assays						
Bovine	22	[^{3}H]pNHppG	1.5	10^{-5}	12	Ref. 20[#]
Amphibian	Room temp	[α-^{32}P]GTP	125	10^{-5}	<300	Ref. 21[#]
Frog	Room temp	[^{3}H]GTP	10	10^{-4}	26	Ref. 22[#]
Frog	Room temp	[^{3}H]GTP	30-60	10^{-6}	24	Ref. 10[#]
		[^{35}S]GTPγS	30-60	$<10^{-6}$	250	
Frog	22	[^{35}S]GTPγS	100	$(1 – 2.3)\times10^{-6}$	~120[^]	Ref. 9
Light-scattering studies						
Frog	23	N.A.	500	$<10^{-3}$	1,100	Ref. 23[#]
Bovine	21	N.A.	100	$<10^{-3}$	>3,300	Ref. 24[#]
Bovine	21	N.A.	Intact retina	$<10^{-4}$	2,500	Ref. 25[#]
Bovine	20	N.A.	Intact retina	$<10^{-4}$	800	Ref. 26[#]

Part of this table is adapted from Ref. 4, with permission from Elsevier. N.A. stands for not applicable.
[#]See Ref. 4 for detailed discussions on these studies.
[^]Value estimated from experiments under the most favorable conditions presented in the study.

2.3 Generation and characterization of *Rho*$^{REY/REY}$ mutant mice

We mutated the G protein-binding motif (E134-R135-Y136) of rhodopsin to REY[27] in mice (denoted as *Rho*$^{REY/REY}$ mice) by using the CRISPR method (see Method). We reasoned that if we could dramatically reduce the binding affinity of transducin to R*, the probability of a R* molecule activating a transducin molecule may become so low that activation would not be effected in all but a handful of R*-transducin binding events. In those cases of successful activation, the chance is high that only one single transducin molecule would be activated. Hence, by comparing the single-photon response amplitude of *Rho*$^{REY/REY}$ rods (which is essentially a single-transducin-mediated response) with that

of wildtype (WT) rods, we can deduce the number of transducin normally being activated in a single-photon response of a WT rod.

We performed some basic characterization of the $Rho^{REY/REY}$ mice. The retina of 2- to 3-month-old $Rho^{REY/REY}$ mice showed normal gross morphology, with no obvious photoreceptor degeneration (Fig. 2-1a). The mutant rhodopsin was correctly targeted to the ROS (Fig. 2-1b). Microspectrophotometry on groups of $Rho^{REY/REY}$ rods gave an absorption spectrum indistinguishable from that of WT rods, with a λ_{max} of ~500 nm (Fig. 2-1c). The peak optical density obtained from $Rho^{REY/REY}$ rods (0.328), which reflects the pigment density in the ROS, was similar to that from WT rods (0.342), supporting a normal expression level of the mutant rhodopsin. We also checked the expression levels of various phototransduction components by Western blot but saw no difference between the retinas of $Rho^{+/+}$, $Rho^{REY/+}$ and $Rho^{REY/REY}$ littermates (Fig. 2-1d). In order to be consistent with electrophysiological experiments below, all of the above analyses were done on mice in which GCAP1 and GCAP2 proteins have both been ablated (i.e., $Gcaps^{-/-}$)[28]; GCAP proteins are responsible for regulating rods' light responses through Ca^{2+}-dependent feedback on guanylate cyclase[8].

2.4 Photoresponses of $Rho^{REY/REY};Gcaps^{-/-}$ rods

Table 2-2 summarizes the kinetic parameters of photoresponses of $Rho^{+/+};Gcaps^{-/-}$ and $Rho^{REY/REY};Gcaps^{-/-}$ rods, which are, although not directly relevant to our immediate question, worth some mentioning here. Overall, $Rho^{REY/REY};Gcaps^{-/-}$ rods responded to light flashes (Fig. 2-2a) with similar saturating current but drastically slower kinetics, which was reflected in a 2- to 3-fold increase in the integration time (t_{int}; see

Methods), the time-to-peak (t_{peak}; see Methods) and the time constant of recovery (τ_{rec}; see Methods) of their dim-flash responses (Fig. 2-2c). The latter two parameters quantify the speed of response termination whereas t_{int} provides a measure of the effective response duration. Pepperberg analyses[29] of saturated responses also revealed a larger dominant time constant (τ_D) for $Rho^{REY/REY};Gcaps^{-/-}$ rods than for $Rho^{+/+};Gcaps^{-/-}$ rods (Fig. 2-2d). The change in these kinetic parameters indicated that the deactivation of rhodopsin, instead of transducin normally in WT rods, probably limited the rate of response termination of $Rho^{REY/REY};Gcaps^{-/-}$ rods. Moreover, we also obtained the amplification factor (A_{amp}) from the initial rising phase of the dim-flash responses (see Methods); the A_{amp} of $Rho^{REY/REY};Gcaps^{-/-}$ rods was 5 orders of magnitude lower than that of $Rho^{+/+};Gcaps^{-/-}$ rods. Furthermore, a slower rising phase was evident from comparing the dim-flash responses of rods of these two genotypes normalized to their transient peak amplitudes (Fig. 2-2c). Taken together, these two observations suggested that response activation was likewise slowed down in $Rho^{REY/REY};Gcaps^{-/-}$ rods. The above kinetic properties were likely intrinsic to the mutant pigment because $Rho^{REY/REY};Gcaps^{-/-}$ rods that expressed also transgenically the human red cone pigment ($hOpn1lw^{+}$)[30] responded with apparently normal kinetics when the transgenic red cone pigment was preferentially stimulated by light flashes at 560 nm; the same stimuli elicited only small and slow responses in $Rho^{REY/REY};Gcaps^{-/-}$ rods that did not express the red cone pigment (Fig. 2-2b).

As a proxy for light sensitivity, we measured the light intensities required for producing half-maximal responses (i.e., half-saturating light intensity, σ) in $Rho^{+/+};Gcaps^{-/-}$ and $Rho^{REY/REY};Gcaps^{-/-}$ rods. The σ's for the two genotypes were about 6

and 46,168 photons μm^{-2}, respectively, giving an over 7,400-fold difference in sensitivity (Fig. 2-3). Since we observed no major deficits in the expressions of core phototransduction components, including rhodopsin itself, in *Rho*$^{REY/REY}$;*Gcaps*$^{-/-}$ rods, this difference in sensitivity was likely attributable to a reduced efficiency of transducin-activation by the mutant rhodopsin. In addition, the magnitude of the sensitivity-reduction (7,400-fold) far exceeded the number of transducin molecules (1,320 G*) activated by a single R* molecule in a photoresponse predicted (see above) from even the largest, acceptable measures of transducin-activation rate (3,300 G* sec^{-1} per R*; Ref. 24) and R* lifetime (0.4 sec; Ref. 15). Although sensitivity does not necessarily follow a simple linear relationship with gain, the vastness of the sensitivity-reduction (and also in A_{amp}) highly suggests that transducin-activation has become so ineffective in *Rho*$^{REY/REY}$;*Gcaps*$^{-/-}$ rods that on average a single R* molecule activates much fewer than one transducin molecule in its lifetime.

Table 2-2 Kinetic parameters of photoresponses of *Rho*$^{+/+}$;*Gcaps*$^{-/-}$ and *Rho*$^{REY/REY}$;*Gcaps*$^{-/-}$ rods

Genotype	R_{max} (pA)	t_{int} (msec)	t_{peak} (msec)	τ_{rec} (sec^{-1})	τ_D (sec^{-1})	σ (photons μm^{-2})	A_{amp} (sec^{-2})
Rho$^{+/+}$;*Gcaps*$^{-/-}$	15.1 ± 0.5 (n = 15)	567 ± 14 (n = 15)	393 ± 8 (n = 15)	247 ± 14 (n = 15)	163 ± 6 (n = 8)	6 ± 0.05 (n = 8)	11.8 ± 1.0 (n = 15)
Rho$^{REY/REY}$;*Gcaps*$^{-/-}$	14.3 ± 0.7 (n = 11)	1304 ± 99 (n = 11)	787 ± 28 (n = 11)	697 ± 96 (n = 15)	467 ± 14 (n = 18)	46168 ± 560 (n = 16)	(48.3 ± 8.6) × 10^{-5} (n = 11)
Fold difference		2.30	2.00	2.82	2.87	7695	1/24426

2.5 Single-photon responses of *Rho*$^{REY/REY}$;*Gcaps*$^{-/-}$ rods

Under the presumption that a single R* molecule in a *Rho*$^{REY/REY}$;*Gcaps*$^{-/-}$ rod activates on average much fewer than one transducin molecule in its lifetime, a single-photon response in such a rod would virtually be mediated by a single transducin

molecule. Thus, we compared the amplitudes (a_{SPR}) of single-photon responses of *Rho*$^{+/+}$;*Gcaps*$^{-/-}$ and *Rho*$^{REY/REY}$;*Gcaps*$^{-/-}$ rods by fluctuation analyses on dim-flash responses. The *Gcaps*$^{-/-}$ background was used here to increase the size of single-photon responses[28], particularly in *Rho*$^{REY/REY}$ rods, which may otherwise be too small to measure reliably. By computing the ensemble variance over mean at the peak of many dim-flash responses[3] (see Methods), we obtained single-photon-response amplitudes (mean ± SEM) of 3.20 ± 0.13 pA (n = 15) and 0.16 ± 0.01 pA (n = 11) for *Rho*$^{+/+}$;*Gcaps*$^{-/-}$ and *Rho*$^{REY/REY}$;*Gcaps*$^{-/-}$ rods, respectively (Fig. 2-4a). Because *Gcaps*$^{-/-}$ rods sometimes produced very large and/or prolonged dim-flash responses[31], saturation may happen around the peak of the dim-flash responses. We therefore separately obtained another set of measures of single-photon-response amplitudes by scaling the square of the ensemble mean of dim-flash responses to fit the ensemble variance[12] (see Methods). The values (mean ± SEM) were 3.11 ± 0.11 pA (n = 15) and 0.13 ± 0.01 pA (n = 11) for *Rho*$^{+/+}$;*Gcaps*$^{-/-}$ and *Rho*$^{REY/REY}$;*Gcaps*$^{-/-}$ rods, respectively (Fig. 2-4b).

2.6 Discussion

We presented here the idea of using the single-photon response amplitude (a_{SPR}) of *Rho*$^{REY/REY}$;*Gcaps*$^{-/-}$ rods, in which the G protein-binding motif of rhodopsin was mutated, as a means for directly estimating the number of transducin molecules activated by a single R* in a photoresponse. The incommensurately large reduction in sensitivity led us to believe that the effectiveness of a R* activating a transducin molecule has been greatly reduced to a degree that most R* failed to activate even one transducin molecule in its lifetime. Currently, we are experimentally testing this notion by introducing an

over-expressing, hyperactive mutant of G protein receptor kinase 1 (GRK1-S561L)[18] into $Rho^{REY/REY};Gcaps^{-/-}$ rods. The expression of this mutant shortens the R* lifetime in $Rho^{+/+};Gcaps^{-/-}$ rods[18]. We expect that the same effect on $Rho^{REY/REY};Gcaps^{-/-}$ rods would further lower the sensitivity of these rods (due to even lower probability of transducin-activation) but keep the a_{SPR} the same (as a single active transducin was already the signaling unit in these rods).

The a_{SPR} of $Rho^{REY/REY};Gcaps^{-/-}$ rods was about 20- to 25-fold lower than that of $Rho^{+/+};Gcaps^{-/-}$ rods, estimated by two separate methods at either the peak or the initial rising phase of the dim-flash responses. As a first approximation, this would suggest that a R* in a $Rho^{+/+};Gcaps^{-/-}$ rod activates about 20 – 25 transducin molecules at the peak of a single-photon response. There are, however, complexities. For example, for a dim-flash response of certain size, the underlying active transducin molecules in a $Rho^{REY/REY};Gcaps^{-/-}$ rod has a different spatial profile from those in a $Rho^{+/+};Gcaps^{-/-}$ rod – the active transducin molecules are distributed over multiple rod discs in the former but confined to a local milieu in the latter, in which case non-linearity may develop. We are now working to refine our analyses to hopefully get a more accurate estimate of the number of transducin molecules that are actually activated per R* over time.

It is interesting that $Rho^{REY/REY};Gcaps^{-/-}$ rods showed slower photoresponses. Preliminary microspectrophotometric experiments on these rods revealed an altered kinetics of the production and decay of meta-II and meta-III states. This, however, probably does not explain the slow recovery of the responses of $Rho^{REY/REY};Gcaps^{-/-}$ rods, because the decay of meta-II and meta-III normally takes minutes even in WT mouse rods[32]. Instead, the slow recovery may be a result of disturbed R* phosphorylation or

arrestin-binding. In fact, the ERY motif is believed to be part of the binding surface between R* and GRK1[33], and between R* and ARR1[34,35]. Nonetheless, it is curious that the dim-flash responses of *Rho*$^{REY/REY}$*;Gcaps*$^{-/-}$ rods also demonstrated a slower rising kinetics; in contrast, *Grk1*$^{-/-}$ or *Arr1*$^{-/-}$ rods show slower kinetics only in the decay phase, but not the rising phase of their dim-flash responses[36,37]. It remained to be studied what actually contributed to the kinetic defects of *Rho*$^{REY/REY}$*;Gcaps*$^{-/-}$ rods.

2.7 Thermal noise from visual pigments

The high amplification discussed above in rods enables the generation of a reliable electrical signal upon absorption of just a single photon[3]. However, as mentioned in Chapter 2.1, our conscious perception of light actually takes more than one photon[1]. What underlies such a higher limit for our visual threshold? By attending to the false perception of light of some human subjects in the dark (so-called dark-light), Barlow[38] pointed out that our visual system is corrupted by intrinsic noise, so it takes a signal sizably larger than the noise to generate a genuine perception. Biological noise has indeed later been observed in rods as discrete electrical events happening in darkness[7]. These events appear identical to single-photon responses in both amplitude and waveform[7], apparently coming from the spontaneous activation of rhodopsin. At the molecular level, rhodopsin is actually remarkably stable, having a half-life of about 1000 years at room temperature[7]; however, when they are packed in thousands of millions or billions in a rod cell, the aggregate noise rate per cell can amount to about one event per minute at physiological temperature (37°C).

Barlow also hypothesized a possible link between the peak-absorption wavelength (λ_{max}) of a pigment and its spontaneous activation rate[39]. Daily experience has long suggested that the level of illumination greatly influences color contrast. Red colors that burn bright in daylight turn even duller than blue colors at dawn or dusk. This phenomenon, known as the Purkinje shift, illustrates a shift in the maximum sensitivity of the human eye toward the blue end of the spectrum (i.e., shorter wavelengths) as vision switches from being cone-based to being rod-based for a decrease in the ambient light level (see, for examples, Ref. 40,41). Barlow recognized the evolutionary value of this shift by proposing that pigments with shorter λ_{max}'s are more thermally stable, thus quieter and more suitable for dim-light detection[39]. This hypothetical connection between the spectral and thermal properties of visual pigments has later been confirmed by several groups, including our laboratory[30,42–46] (summarized in Table S3 of Ref. 47).

One question remains: how do visual pigments become spontaneously activated? The close resemblance of the dark events to single-photon responses, on the one hand, suggests that they originate from canonical isomerization of the pigments as in the case of light-activation, but, in this case, harness thermal energy intrinsic to the pigment molecule instead of photon energy. On the other hand, spontaneous pigment-activation appears to require an activation energy (also termed the ground-state isomerization energy barrier E_a^T) much less than the minimal energy it would take for a pigment to get to the early photoisomerized "bathorhodopsin" state (Fig. 2-5). Specifically, by measuring spectroscopically the rate of spontaneous isomerization of free 11-cis-retinal in various solvents, Hubbard[48] found an Arrhenius activation energy for spontaneous isomerization, $E_a^{T(app)}$, of ~22-26 kcal mole^{-1}. Single-cell recordings of dark events in live

toad rods gave a similar estimate of 21.9 kcal mole^{-1} for spontaneous activation of rhodopsin[7]. Both these values are much smaller than the generally accepted ground-state energy of bathorhodopsin (35 kcal mole^{-1}) measured by calorimetry[49].

Over the past thirty years, several mechanistic models for spontaneous pigment-activation have been put forward to explain the above energy discrepancy. An early idea was that deprotonation at the Schiff base between the chromophore and the opsin protein would transform a population of rhodopsin into a relatively unstable form that is prone to thermal isomerization[50,51]. It was calculated that deprotonation should reduce E_a^T to ~23 kcal mole^{-1} (Ref. 50), thus consistent with the experimentally measured $E_a^{T(app)}$. This proposal, however, was later dismissed when pH changes were found not to affect the rates of dark events in both rods and cones[42,52]. More recently, a variation of this model has been devised from measuring the hydrogen/deuterium exchange at the –OH group of residue Thr118 in the chromophore-binding pocket of rhodopsin[53]. It was suggested that infrequent structural fluctuations in rhodopsin may transiently open its chromophore-binding pocket to allow the chromophore inside to thermally isomerize in a less-constrained, solvent-like environment, thus accounting for the low $E_a^{T(app)}$ (Ref. 53). Nevertheless, it is not obvious how the rate of spontaneous activation can be correlated with λ_{max} (see above) under this model, given that all cone pigments, regardless of their λ_{max}'s, have constitutively more open chromophore-binding pockets than has rhodopsin. Other proposals include the notion of bioluminescent photons emitted from natural redox reactions in the retina[54]. These proposals are likewise speculative or defective in certain ways.

In 2004, a new insight emerged when Ala-Laurila *et al.*[55] pointed out that the low $E_a^{T(app)}$ value compared to E_a^T may simply be the result of a misuse of thermal statistics (see Chapter 2.8). Their work reopened the possibility that photo- and thermal-activation of visual pigments follow a common isomerization pathway. Expanding on their idea, I participated in an ongoing project of our laboratory to develop a quantitative relation that would account for: (1) the correlation between the rate of spontaneous pigment-activation and λ_{max}, (2) the general observation that cone pigments are noisier than rod pigment of a given λ_{max}, and (3) the discrepancy between E_a^T and $E_a^{T(app)}$. Here, I shall only give a brief account of the key findings of this piece of work, now published as Luo *et al.*[47], in connection to our later study of thermal noise from a number of native and mutant rod and cone opsins.

2.8 Theoretical predictions of pigment noise

In Luo *et al.*[47], we undertook three major steps to develop a comprehensive theory of pigment noise that would apply well to both rod and cone pigments.

To begin, we have discovered a fundamental, quantitative principle that relates the minimum photoactivation energy (E_a^P) of a pigment (i.e., the minimum energy required for a pigment to reach its photoexcited state) to its λ_{max}, namely,

$$E_a^P = 0.84hc/\lambda_{max} \qquad \text{(Eqn. 1)}$$

where h is the Planck's constant and c is the velocity of light. This principle holds for all the pigments we have examined, regardless whether it is a rod or cone pigment, being UV- or non-UV-sensitive, or having A_1- or A_2-chromophore[47] [11-*cis*-retinal (A_1) is used

by land-based animals whereas 11-*cis*-3-dehydroretinal (A_2) is used by some aquatic or amphibian species[56]]. Thus, we were able to calculate for the first time the E_a^P of a pigment from its λ_{max}.

Meanwhile, we have also achieved precise measurement of the thermal rate constant of blue cone pigment, which happens to be expressed naturally in toad green rods[47]. Importantly, this noise is very low[47]. Because of the low gain in cone phototransduction, it has traditionally been difficult to measure cone pigment noise directly from native cones. Previously, by expressing the human red cone pigment transgenically in *Xenopus*[43] or mouse[30] rods, we were able to take advantage of the high amplification in rod phototransduction to count the spontaneous pigment-activation events in dark recordings, which we found to be remarkably frequent. Together with the measurements on blue cone pigment, we have now quantitatively established that the thermal-noise rate is indeed higher for longer λ_{max}, varying by 10-million-fold from blue cone pigment (λ_{max} = 432 nm, with A_1 chromophore)[47] through rhodopsin (λ_{max} = 500 nm, with A_1 chromophore)[7] to red cone pigment (λ_{max} = 620 nm, with A_2 chromophore)[43].

Finally, by applying the statistical-mechanical distribution depicted in Eqn. 2, we have been able to predict the thermal noise rates of various pigments from their λ_{max}'s. This distribution was first derived by Hinshelwood[57] for describing unimolecular reactions involving thermal contribution from multiple vibrational modes internal to the reactant molecules; it was first applied to visual pigments by St. George[58] in 1952 and by Ala-Laurila *et al.*[55] more recently. According to the Hinshelwood theory[57], the probability, $f_{\geq E_a^T}$, of a pigment molecule having relevant thermal energy (coming from *m* vibrational modes) equal to or greater than E_a^T and thus being capable of isomerization, is given by:

$$f_{\geq E_a^T} = e^{-\frac{E_a^T}{RT}} \sum_1^m \frac{1}{(m-1)!} \left(\frac{E_a^T}{RT} \right)^{m-1} \qquad \text{(Eqn. 2)}$$

where R is the universal gas constant and T is the absolute temperature. When $m = 1$, the Hinshelwood distribution reduces to the commonly-used Boltzmann distribution, which, strictly speaking, applies only to an ideal gas with a thermal energy of RT, as opposed to a polyatomic biomolecule with a total usable thermal energy of mRT (see Ref. 57). In fact, it is this difference that explains the aforementioned energy discrepancy between E_a^T and $E_a^{T(app)}$ (see Ref. 47). We assumed the simple picture that thermal activation is a canonical isomerization reaction. Hence, by taking $E_a^T = \alpha E_a^P$ in Eqn. 1 (the exact value of α turns out to be unimportant, see Ref. [47]), we were able to predict the absolute rate of thermal activation of various pigments by $A \times f_{\geq E_a^T}$, where A is the pre-exponential factor representing the frequency at which thermal activation is attempted by the pigment molecule[47]. As shown in Fig. 2-6, for the three native pigments (red squares) the thermal-noise rate of which we have measured, our theoretical predictions (red curve) match the measured values reasonably well, suggesting that pigment noise indeed arises from isomerization. At a given λ_{max}, rod pigments (black squares) are generally less thermally active than cone pigments; this phenomenon can be captured by lowering the A factor by about 26 fold[47] (Fig. 2-6). We interpreted this difference to reflect the more open chromophore-binding pocket known to exist in cone pigments[59,60], which may allow for more frequent isomerization-attempts by the molecule.

In the following work, we aimed at furthering our understanding on how the rate of thermal activation of visual pigments may be affected by their molecular/structural features. For this, we extended the above analyses to the native green-cone pigment not

covered in the earlier work, and to mutant pigments that show uniquely interesting activation properties.

2.9 Thermal-noise measurements on green cone pigment

Based on the theoretical estimations described in Chapter 2.8, we calculated a thermal-noise rate constant of 7.4×10^{-9} sec^{-1} for the mouse green-cone pigment (λ_{max} = 510 nm) and of 2.6×10^{-8} sec^{-1} for the human green-cone pigment (λ_{max} = 530 nm) at 37°C (assuming $\alpha = 1$, $m = 45$ and $A = 1.88 \times 10^{-4}$ sec^{-1} as for other cone pigments[47]). Nonetheless, existing noise-rate measurements seemed to disagree with our predictions. By replacing rhodopsin with the mouse green cone pigment in a knock-in mouse line, Sakurai *et al*.[46] have obtained a rate constant of 1.7×10^{-7} sec^{-1} at 34-37°C, or 23-fold higher than our prediction. In macaque monkey red/green cones (not specified explicitly; green cones: λ_{max} = 530 nm), Schneeweis and Schnapf[61] have also reported very high equivalent dark pigment-noise rates of 3,800 sec^{-1} $cell^{-1}$ from voltage-recordings, and of 6,400 sec^{-1} $cell^{-1}$ by correction from earlier current-recordings, both at unknown temperatures. Because individual thermal-activation events were below resolution, the above studies have all relied on less-direct approaches such as power spectral analysis, which suffered from contamination by other phototransduction noise. In great contrast, pigment thermal noise was reportedly not detectable in goldfish green cones (λ_{max} = 537 nm)[62].

We decided to re-measure the thermal-noise rate constant of (human) green cone pigment (hOPN1MW) by directly counting spontaneous-activation events in dark recordings made from rods transgenically expressing this pigment, as was done for the

human red-cone pigment. We did not consider the generation of knock-in animals as a viable strategy because a high expression level may lead to cell desensitization (hence smaller single-photon responses) as well as superposition of the too-frequent thermal-activation events over each other, as had happened in the study by Sakurai *et al*[46]. In collaboration with Dr. Nicholas Marsh-Armstrong, we created a few transgenic *Xenopus* lines expressing the human green cone opsin under the ubiquitous cytomegaloviral (CMV) promoter (Fig. 2-7a). *Xenopus* was chosen because their green rods, as in other amphibians[63–65], naturally express a blue-cone pigment (λ_{max} = 445 nm)[66,67] instead of rhodopsin (λ_{max} = 500 nm) and because their use of A_2 chromophore would red-shift the λ_{max} of the human green cone pigment from 530 nm to 579 nm[56]; both of these characteristics served to exaggerate the spectral difference between the endogenous and the transgenic pigments, therefore allowing more accurate quantification of the transgenic expression levels (information necessary for calculating the molecular rate constant of thermal activation) based on the red-shifts in the rods' action spectra. Indeed, the quantification could be achieved in the two cells shown in Fig. 2-7b and c. Disappointingly, however, the single-photon response of the transgenic rods, as calculated from the ensemble variance over mean, was below 0.2 pA (Fig. 2-7b, c). This precluded the resolution of pigment-activation events from background noise for estimating the thermal rate constant reliably.

As demonstrated in Chapter 2.5, single-photon response amplitude can reach ~3 pA in *Gcaps*$^{-/-}$ mouse rods. In fact, we have previously succeeded in counting thermal-activation events and measuring the thermal rate constant of the human red cone pigment by transgenically expressing it in *Gcaps*$^{-/-}$ mice[30]. This strategy, however, could not be

identically replicated on the green cone pigment because the very similar λ_{max}'s of the green cone pigment and the endogenous mouse rhodopsin would prevent accurate determination of the transgenic expression levels from spectral shifts. Rhodopsin is structurally required for rods to develop outer segments[68], so we avoided resorting to the rhodopsin-knockout background for removing the contribution from endogenous rhodopsin. At this point, we recognized the value of the $Rho^{REY/REY}$ mutant: it would silence downstream signaling from rhodopsin while maintaining structural support.

Thus far, we have generated 14 transgenic human green-cone pigment ($hOpn1mw^{+}$) mouse lines. Expressions of the green-cone pigment were too low to be reliably confirmed by immunohistochemistry or Western blotting. Instead, we screened for transgenic expression by breeding all the lines (except for the 3 lines that experienced germ-line-transmission problem) into the $Rho^{REY/REY};Gcaps^{-/-}$ background. The expression levels of the green-cone pigment were calculated as follows (see also Ref. 3). Rods were challenged with ~100 trials of light flashes at an intensity (i) that would elicit only tiny responses from the mutant rhodopsin, but large (~3 pA), quantized responses from the green-cone pigment (Fig. 2-8a). The number of these large responses was counted and the overall probability of success (p_s) was computed. This probability is related to the effective collecting area (A_e) by:

$$p_s = 1 - e^{-A_e i} \qquad \text{(Eqn. 3)}$$

The effective collecting area is defined by the diameter (d) and length (l) of the ROS, the quantum efficiency of rhodopsin ($Q_{isom} = 0.67$), the correction factor for light polarization (0.5 if unpolarized) as well as the axial pigment density (ρ) in question by the equation:

$$A_e = 2.303 \frac{\pi d^2 l}{4} Q_{isom} f \rho \qquad \text{(Eqn. 4)}$$

Only four transgenic lines gave detectable expression of green-cone pigment; the expression level varied hugely from animals to animals of the same line, and even from cell to cell of the same retina. Based on the expression levels and the molecular thermal rate constant of 2.6×10^{-8} sec^{-1} predicted for the human green-cone pigment from its λ_{max} at the beginning of this section, we plotted in Fig. 2-8b the half-time of a spontaneous green-cone-pigment-activation event in different recorded transgenic rods. In 3 of the 4 lines, the expression levels of the green-cone pigment in most cells were so low that it would take on average at least an hour to see a spontaneous event in a recorded cell. Obtaining a reliable measure of the thermal rate constant from these lines would be experimentally difficult. Therefore, we are currently focusing on line Wz11 only. Measurements are still pending.

2.10 Thermal-noise measurements on E122Q-rhodopsin and D190N-rhodopsin

Based on work discussed in Chapter 2.8, we speculated that the less-restricted chromophore-binding pocket of cone pigments may contribute to their higher thermal rate constants compared to those of rhodopsins having the same λ_{max}'s (Fig. 2-6). We explored this idea here by examining two knock-in mouse lines that carried different amino-acid substitutions around the chromophore-binding pocket of rhodopsin.

Residue E122 of rhodopsin situates close to the β-ionone ring of the chromophore[69]. Rhodopsin with a glutamate-to-glutamine mutation (glutamine being the equivalent residue in cone pigments) at this residue shows a number of cone-pigment

properties in terms of its photoactivation kinetics, for example, a faster decay of meta-II and meta-III (see Fig. 2-5 for descriptions about the photointermediate states)[70,71]. However, the Schiff-base linkage of E122Q-rhodopsin to the chromophore is resistant to hydroxylamine[46,72], indicative of a restricted chromophore-binding pocket similar to WT rhodopsin. We are interested to see if E122Q-rhodopsin behaves like rod or cone pigments with respect to thermal activation. We obtained the knock-in $Rho^{E122Q/E122Q}$ mouse line[71] from Dr. Yoshinori Shichida and bred it with $Gcaps^{-/-}$ mice. We confirmed that the mutant rods showed a ~20% reduction in the single-photon-response amplitude[71], but this did not pose any major problem for noise recordings under the $Gcaps^{-/-}$ background. Dark recordings from $Rho^{E122Q/E122Q};Gcaps^{-/-}$ rods (n = 18) gave a thermal rate constant of 3.60×10^{-11} sec^{-1} at 37.5°C by event-counting (Fig. 2-9a), close to the 3.40×10^{-11} sec^{-1} predicted from our theory (see Chapter 2.8) by assuming λ_{max} = 480 nm (Ref. [71]), $\alpha = 1$, $m = 45$ and $A = 7.19 \times 10^{-6}$ sec^{-1} as for rod pigments. In collaboration with Dr. Carter Cornwall, we also found that E122Q-rhodopsin showed minimal exchange of its 11-cis-retinal with exogenous chromophore in the dark, but readily took up the exogenous chromophore after bleaching (n = 5), as reflected by a spectral shift in microspectphotometric measurements (Fig. 2-9b). Such a behavior was reminiscent of that of WT rhodopsin but contrary to that of cone pigments, verifying that E122Q-rhodopsin has a restricted chromophore-binding pocket.

Residue D190 of rhodopsin forms part of a highly-conserved salt bridge at the end of a twisted β-hairpin that lies beside the chromophore[73]. Mutation of this residue to asparagine, tyrosine or glycine leads to autosomal-dominant retinitis pigmentosa in human[74–76]. Spectroscopic measurements showed that D190N mutant rhodopsin has an at

least 10-fold higher thermal decay rate in darkness[77,78]. Nevertheless, it is uncertain whether the higher thermal decay rate would translate to a higher thermal activation rate *in vivo*, and if so, whether this contributes to the pathophysiology associated with the mutation. Although the λ_{max} of D190N-rhodopsin stays normal[77,78], it is possible that the disruption of the salt bridge relieves some structural constraints at the chromophore-binding pocket, permitting more frequent thermal pigment activation. Because $Rho^{D190N/D190N};Gcaps^{-/-}$ rods and $Rho^{D190N/-};Gcaps^{-/-}$ rods degenerated at early age, we have not been able to record from rods expressing only the D190N-rhodopsin. Instead, we measured from the more slowly-degenerating $Rho^{D190N/+};Gcaps^{-/-}$ rods (n = 16), which still maintained roughly half the length of the ROS at postnatal day 18 (i.e., P18). By event-counting, the thermal rate constant of D190N-rhodopsin was estimated to be 2.25×10^{-10} sec^{-1} at 37.5°C after being corrected for the smaller dimensions of the mutant rods (Fig. 2-10a). This measured value was about 1.5-fold of the value (1.52×10^{-10} sec^{-1}) predicted from our theory (see Chapter 2.8) by assuming λ_{max} = 500 nm (Ref. 77,78), α = 1, m = 45 and $A = 7.19 \times 10^{-6}$ sec^{-1} as for rod pigments. Superficially, the discrepancy probably only reflected a margin of error in the measured rate of thermal events and the results would argue for D190N-rhodopsin having a similar thermal-activation rate as WT rhodopsin. Consistently, D190N-rhodopsin has been shown to be resistant to hydroxylamine[77], suggesting a restricted chromophore-binding pocket as in WT rhodopsin. To ascertain the above conclusion, we are currently repeating the noise measurements on $Rho^{D190N/REY};Gcaps^{-/-}$ rods, in which D190N-rhodopsin is the only rhodopsin species with normal signaling capability. Separately, in collaboration with Dr. Stephen Tsang's laboratory, we have also found that photoreceptor degeneration in

Rho$^{D190N/D190N}$ mice persisted even in transducin-knockout background (Fig. 2-10b), thus making increased spontaneous pigment activity an unlikely cause of cell degeneration.

In sum, our results on E122Q- and D190N-rhodopsins currently still support a relationship between a pigment's thermal rate constant and the openness of its chromophore-binding pocket. The true test will come from noise measurements on a rhodopsin mutant with an open binding pocket or a cone pigment mutant with its binding pocket engineered to be more restricted.

2.11 Figures

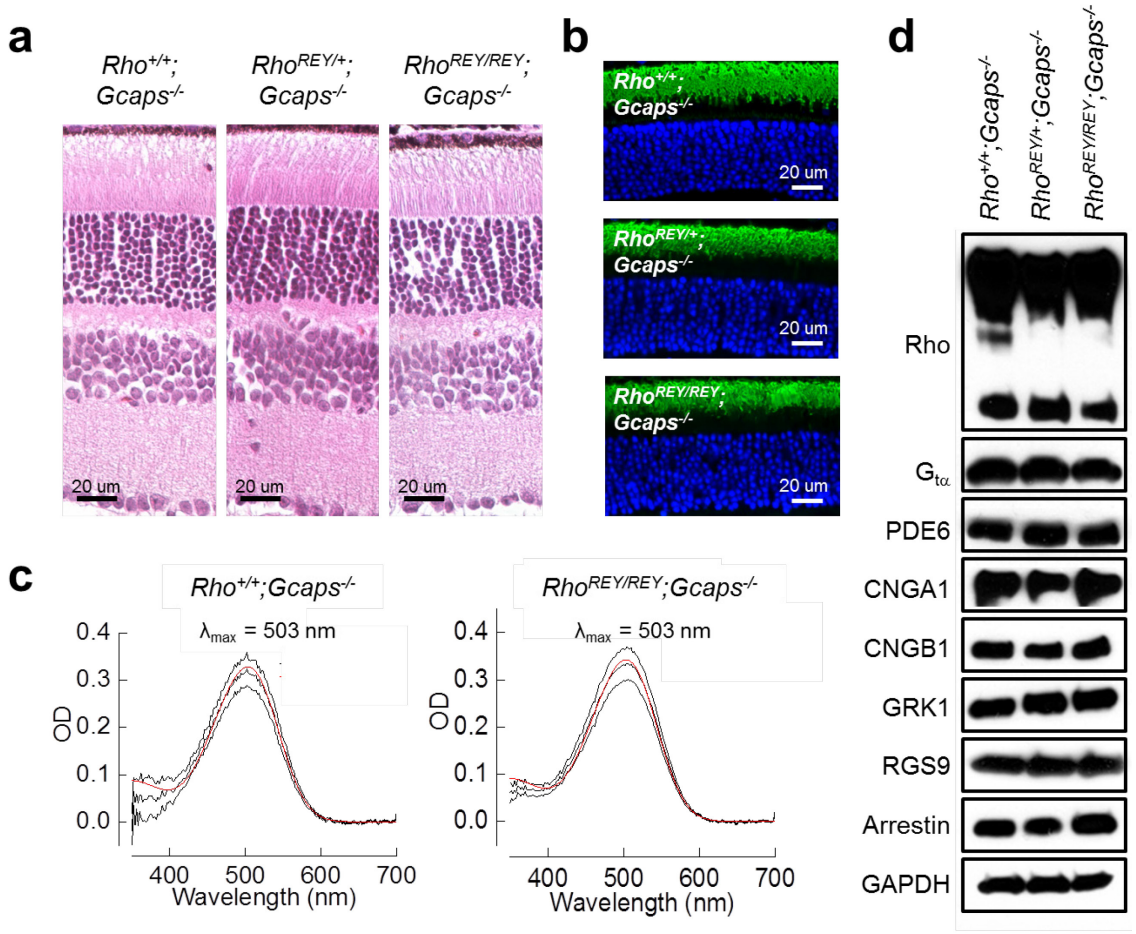
a
Rho+/+; Gcaps-/-
RhoREY/+; Gcaps-/-
RhoREY/REY; Gcaps-/-
20 um
b
Rho+/+; Gcaps-/-
RhoREY/+; Gcaps-/-
RhoREY/REY; Gcaps-/-
20 um
c
Rho+/+;Gcaps-/-
λmax = 503 nm
RhoREY/REY;Gcaps-/-
λmax = 503 nm
OD
0.4
0.3
0.2
0.1
0.0
400 500 600 700
Wavelength (nm)
d
Rho+/+;Gcaps-/-
RhoREY/+;Gcaps-/-
RhoREY/REY;Gcaps-/-
Rho
Gtα
PDE6
CNGA1
CNGB1
GRK1
RGS9
Arrestin
GAPDH

Fig. 2-1 Characterization of *Rho$^{REY/REY}$;Gcaps$^{-/-}$* retinas. a, Paraffin sections of 2-month-old *Rho$^{+/+}$;Gcaps$^{-/-}$* (left), *Rho$^{REY/+}$;Gcaps$^{-/-}$* (middle) and *Rho$^{REY/REY}$;Gcaps$^{-/-}$* (right) retinas stained by haematoxylin and eosin. **b,** Paraffin sections of 2-month-old *Rho$^{+/+}$;Gcaps$^{-/-}$* (top), *Rho$^{REY/+}$;Gcaps$^{-/-}$* (middle) and *Rho$^{REY/REY}$;Gcaps$^{-/-}$* (bottom) retinas immunostained for rhodopsin. DAPI marks the outer nuclear layer. **c,** Absorption spectra of *Rho$^{+/+}$;Gcaps$^{-/-}$* (left) and *Rho$^{REY/REY}$;Gcaps$^{-/-}$* (right) rods measured by microspectrophotometry (See Methods). Noisy traces are average ± SEM. Fits with the spectral template for A_1-pigments (red curves) yield λ_{max} = 503 nm for both genotypes. The peak optical densities for *Rho$^{+/+}$;Gcaps$^{-/-}$* and *Rho$^{REY/REY}$;Gcaps$^{-/-}$* rods are 0.342 and 0.328, respectively. n = 8 for both genotypes. **d,** Western blots showing the expression of various phototransduction components in extracts of *Rho$^{+/+}$;Gcaps$^{-/-}$* (left), *Rho$^{REY/+}$;Gcaps$^{-/-}$* (middle) and *Rho$^{REY/REY}$;Gcaps$^{-/-}$* (right) retinas. Rho: rhodopsin; $G_{t\alpha}$: α subunit of transducin; PDE6: phosphodiesterase isoform 6; CNGA1: A1 subunit of the cyclic nucleotide-gated (CNG) channel; CNGB1: B1 subunit of the CNG channel; GRK1: G protein receptor kinase isoform 1; RGS9: regulator of G protein signaling isoform 9; GAPDH: glyceraldehyde 3-phosphate dehydrogenase (as loading control).

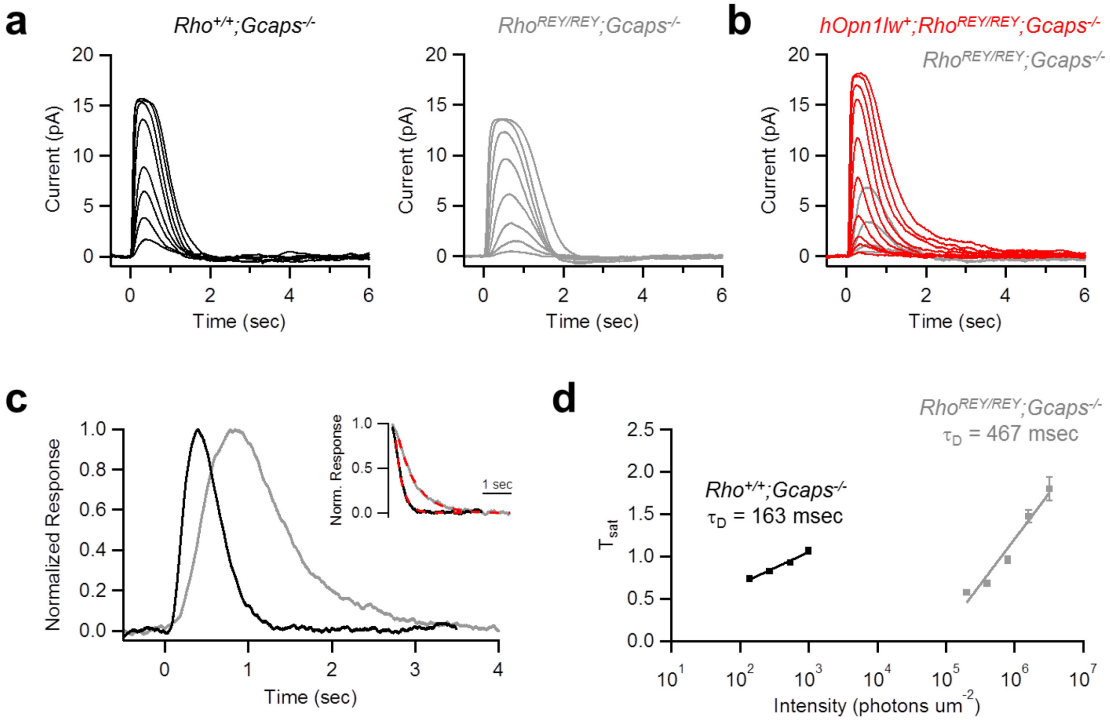
a
Rho+/+;Gcaps-/-
RhoREY/REY;Gcaps-/-
b
hOpn1lw+;RhoREY/REY;Gcaps-/-
RhoREY/REY;Gcaps-/-
Current (pA)
Time (sec)
c
Normalized Response
Norm. Response
1 sec
Time (sec)
d
RhoREY/REY;Gcaps-/-
τD = 467 msec
Rho+/+;Gcaps-/-
τD = 163 msec
Tsat
Intensity (photons um-2)

Fig. 2-2 Kinetics of photoresponses of *Rho$^{REY/REY}$;Gcaps$^{-/-}$* rods. a, Responses of a *Rho$^{+/+}$;Gcaps$^{-/-}$* (left) rod and a *Rho$^{REY/REY}$;Gcaps$^{-/-}$* (right) rod to 10-msec of light flashes of various intensities. Monochromatic 500-nm light was used for the *Rho$^{+/+}$;Gcaps$^{-/-}$* rod whereas white light was used for the *Rho$^{REY/REY}$;Gcaps$^{-/-}$* rod due to its very much reduced sensitivity. Average responses, flashes delivered at time zero. **b,** Responses of a *hOpn1lw^{+};Rho$^{REY/REY}$;Gcaps$^{-/-}$* (red) rod and a *Rho$^{REY/REY}$;Gcaps$^{-/-}$* (gray) rod to 560-nm light flashes of the same set of intensities. Note the smaller and slower responses of the *Rho$^{REY/REY}$;Gcaps$^{-/-}$* rod. Average responses, 30-msec flashes at time zero. **c,** Dim-flash responses a *Rho$^{+/+}$;Gcaps$^{-/-}$* (black) rod and a *Rho$^{REY/REY}$;Gcaps$^{-/-}$* (gray) rod normalized to the same peak amplitude for comparing their kinetics. Average responses, flashes at time zero, 500-nm light for *Rho$^{+/+}$;Gcaps$^{-/-}$* rod and white light for *Rho$^{REY/REY}$;Gcaps$^{-/-}$* rod. Inset shows the same responses aligned in time by their transient peaks. Red dashed curves are single-exponential fits for estimating the time constants of response recovery (τ_{rec}). **d,** Pepperberg analysis (see Methods) of saturated responses of *Rho$^{+/+}$;Gcaps$^{-/-}$* (black) rods and *Rho$^{REY/REY}$;Gcaps$^{-/-}$* (gray) rods. The time (T_{sat}) that the responses remained in saturation (90% of peak responses) is plotted against the intensity of the light stimuli. The slopes give dominant time constants (τ_D) of 163 msec for *Rho$^{+/+}$;Gcaps$^{-/-}$* rods and 467 msec for *Rho$^{REY/REY}$;Gcaps$^{-/-}$* rods. Data points are average ± SEM. *Rho$^{+/+}$;Gcaps$^{-/-}$*: n = 8 cells; *Rho$^{REY/REY}$;Gcaps$^{-/-}$*: n = 18 cells.

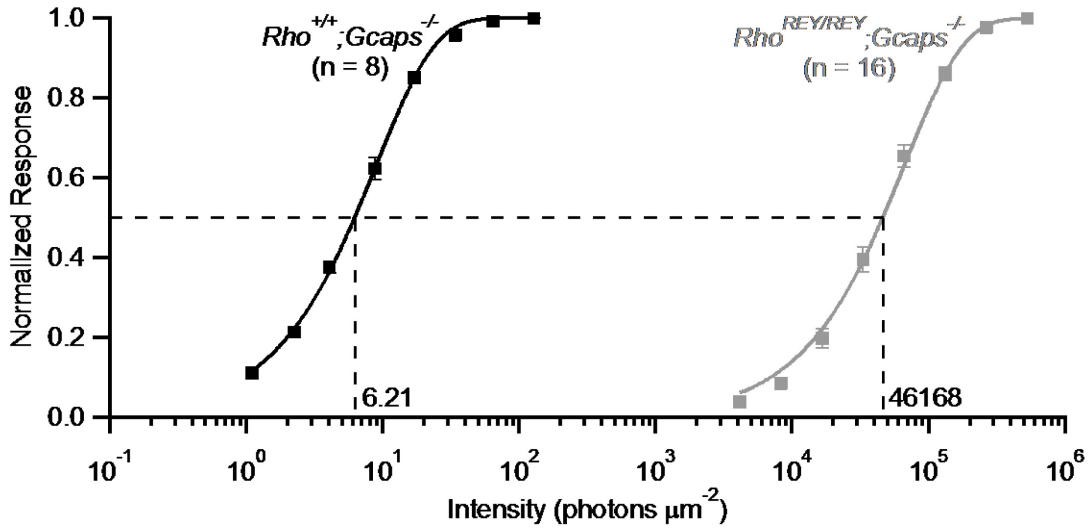

Fig. 2-3 Intensity-response relation of *Rho$^{REY/REY}$;Gcaps$^{-/-}$* rods. *Rho$^{+/+}$;Gcaps$^{-/-}$* (black) rods were stimulated with 500-nm light flashes. *Rho$^{REY/REY}$;Gcaps$^{-/-}$* (gray) rods were stimulated with white light, with intensities converted to 500-nm equivalents (see Methods) for comparisons. Response amplitudes were measured at the transient peak and normalized by the saturated responses. Fits are with a saturating-exponential function (see Methods). The half-saturating flash intensities (σ) are 6.21 and 46,168 photons μm^{-2} for *Rho$^{+/+}$;Gcaps$^{-/-}$* and *Rho$^{REY/REY}$;Gcaps$^{-/-}$*rods, respectively. Data points are average ± SEM. *Rho$^{+/+}$;Gcaps$^{-/-}$*: n = 8 cells; *Rho$^{REY/REY}$;Gcaps$^{-/-}$*: n = 16 cells.

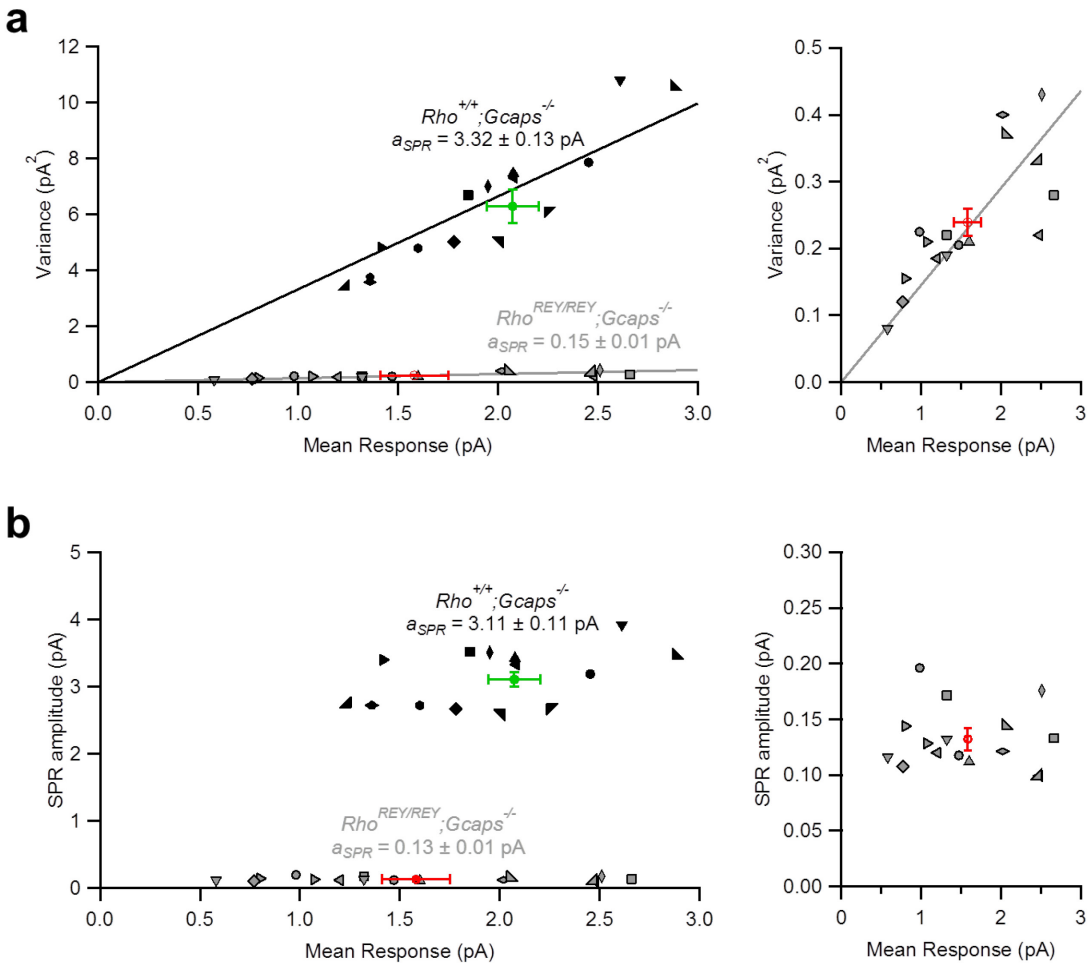
a
Variance (pA²)
Mean Response (pA)
Rho+/+;Gcaps-/-
aSPR = 3.32 ± 0.13 pA
RhoREY/REY;Gcaps-/-
aSPR = 0.15 ± 0.01 pA
b
SPR amplitude (pA)
Mean Response (pA)
Rho+/+;Gcaps-/-
aSPR = 3.11 ± 0.11 pA
RhoREY/REY;Gcaps-/-
aSPR = 0.13 ± 0.01 pA

Fig. 2-4 Single-photon-response amplitudes of *Rho*$^{REY/REY}$;*Gcaps*$^{-/-}$ rods. a, (Left) Plot of the ensemble variance against mean of dim-flash responses of *Rho*$^{+/+}$;*Gcaps*$^{-/-}$ (black) rods and *Rho*$^{REY/REY}$;*Gcaps*$^{-/-}$ (gray) rods. Each symbol represents a cell; cells tested at two light intensities are marked by the same symbol. Green and red points are average ± SEM for *Rho*$^{+/+}$;*Gcaps*$^{-/-}$ and *Rho*$^{REY/REY}$;*Gcaps*$^{-/-}$ rods, respectively. Single-photon-response amplitudes (a_{SPR}) are given by the slopes (variance/mean) of the linear fits (constrained to pass through origin) to the data points. (Right) an enlarged view of the plot on left with only the data points for *Rho*$^{REY/REY}$;*Gcaps*$^{-/-}$ rods. **b,** (Left) Plot of the single-photon-response amplitude of *Rho*$^{+/+}$;*Gcaps*$^{-/-}$ (black) rods and *Rho*$^{REY/REY}$;*Gcaps*$^{-/-}$ (gray) rods estimated by fitting the initial rising phase of the ensemble variance of dim-flash responses with a scaled square of the mean response (see Methods). Each symbol represents a cell; cells tested at two light intensities are marked by the same symbol. Green and red points are average ± SEM for *Rho*$^{+/+}$;*Gcaps*$^{-/-}$ and *Rho*$^{REY/REY}$;*Gcaps*$^{-/-}$ rods, respectively. (Right) an enlarged view of the plot on left with only the data points for *Rho*$^{REY/REY}$;*Gcaps*$^{-/-}$ rods. *Rho*$^{+/+}$;*Gcaps*$^{-/-}$: n = 15 cells; *Rho*$^{REY/REY}$;*Gcaps*$^{-/-}$: n = 11 cells.

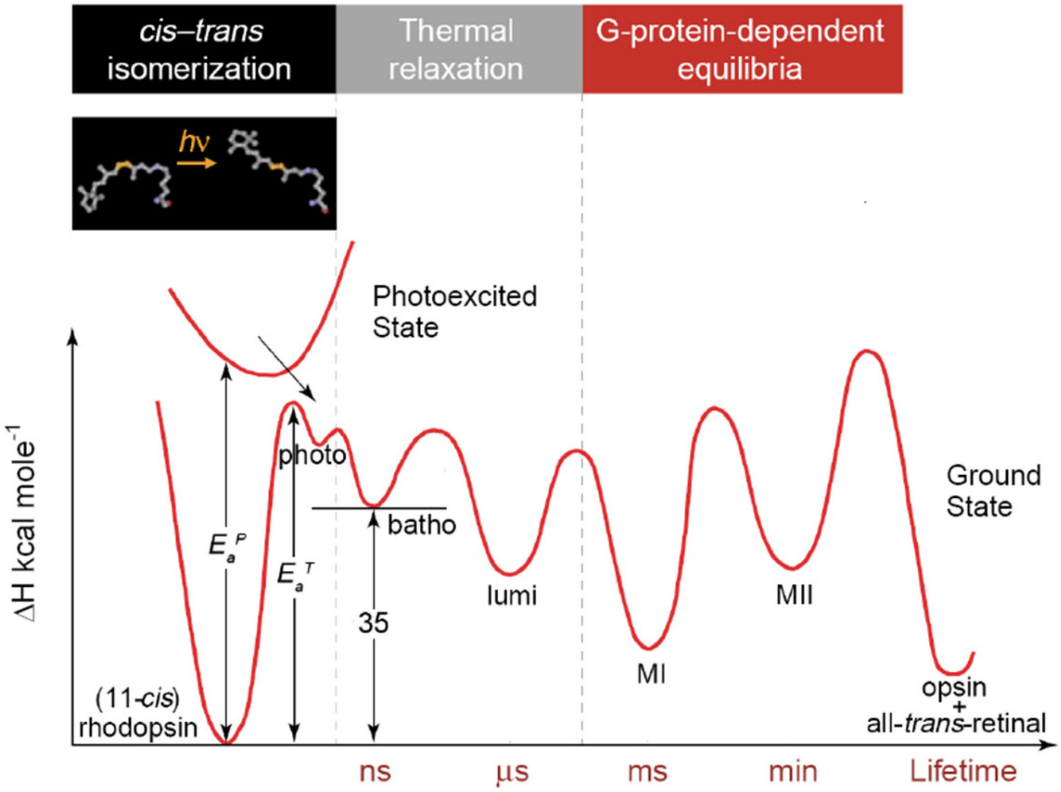
cis–trans isomerization
Thermal relaxation
G-protein-dependent equilibria
hν
Photoexcited State
photo
batho
lumi
MI
MII
Ground State
opsin + all-trans-retinal
(11-cis) rhodopsin
35
ΔH kcal mole-1
ns
µs
ms
min
Lifetime

Fig. 2-5 Schematic energy diagram for activation of rhodopsin. Ordinate gives the energy of the different states of rhodopsin as photoisomerization progresses with time (abscissa). Absorption of a photon provides energy (that acts alone or in combination with rhodopsin's internal thermal energy) for promoting the transition of dark (11-cis) rhodopsin to the photoexcited state. The energy difference between the lowest photoexcited state and the dark state is denoted the minimum photoactivation energy (E_a^P). Photoexcited rhodopsin relaxes rapidly back to the ground state, and in so doing, overcomes the ground-state isomerization energy barrier (E_a^T) with a quantum efficiency of 0.67. It then thermally decays through various photointermediate states, including the Meta-II (MII) state responsible for activating transducin and thereby triggering phototransduction. Finally, MII decays either directly or through the Meta-III state (not shown) into free opsin and all-trans-retinal. Bathorhodopsin, an early photoproduct of rhodopsin, stores up to 35 kcal mol^{-1} of the absorbed photon energy (Ref. 49). Figure from Luo *et al*.[47]. Reprinted with permission from AAAS.

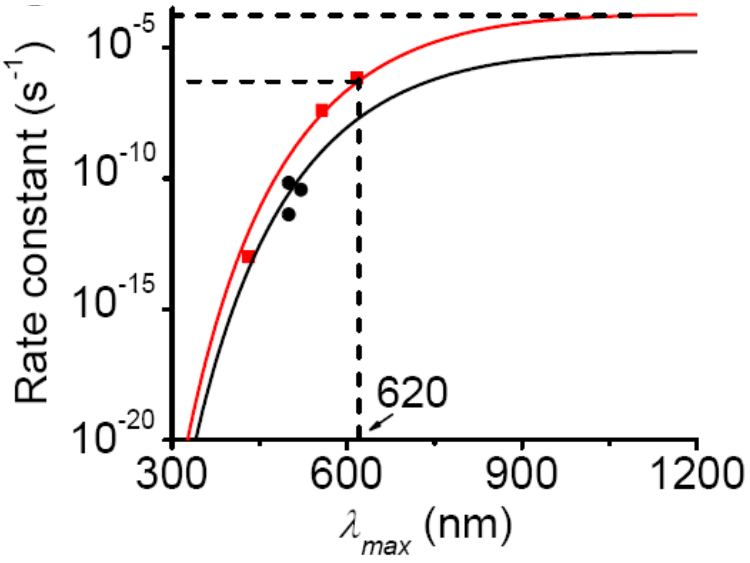

Fig. 2-6 Noise predictions for various rod and cone pigments. Plot of thermal-noise rate constants (measured by direct event-counting) of various rod (black circles) and cone (red squares) pigments at 23°C against pigments' peak-absorption wavelength (λ_{max}). Black and red curves are $A \times f_{\geq E_a^T}$, with A = 7.19 × 10^{-6} sec^{-1} for rhodopsin and 1.88 × 10^{-4} sec^{-1} for cone pigments as well as $\alpha = 1$ and $m = 45$ in the calculations of $f_{\geq E_a^T}$ (see Chapter 2.8). Figure from Luo *et al.*[47]. Reprinted with permission from AAAS.

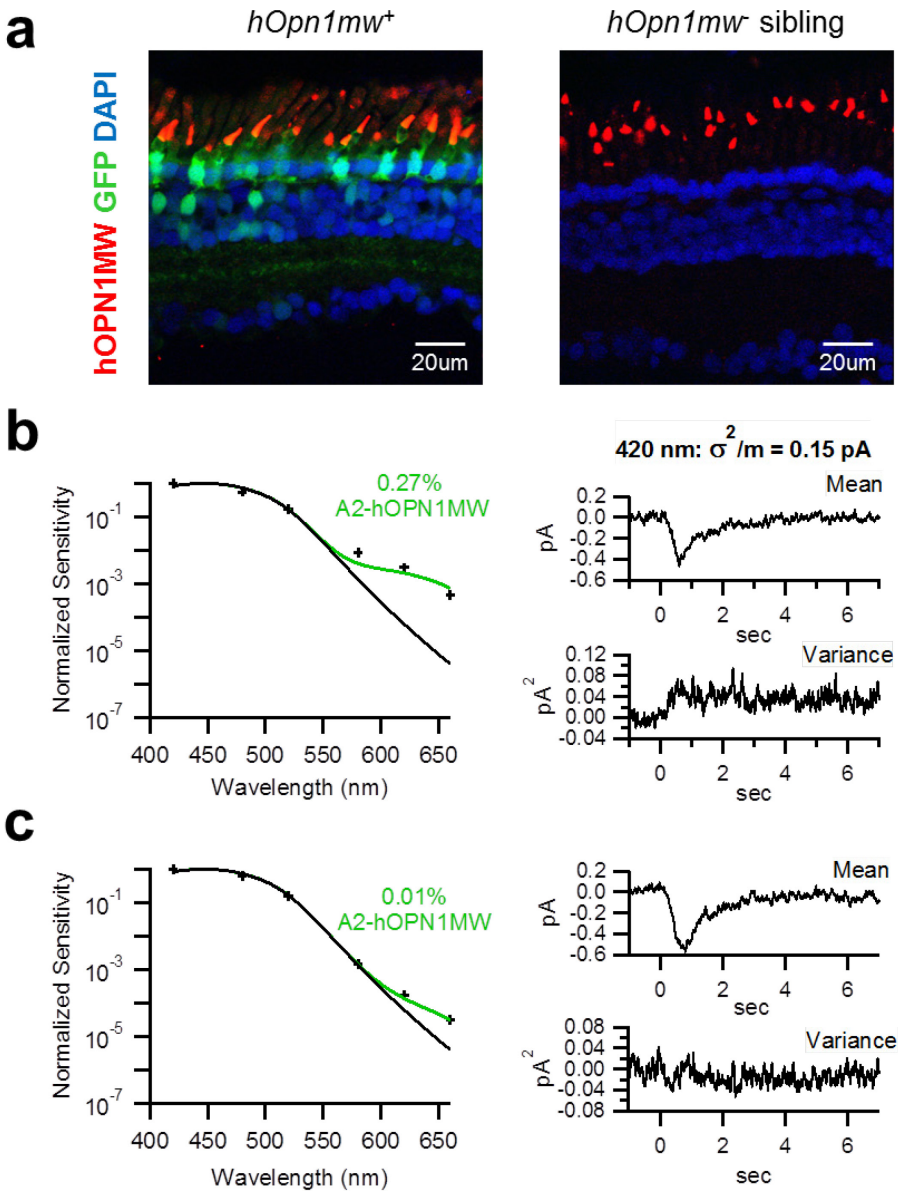
a
hOpn1mw+
hOpn1mw- sibling
hOPN1MW GFP DAPI
20um
20um
b
420 nm: σ2/m = 0.15 pA
0.27%
A2-hOPN1MW
Normalized Sensitivity
Wavelength (nm)
Mean
Variance
pA
pA2
sec
c
0.01%
A2-hOPN1MW
Normalized Sensitivity
Wavelength (nm)
Mean
Variance
pA
pA2
sec

Fig. 2-7 Characterization of transgenic *Xenopus* rods expressing the human green-cone pigment (hOpn1mw). a, Retinal cryosections of a *hOpn1mw*$^{+}$ *Xenopus* and its *hOpn1mw*$^{-}$ sibling immunostained for the human green-cone pigment (red). The antibody labels native red cones in both *hOpn1mw*$^{+}$ and *hOpn1mw*$^{-}$ retinas. Dim immunosignal can also be recognized in the rods of the *hOpn1mw*$^{+}$ retina. GFP was co-introduced as a transgene for identifying transgenic animals. Cellular layers are marked by DAPI. **b,** (Left) Action spectrum of a *hOpn1mw*$^{+}$green rod (data points). Black curve is the absorption template of endogenous A_2-rhodopsin. The percentage expression level is calculated by fitting the data points (green curve) with a linear combination of the black curve and the absorption template of A_2-human green-cone pigment. (Right) Ensemble mean and variance of dim-flash responses of the same cell. The single-photon-response amplitude is 0.15 pA for this cell. **c,** Same as in **b** but with a different *hOpn1mw*$^{+}$green rod. Single-photon-response amplitude is too small to be estimated.

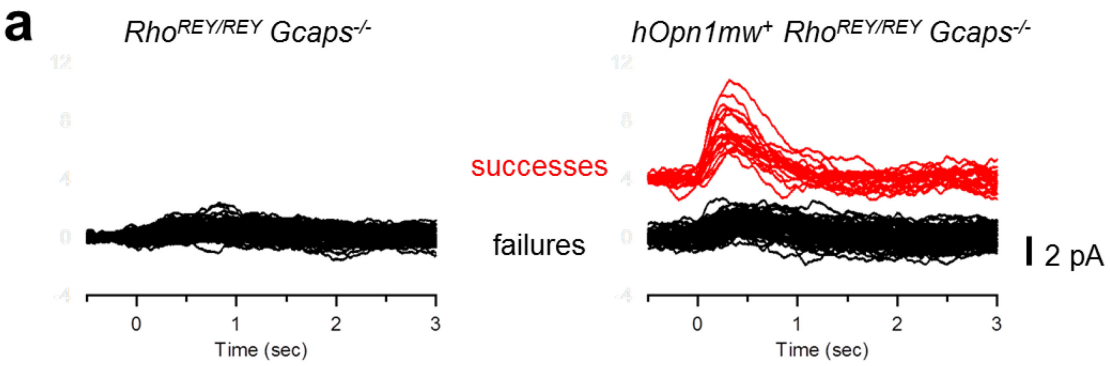

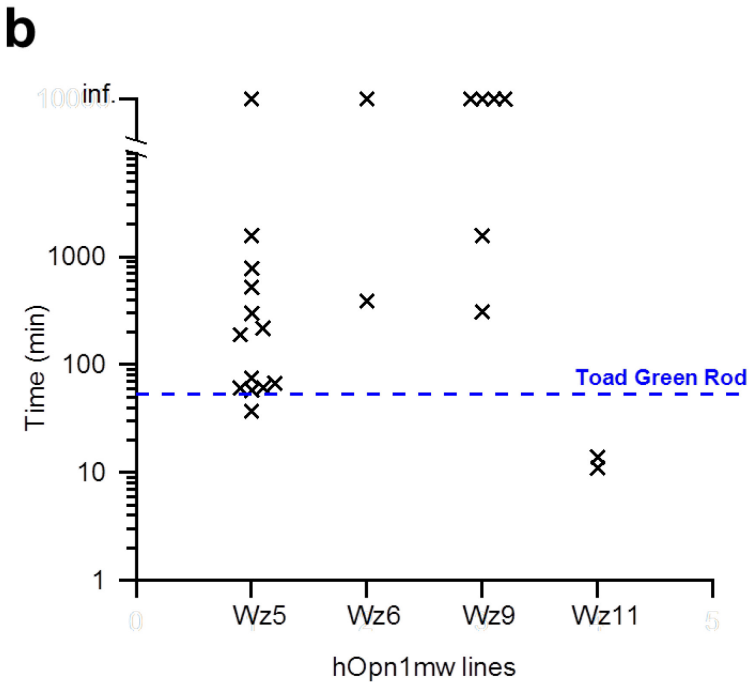

hOpn1mw lines	% expression
Wz1	Undetectable
Wz2	Very infrequent germ-line transmission
Wz3	Undetectable
Wz4	Undetectable
Wz5	Undetectable to 0.0273%
Wz6	Undetectable to 0.0026%
Wz7	Very infrequent germ-line transmission
Wz8	Undetectable
Wz9	Undetectable to 0.0032%
Wz10	Undetectable
Wz11	0.0696% to 0.0934%
Wz12	Undetectable
Wz13	Very infrequent germ-line transmission
Wz14	Undetectable

Fig. 2-8 Characterization of transgenic mouse rods expressing the human green-cone pigment (hOpn1mw). a, Responses of a $Rho^{REY/REY};Gcaps^{-/-}$ (left) rod and a $hOpn1mw^{+};Rho^{REY/REY};Gcaps^{-/-}$ (right) rod to dim 530-nm flashes of the same intensity. A response is defined as a success (red traces) or a failure (black traces) by the presence or absence of an obvious current response of ~3 pA. **b,** (Right), Table showing the percentage expression levels of the transgenic human green-cone pigment in different $hOpn1mw^{+};Rho^{REY/REY};Gcaps^{-/-}$ (Wz1 to Wz14) lines (see Chapter 2.9 and Methods for derivations). (Left) Predicted half-time for detecting a spontaneous pigment-activation event in four transgenic mouse lines. Predictions are based on the percentage expression levels and $f_{\geq E_a^T}$ calculations (see Methods). Each symbol represents a cell.

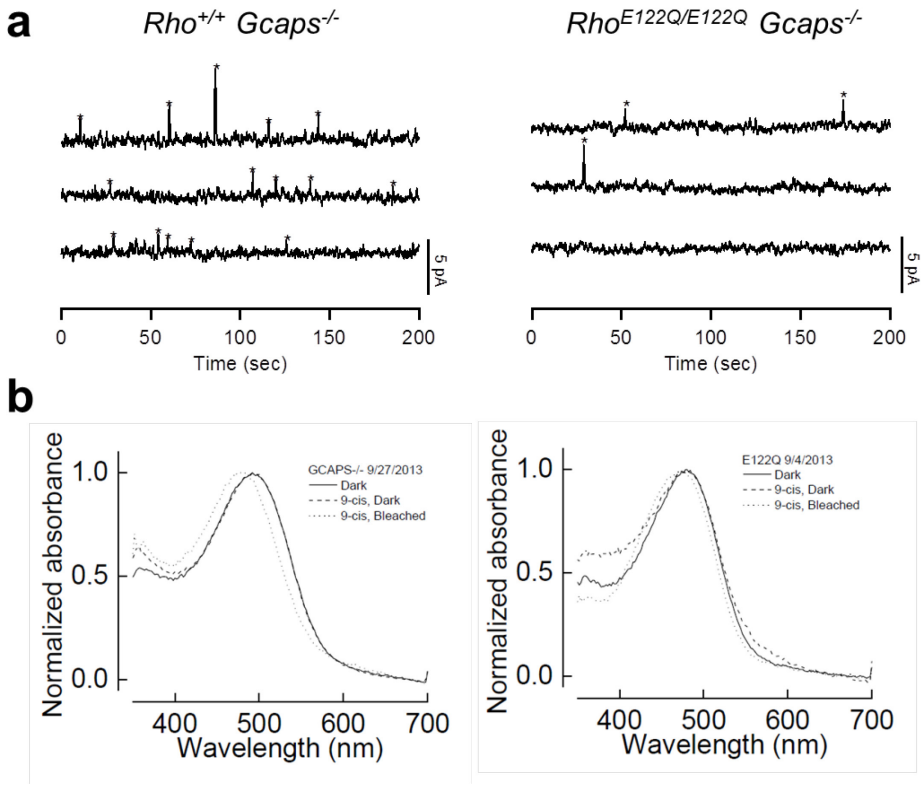

Fig. 2-9 Thermal-noise measurements and chromophore-exchange experiments on *Rho$^{E122Q/E122Q}$;Gcaps$^{-/-}$* rods. a, Samples of 10-min continuous dark-recording from a *Rho$^{+/+}$;Gcaps$^{-/-}$* (left) rod and a *Rho$^{E122Q/E122Q}$;Gcaps$^{-/-}$* (right) rod. Signals were low-pass filtered at 3 Hz for lower baseline noise. **b,** Examples of absorption spectra from a *Rho$^{+/+}$;Gcaps$^{-/-}$* (left) rod and a *Rho$^{E122Q/E122Q}$;Gcaps$^{-/-}$* (right) rod measured by microspectrophotometry in the absence (solid trace) or presence (dashed trace) of exogenous 9-cis-retinal in the dark or after 99% bleaching with light and subsequent regeneration with 9-cis-retinal (dotted trace). For both genotypes, incubation with exogenous chromophore produced a spectral shift only after bleaching, but not in the dark. Data by Rikard Frederiksen of Dr. Carter Cornwall's laboratory.

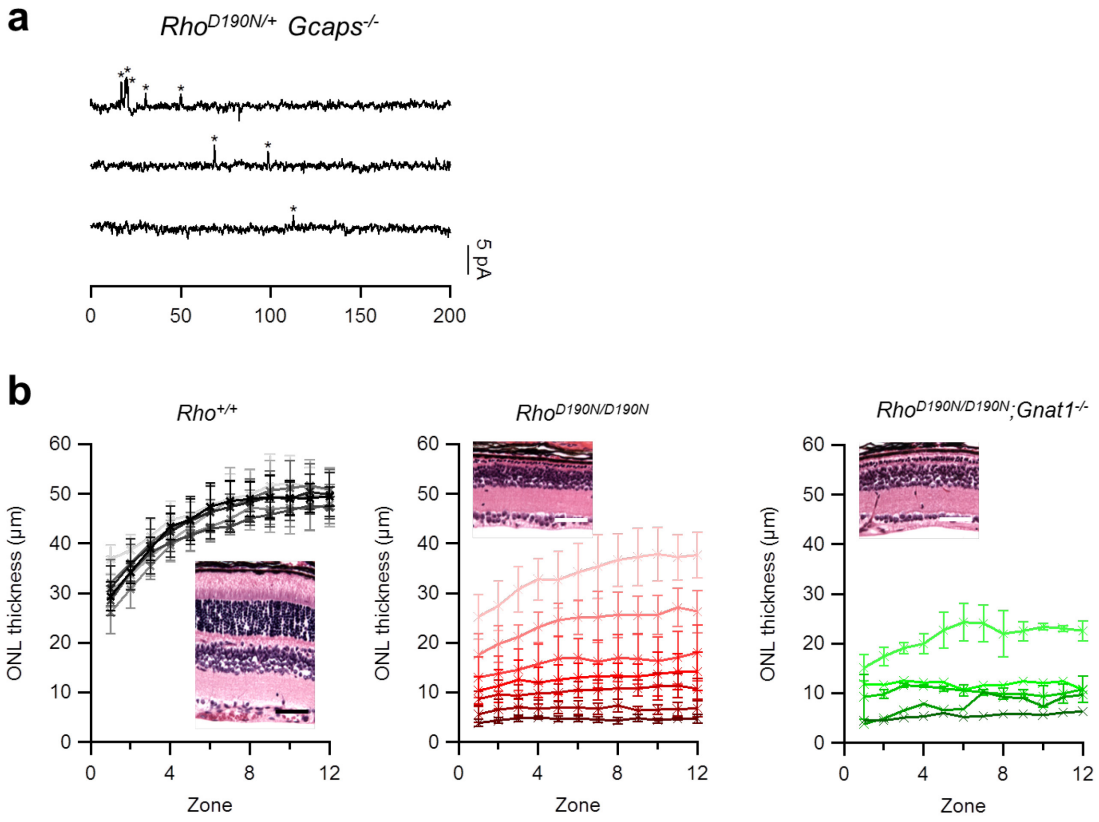

Fig. 2-10 Thermal-noise measurements and chromophore-exchange experiments on *Rho*$^{D190N/+}$;*Gcaps*$^{-/-}$ rods. a, Samples of 10-min continuous dark-recording from a *Rho*$^{D190N/+}$;*Gcaps*$^{-/-}$ rod at P18. Signals were low-pass filtered at 3 Hz for lower baseline noise. **b,** Thickness of the outer nuclear layer (ONL) in *Rho*$^{+/+}$ (left), *Rho*$^{D190N/D190N}$ (middle) and *Rho*$^{D190N/D190N}$;*Gnat1*$^{-/-}$ (right) retinas measured at various locations (zone 1 to zone 12) away from the optic disk (see Methods). Darker colors correspond to older age. *Rho*$^{+/+}$: n = 6 (P12), 5 (P14), 5 (P16), 5 (P18), 5 (P21), 8 (P24), 5 (P30); *Rho*$^{D190N/D190N}$: n = 5 (P12), 6 (P14), 5 (P16), 5 (P18), 4 (P21), 6 (P24), 6 (P30); *Rho*$^{D190N/D190N}$;*Gnat1*$^{-/-}$: n = 2 (P16), 1 (P18), 2 (P21), 1 (P24), 3 (P30).

2.12 References

1. Hecht, S., Shlaer, S. & Pirenne, M. H. Energy, quanta and vision. *J. Gen. Physiol.* **25,** 819–840 (1942).

2. Yau, K.-W., Lamb, T. D. & Baylor, D. A. Light-induced fluctuations in membrane current of single toad rod outer segments. *Nature* **269,** 78–80 (1977).

3. Baylor, D. A., Lamb, T. D. & Yau, K.-W. Responses of retinal rods to single photons. *J. Physiol.* **288,** 613–634 (1979).

4. Pugh, E. N. & Lamb, T. D. Amplification and kinetics of the activation steps in phototransduction. *Biochim. Biophys. Acta* **1141,** 111–149 (1993).

5. Arshavsky, V. Y., Lamb, T. D. & Pugh, E. N. G proteins and phototransduction. *Annu. Rev. Physiol.* **64,** 153–187 (2002).

6. Arshavsky, V. Y. & Burns, M. E. Current understanding of signal amplification in phototransduction. *Cell. Logist.* **4,** e29390 (2014).

7. Baylor, D. A., Matthews, G. & Yau, K.-W. Two components of electrical dark noise in toad retinal rod outer segments. *J. Physiol.* **309,** 591–621 (1980).

8. Luo, D.-G., Xue, T. & Yau, K.-W. How vision begins: an odyssey. *Proc. Natl. Acad. Sci. U. S. A.* **105,** 9855–9862 (2008).

9. Leskov, I. B. *et al.* The gain of rod phototransduction: reconciliation of biochemical and electrophysiological measurements. *Neuron* **27,** 525–537 (2000).

10. Gray-Keller, M. P., Biernbaum, M. S. & Bownds, M. D. Transducin activation in electropermeabilized frog rod outer segments is highly amplified, and a portion equivalent to phosphodiesterase remains membrane-bound. *J. Biol. Chem.* **265,** 15323–32 (1990).

11. Uhl, R. & Ryba, N. J. Transducin activation and deactivation in rod systems of different structural integrity. Attempts at a focussed view through scattered light. *Biochim. Biophys. Acta* **1054,** 56–68 (1990).

12. Rieke, F. & Baylor, D. A. Origin of reproducibility in the responses of retinal rods to single photons. *Biophys. J.* **75,** 1836–57 (1998).

13. Krispel, C. M. *et al.* RGS Expression Rate-Limits Recovery of Rod Photoresponses. *Neuron* **51,** 409–416 (2006).

14. Chen, C.-K., Woodruff, M. L., Chen, F. S., Chen, D. & Fain, G. L. Background Light Produces a Recoverin-Dependent Modulation of Activated-Rhodopsin Lifetime in Mouse Rods. *J. Neurosci.* **30,** 1213–1220 (2010).

15. Doan, T., Azevedo, a. W., Hurley, J. B. & Rieke, F. Arrestin Competition Influences the Kinetics and Variability of the Single-Photon Responses of Mammalian Rod Photoreceptors. *J. Neurosci.* **29,** 11867–11879 (2009).

16. Gross, O. P. & Burns, M. E. Control of rhodopsin's active lifetime by arrestin-1 expression in mammalian rods. *J. Neurosci.* **30,** 3450–7 (2010).

17. Burns, M. E. & Pugh, E. N. RGS9 concentration matters in rod phototransduction. *Biophys. J.* **97,** 1538–47 (2009).

18. Gross, O. P., Pugh, E. N. & Burns, M. E. Calcium Feedback to cGMP Synthesis Strongly Attenuates Single-Photon Responses Driven by Long Rhodopsin Lifetimes. *Neuron* **76,** 370–382 (2012).

19. Hamer, R. D., Nicholas, S. C., Tranchina, D., Liebman, P. A. & Lamb, T. D. Multiple Steps of Phosphorylation of Activated Rhodopsin Can Account for the Reproducibility of Vertebrate Rod Single-photon Responses. *J. Gen. Physiol.* **122,** 419–444 (2003).

20. Kwok-Keung Fung, B. & Stryer, L. Photolyzed rhodopsin catalyzes the exchange of GTP for bound GDP in retinal rod outer segments. *Proc. Natl. Acad. Sci. U. S. A.* **77,** 2500–2504 (1980).

21. Liebman, P. A. & Pugh, E. N. Gain, speed and sensitivity of GTP binding vs PDE activation in visual excitation. *Vision Res.* **22,** 1475–80 (1982).

22. Robinson, P. R., Radeke, M. J., Cote, R. H. & Bownds, M. D. cGMP influences guanine nucleotide binding to frog photoreceptor G-protein. *J. Biol. Chem.* **261,** 313–318 (1986).

23. Vuong, T. M., Chabre, M. & Stryer, L. Millisecond activation of transducin in the cyclic nucleotide cascade of vision. *Nature* **311,** 659–661 (1984).

24. Wagner, R., Ryba, N. & Uhl, R. Sub-second turnover of transducin GTPase in bovine rod outer segments. A light scattering study. *FEBS Lett.* **234,** 44–48 (1988).

25. Pepperberg, D. R., Kahlert, M., Krause, A. & Hofmann, K. P. Photic modulation of a highly sensitive, near-infrared light-scattering signal recorded from intact retinal photoreceptors. *Proc. Natl. Acad. Sci. U. S. A.* **85,** 5531–5535 (1988).

26. Kahlert, M. & Hofmann, K. P. Reaction rate and collisional efficiency of the rhodopsin-transducin system in intact retinal rods. *Biophys. J.* **59,** 375–86 (1991).

27. Franke, R. R., König, B., Sakmar, T. P., Khorana, H. G. & Hofmann, K. P. Rhodopsin mutants that bind but fail to activate transducin. *Science* **250,** 123–125 (1990).

28. Mendez, A. *et al.* Role of guanylate cyclase-activating proteins (GCAPs) in setting the flash sensitivity of rod photoreceptors. *Proc. Natl. Acad. Sci. U. S. A.* **98,** 9948–53 (2001).

29. Pepperberg, D. R. *et al.* Light-dependent delay in the falling phase of the retinal rod photoresponse. *Vis. Neurosci.* **8,** 9–18 (1992).

30. Fu, Y., Kefalov, V., Luo, D.-G., Xue, T. & Yau, K.-W. Quantal noise from human red cone pigment. *Nat. Neurosci.* **11,** 565–571 (2008).

31. Gross, O. P., Pugh, E. N. & Burns, M. E. Spatiotemporal cGMP dynamics in living mouse rods. *Biophys. J.* **102,** 1775–1784 (2012).

32. Nymark, S., Frederiksen, R., Woodruff, M. L., Cornwall, M. C. & Fain, G. L. Bleaching of mouse rods: microspectrophotometry and suction-electrode recording. *J. Physiol.* **590,** 2353–2364 (2012).

33. Palczewski, K., Buczyłko, J., Kaplan, M. W., Polans, A. S. & Crabb, J. W. Mechanism of rhodopsin kinase activation. *J. Biol. Chem.* **266,** 12949–55 (1991).

34. Kang, Y. *et al.* Crystal structure of rhodopsin bound to arrestin by femtosecond X-ray laser. *Nature* **523,** 561–567 (2015).

35. Szczepek, M. *et al.* Crystal structure of a common GPCR-binding interface for G protein and arrestin. *Nat. Commun.* **5,** 4801 (2014).

36. Chen, C. K. *et al.* Abnormal photoresponses and light-induced apoptosis in rods lacking rhodopsin kinase. *Proc. Natl. Acad. Sci. U. S. A.* **96,** 3718–22 (1999).

37. Xu, J. *et al.* Prolonged photoresponses in transgenic mouse rods lacking arrestin. *Nature* **389,** 505–509 (1997).

38. Barlow, H. B. Retinal noise and absolute threshold. *J. Opt. Soc. Am.* **46,** 634–639 (1956).

39. Barlow, H. B. Purkinje shift and retinal noise. *Nature* **179,** 255–256 (1957).

40. Wald, G. Human Vision and the Spectrum. *Science* **101,** 653–658 (1945).

41. Dowling, J. E. The Site of Visual Adaptation. *Adv. Sci.* **155,** 273–279 (2009).

42. Firsov, M. L., Donner, K. & Govardovskii, V. I. pH and rate of 'dark' events in toad retinal rods: test of a hypothesis on the molecular origin of photoreceptor noise. *J. Physiol.* **539,** 837–846 (2002).

43. Kefalov, V., Fu, Y., Marsh-Armstrong, N. & Yau, K.-W. Role of visual pigment properties in rod and cone phototransduction. *Nature* **425,** 526–531 (2003).

44. Rieke, F. & Baylor, D. A. Origin and functional impact of dark noise in retinal cones. *Neuron* **26,** 181–186 (2000).

45. Ala-Laurila, P., Donner, K., Crouch, R. K. & Cornwall, M. C. Chromophore switch from 11-cis-dehydroretinal (A2) to 11-cis-retinal (A1) decreases dark noise in salamander red rods. *J. Physiol.* **585,** 57–74 (2007).

46. Sakurai, K. *et al.* Physiological properties of rod photoreceptor cells in green-sensitive cone pigment knock-in mice. *J. Gen. Physiol.* **130,** 21–40 (2007).

47. Luo, D.-G., Yue, W. W. S., Ala-Laurila, P. & Yau, K.-W. Activation of visual pigments by light and heat. *Science* **332,** 1307–1312 (2011).

48. Hubbard, R. The thermal stability of rhodopsin and opsin. *J. Gen. Physiol.* **42,** 259–280 (1958).

49. Cooper, A. Energy uptake in the first step of visual excitation. *Nature* **282,** 531–533 (1979).

50. Barlow, R. B., Birge, R. R., Kaplan, E. & Tallent, J. R. On the molecular origin of photoreceptor noise. *Nature* **366,** 64–66 (1993).

51. Birge, R. R. & Barlow, R. B. On the molecular origins of thermal noise in vertebrate and invertebrate photoreceptors. *Biophys. Chem.* **55,** 115–126 (1995).

52. Sampath, A. P. & Baylor, D. A. Molecular mechanism of spontaneous pigment activation in retinal cones. *Biophys. J.* **83,** 184–93 (2002).

53. Lórenz-Fonfría, V. A., Furutani, Y., Ota, T., Ido, K. & Kandori, H. Protein fluctuations as the possible origin of the thermal activation of rod photoreceptors in the dark. *J. Am. Chem. Soc.* **132,** 5693–5703 (2010).

54. Bókkon, I. & Vimal, R. L. P. Retinal phosphenes and discrete dark noises in rods: A new biophysical framework. *J. Photochem. Photobiol. B Biol.* **96,** 255–259 (2009).

55. Ala-Laurila, P., Donner, K. & Koskelainen, A. Thermal Activation and Photoactivation of Visual Pigments. *Biophys. J.* **86,** 3653–3662 (2004).

56. Hárosi, F. I. An analysis of two spectral properties of vertebrate visual pigments. *Vision Res.* **34,** 1359–1367 (1994).

57. Hinshelwood, C. N. *The kinetics of chemical change*. (The Clarendon Press, 1940).

58. St George, R. C. C. The interplay of light and heat in bleaching rhodopsin. *J. Gen. Physiol.* **35,** 495–517 (1952).

59. Matsumoto, H., Tokunaga, F. & Yoshizawa, T. Accessibility of the iodopsin

chromophore. *Biochim. Biophys. Acta* **404,** 300–8 (1975).

60. Kefalov, V. J. *et al.* Breaking the covalent bond - A pigment property that contributes to desensitization in cones. *Neuron* **46,** 879–890 (2005).

61. Schneeweis, D. M. & Schnapf, J. L. The photovoltage of macaque cone photoreceptors: adaptation, noise, and kinetics. *J. Neurosci.* **19,** 1203–1216 (1999).

62. Holcman, D. & Korenbrot, J. I. The limit of photoreceptor sensitivity: molecular mechanisms of dark noise in retinal cones. *J. Gen. Physiol.* **125,** 641–660 (2005).

63. Hisatomi, O., Takahashi, Y., Taniguchi, Y., Tsukahara, Y. & Tokunaga, F. Primary structure of a visual pigment in bullfrog green rods. *FEBS Lett.* **447,** 44–48 (1999).

64. Ma, J. *et al.* A Visual Pigment Expressed in Both Rod and Cone Photoreceptors. *Neuron* **32,** 451–461 (2001).

65. Takahashi, Y., Hisatomi, O., Sakakibara, S., Tokunaga, F. & Tsukahara, Y. Distribution of blue-sensitive photoreceptors in amphibian retinas. *FEBS Lett.* **501,** 151–155 (2001).

66. Witkovsky, P., Levine, J. S., Engbretson, G. a, Hassin, G. & MacNichol, E. F. A microspectrophotometric study of normal and artificial visual pigments in the photoreceptors of Xenopus laevis. *Vision Res.* **21,** 867–873 (1981).

67. Witkovsky, P. Photoreceptor classes and transmission at the photoreceptor synapse in the retina of the clawed frog, Xenopus laevis. *Microsc. Res. Tech.* **50,** 338–346 (2000).

68. Humphries, M. M. *et al.* Retinopathy induced in mice by targeted disruption of the rhodopsin gene. *Nat. Genet.* **15,** 216–9 (1997).

69. Palczewski, K. *et al.* Crystal Structure of Rhodopsin: A G Protein - Coupled Receptor. *Science (80-.).* **289,** 739–745 (2000).

70. Imai, H. *et al.* Single amino acid residue as a functional determinant of rod and cone visual pigments. *Proc. Natl. Acad. Sci. U. S. A.* **94,** 2322–2326 (1997).

71. Imai, H. *et al.* Molecular Properties of Rhodopsin and Rod Function. *J. Biol. Chem.* **282,** 6677–6684 (2006).

72. Nathans, J. Determinants of visual pigment absorbance: role of charged amino acids in the putative transmembrane segments. *Biochemistry* **29,** 937–942 (1990).

73. Janz, J. M., Fay, J. F. & Farrens, D. L. Stability of dark state rhodopsin is mediated by a conserved ion pair in intradiscal loop E-2. *J. Biol. Chem.* **278,** 16982–16991 (2003).

74. Kaushal, S. & Khorana, H. G. Structure and function in rhodopsin. 7. Point mutations associated with autosomal dominant retinitis pigmentosa. *Biochemistry* **33,** 6121–8 (1994).

75. Tsui, I., Chou, C. L., Palmer, N., Lin, C. S. & Tsang, S. H. Phenotype-genotype correlations in autosomal dominant retinitis pigmentosa caused by RHO, D190N. *Curr Eye Res* **33,** 1014–1022 (2008).

76. Sung, C. H. *et al.* Rhodopsin mutations in autosomal dominant retinitis pigmentosa. *Proc Natl Acad Sci U S A* **88,** 6481–6485 (1991).

77. Janz, J. M. & Farrens, D. L. Assessing structural elements that influence Schiff base stability: Mutants E113Q and D190N destabilize rhodopsin through different mechanisms. *Vision Res.* **43,** 2991–3002 (2003).

78. Liu, M. Y. *et al.* Thermal Stability of Rhodopsin and Progression of Retinitis Pigmentosa: Comparison of S186W and D190N Rhodopsin Mutants. *J. Biol. Chem.* **288,** 17698–17712 (2013).

Chapter 3 Extra-retinal Expression of Melanopsin

3.1 Introduction

Rods and cones have traditionally been regarded as the only photoreceptors in mammals, mediating essentially all visual functions. Some early evidence for the presence of another ocular photoreceptor did exist. For instance, the sensitivity of human pupillary light reflex (PLR) at short wavelengths, measured as early as in 1923 (see Ref. 1) and also in 1962 (see Ref. 2), did not actually correspond well to the action spectra of our rods and blue cones (see discussions in Ref. 3). Nonetheless, more solid evidence for a novel photoreceptor did not surface until the past 20 years. It was then observed that light could induce activity in the suprachiasmatic nucleus (SCN), the master circadian pacemaker in the brain, of newborn mice even before the complete development of rods and cones[4]. Moreover, mice with degenerated or functionless rods and cones could still shift their circadian rhythms normally according to the external light/dark cycle[5–9] (known as photoentrainment), and fully constrict their pupils (though more slowly) to bright light[10–12]. In these latter two situations, the spectral sensitivity reflected a retinal-based photopigment with a wavelength of maximal absorption (λ_{max}) at ~480 nm[9,13], distinct from rhodopsin and cone opsins. Incidentally, some humans with severe loss of rods and cones have also been reported to show intact photoentrainment[14].

In parallel with the accumulation of evidence for some rod- and cone-independent light sensitivity in the eye, a search for its cellular and molecular underpinnings had also been underway. A group of inner retinal neurons[15], or specifically retinal ganglion cells (RGCs)[16] that projected to the SCN, were shown to express transcripts of melanopsin

(*Opn4*), an opsin first identified in light-sensitive melanophores in the skin of *Xenopus laevis*[17]. A further breakthrough came when Berson *et al.*[18] performed patch-clamp recordings on RGCs labeled by injecting a retrograde tracer into the rat SCN. Importantly, they found that the labeled cells depolarized to light even after inputs from the rod- and cone-pathways were pharmacologically blocked. Notably, the spectral sensitivity and slow kinetics of the light responses were also consistent with those of circadian photoentrainment. At the same time, work from our laboratory[19] demonstrated that these intrinsically photosensitive RGCs (ipRGCs) indeed expressed melanopsin protein. Subsequent work on melanopsin-knockout ($Opn4^{-/-}$) mice confirmed that melanopsin is the photopigment underlying the intrinsic photosensitivity of ipRGCs[10]. Remarkably, melanopsin-expressing RGCs are present in virtually all mammalian species examined thus far, including rabbit[20,21], monkey[22,23] and human[22,24].

IpRGCs are heterogeneous in their morphology, absolute photosensitivity, intrinsic electrophysiological properties and central projection pattern (summarized in Table 3-1). At least five subtypes of ipRGCs have been described, classified largely based on dendritic arborization and cell morphology. M1 cells' dendrites stratify at the outermost margin of the inner plexiform layer (IPL), within the so-called OFF-sublamina where OFF-bipolar cells' axon terminals locate[25]. Oddly, M1 cells do not receive synaptic input from OFF-bipolar cells; instead, they form *en passant* synapses with ON-bipolar cells[20,26]. M2, M4 and M5 cells all stratify their dendrites in the ON-sublamina of the IPL[25,27], but have perhaps minute differences in the exact plane of arborization[28]. Some differences in soma size and dendritic field size also exist. It is of note that M4 and M5 cells give no obvious melanopsin immunosignal under regular staining conditions

(they are revealed by genetic labeling in *Opn4-Cre* mice)[27,28], indicative of very low melanopsin expression. Consistently, they have relatively low photosensitivity compared with M2 cells[27], which are themselves 10-fold less sensitive than M1 cells[29]. Finally, M3 cells bi-stratify their dendrites in both the ON- and OFF-sublamina[30–32]. Altogether, ipRGCs constitute 2-3% of the total RGC population in mice[19,32,33], and ~0.2% in macaque monkey[22]. There have been continual discussions about whether certain subtype, such as the less-characterized M3 cells, represents a true cell type, because their dendritic fields apparently do not tile the entire retina as do M1 and M2 cells[32]. Most recently, a new M6 subtype[34] has also been suggested, but its full characterization is still pending.

Table 3-1 Properties of ipRGC subtypes

	M1	M2	M3	M4	M5
Morphology					
Dendritic stratification† (sublamina of IPL)	OFF	ON	ON and OFF	ON	ON
Dendritic field diameter†	290-370 μm	320-430 μm	~480 μm	~360 μm	?
Dendritic branching†	Fewest	Medium	Similar to M2	Most	?
Soma diameter†	14-17 μm	16-22 μm	~18 μm	~21 μm	?
Central projection#	SCN, OPN shell, IGL	OPN core, dLGN, SC	?	OPN core, dLGN, SC	OPN core, dLGN, SC
Genetic and Molecular Labeling#					
Opn4$^{\tau lacZ/\tau lacZ}$	+	–	+?	–	–
Opn4-Cre	+	+	+	+	+
OPN4 immunosignal	+	+	+	–	–
Other molecular markers	Brn3b+ (some)	Brn3b+	Brn3b+	Brn3b+ SMI32+	Brn3b+
Physiology*					
Half-saturating intensity	12.5 log photons cm^{-2} sec^{-1}	13.5 log photons cm^{-2} sec^{-1}	12.8 log photons cm^{-2} sec^{-1}	13.9 log photons cm^{-2} sec^{-1}	?
Peak voltage response	Highest	>2-fold lower than M1	Similar to M2	Similar to M2	Similar to M2
Peak latency	Shortest	Medium	Medium	Longest	Medium

† Summarized from Ref. 27–30,35. Diameters are given in ranges if information comes from more than one source and as approximate values if information is only available from one reference. The differences among subtypes are not obvious due to measurement-variations across studies. Qualitatively, it is believed that dendritic field size and soma size follow the sequence: M4 > M2 ≈ M3 > M1.

Reviewed in Ref. 36.

* Summarized from Ref. 28–30,35,37.

IpRGCs project axons to various brain regions that subserve a multitude of visual tasks, especially non-image-forming functions. Primary targets of ipRGCs include the SCN, the intergeniculate leaflet (IGL, for intergrating photic and non-photic circadian signals) and the olivary pretectal nucleus (OPN, for controlling PLR)[19,38–40]. Less prominent innervations were found also in the ventral subparaventricular zone (vSPZ, for light-induced acute arrest of locomotor activity in nocturnal animals or negative masking), the dorsal lateral geniculate nucleus (dLGN, for image-forming vision) and the superior colliculus (SC, for gaze control)[19,38–40]. Accordingly, *Opn4*$^{-/-}$ mice showed various degrees of deficiency in the corresponding visual behaviors. For example, *Opn4*$^{-/-}$ mice achieved only ~80% of maximal pupillary constriction (cf. full constriction in wildtype) in response to bright light[10,41], and failed to maintain the constriction for long durations of light[42]. In addition, *Opn4*$^{-/-}$ mice reset their phases of circadian wheel-running activity to a smaller extent when a light pulse was given amid periods of constant darkness to photoentrain the mice's endogenous circadian clock; the defect grew more severe with brighter light stimuli[43,44]. Lastly, *Opn4*$^{-/-}$ mice experienced less-sustained negative-masking by light[41,45]. The picture thus emerged is that, whereas rods and cones mediate non-image-forming visual functions at low light intensity, melanopsin takes part at high light intensity and contributes to the sustainability of the visual responses. Melanopsin has also been implicated in image-forming vision[27], negative-phototaxis[46], exacerbation of migraine[47], etc.

In 2011, a surprising extra-retinal function of mammalian melanopsin was discovered – melanopsin confers intrinsic photosensitivity to the iris and mediates local PLR[48]. Animals such as fish, amphibians and birds were known to have irises that can

constrict autonomously upon light stimulation, independent of neural regulation through the brain[49–53]. In mammals, however, it was generally believed that a brain circuitry (see Chapter 1.2) is completely necessary, despite some sporadic reports suggesting otherwise[53–55]. By measuring the contractive force generated by isolated sphincter muscles to light, our laboratory[48] found that the irises of many nocturnal or crepuscular non-primate mammals, including mouse, rat, rabbit, cat and dog, are actually intrinsically photosensitive. In mouse, the muscle-contraction responses gave an action spectrum matching that of melanopsin, which, by immunohistochemistry on sections of the iris, appeared to be present in sphincter muscles. The responses were lost in *Opn4*$^{-/-}$ mice. In whole animal, this intrinsic photosensitivity is manifested by a larger pupil constriction in the illuminated eye versus the contralateral eye at high light intensity. Such a local PLR may allow nocturnal/crepuscular animals, whose rod-dominant retinas are especially susceptible to light damage, to stably maintain pupil constriction even when retinal illumination through the already-constricted pupil is weak.

Following our laboratory's initial report of a melanopsin-mediated intrinsic photosensitivity of the iridal sphincter ring, two groups have suggested the involvement of ipRGCs in directly regulating local PLR through axon collaterals that project to the ciliary marginal zone (CMZ) encircling the iris[56] or into the iris itself[57]. Vugler et al.[56] noted that lesions at the CMZ significantly reduced pupil constriction to light in isolated anterior-chamber preparations and that the cholinergic blocker, atropine, partially dampened local PLR *in vivo*. The authors thus proposed that the major mechanism for local PLR in intact animals is a cholinergic-dependent relaxation of the iris dilator muscles driven by ipRGCs that extend processes in the CMZ. Another related model also

invoked ipRGC-driven cholinergic neurotransmission, but inducing, instead, sphincter muscle contraction[57]. To examine these possibilities more closely, we performed various histochemical experiments in an attempt to visualize ipRGCs' projections in the iris. Unexpectedly, we found some melanopsin-immunopositive neuronal processes in the rat iris that appeared to come from the trigeminal ganglia. The discovery and characterization of these neuronal processes are detailed below.

3.2 Melanopsin expression in mouse irises

We first checked the expression of melanopsin by immunohistochemistry on whole-mount mouse irises. Despite an overall mildly-higher signal intensity in the sphincter muscles, no sphincter muscle cells or axon-like structures could be unequivocally labeled with either the regular or Tyramide-amplified staining procedures. This was not in contrast with earlier immunohistochemical results on cryosections of mouse irises (see above), in which immunoreactivity likewise could not be assigned to any cellular structures.

To test whether melanopsin was expressed at levels undetectable by immunohistochemistry as in, for examples, M4 and M5 ipRGCs (see above), we turned to genetic-labeling methods. We performed X-gal labeling on irises of albino *Opn4*$^{tlacZ/tlacZ}$ mice, in which the *tau-lacZ* cDNA was knocked into the melanopsin locus[19], but found no signals in all areas of the irises despite good labeling in the retinas (data by Qian Wang, not shown). We reasoned that the use of an Internal Ribosome Entry Site (IRES) sequence for permitting tau-lacZ expression in the *Opn4*$^{tlacZ/tlacZ}$ mice could have limited the expression level. Thus, we generated an *Opn4-Cre* bacterial artificial

chromosome (BAC) transgenic mouse line (see Methods) and crossed it to a *Rosa-tdTomato* reporter (Ai9) line to take advantage of the high amplification enabled by the *Rosa* promoter and strongly label melanopsin-expressing cells with the fluorescent protein tdTomato. Specificity of the Cre-mediated recombination was confirmed in the retina (Fig. 3-1, see Methods). In the iris (visualized by breeding into the albino C57BL/6J background), tdTomato marked some, but not all, sphincter muscle cells, identified by their characteristic elongated morphology and their expression of smooth muscle actin (data by Qian Wang, not shown). Nevertheless, no neuronal processes were evident.

3.3 Melanopsin-immunopositive neuronal processes in rat irises

We asked where melanopsin may be expressed in the irises of other mammalian species that also demonstrate local PLR[48]. Immunohistochemistry on whole-mount albino rat irises with an antibody against the C-terminus of rat melanopsin[19] again revealed no well-defined sphincter muscle cells, possibly due to low expression level. Curiously, however, we consistently observed about 10-20 immunolabeled neuronal processes which coursed into each iris through the surrounding ciliary body (Fig. 3-2a). These processes meandered with little branching over the dilator muscles of the iris to cover it fairly evenly. They terminated rather abruptly with no discernible swellings at their ends over either the sphincter or the dilator muscles. No processes were seen when the melanopsin antibody was omitted (Fig. 3-3a) or when the irises were pre-incubated with the immunizing peptide[19] used for producing the antibody (Fig. 3-3b). By using an antibody against the N-terminus of rabbit melanopsin[21], we also detected a similar

number of melanopsin-positive neuronal processes in the rabbit iris (Fig. 3-2b), although their density was lower there because of the larger iris size. As in mice and rats, we did not find any immunosignals in the rabbit sphincter muscles (data not shown).

We further characterized the melanopsin-immunopositive neuronal processes in the rat iris. One prominent feature of these processes was their large caliber: the typical diameter was ~3 μm (Fig. 3-2d, e). Interestingly, these processes were punctuated with gaps in immunoreactivity at roughly regular distances along their lengths, which appeared to indicate nodes of Ranvier (Fig. 3-2c). Consistently, the melanopsin-immunopositive processes overlapped almost completely with the population of myelinated neuronal processes in the iris (Fig. 3-2c). Most melanopsin-immunopositive processes expressed tyrosine hydroxylase (TH), which seemed to occur in a membrane-bound form[58] as defined by their spatial coincidence with transmembrane melanopsin (Fig. 3-2d). Besides, a few of the melanopsin-positive processes appeared to express choline acetyl-transferase (ChAT) (Fig. 3-2e).

3.4 Possible sources of melanopsin-immunopositive neuronal processes

Because ipRGCs have recently been suggested to extend axon collaterals into the iris[57] (see above), we examined the possibility that the melanopsin-immunopositive neuronal processes we found in the rat iris represented ipRGCs' axons. We immunostained flat-mount rat retinas for TH and ChAT. While the two markers labeled dopaminergic and cholinergic amacrine cells, respectively, both of them were absent in ipRGCs of the same retinas (Fig. 3-4a). In addition, the melanopsin-positive neuronal

processes in the iris appeared much thicker than ipRGCs' axons of the same eye (Fig. 3-4b). Hence, it is unlikely that the iridal processes would have originated from ipRGCs.

Neuronal control of iridal dilator and sphincter muscles were conducted by neurons in the superior cervical ganglion (SCG) and the ciliary ganglion, respectively (see Chapter 1.2). We next investigated whether SCG neurons, which were known to express TH for the production of norepinephrine, could have provided the melanopsin-immunopositive neuronal processes in the iris. We obtained rats that have undergone surgical denervation of their left SCGs (Charles River) and checked for degeneration of the iridal processes at least one month after the surgery. Immunostaining of the iris for TH revealed two kinds of TH-positive neuronal innervations: a population of thin, melanopsin-negative processes and a population of thick, melanopsin-positive processes. Upon SCG denervation, the former population experienced severe degeneration but the latter was largely resistant (Fig. 3-5). Thus, the melanopsin-immunopositive processes in the iris did not seem to arise from SCG neurons. We did not study the contribution from the ciliary ganglion as its projections in the iris are predominantly cholinergic[59] and it is difficult to be surgically manipulated due to its small size and close location to the optic nerve and blood supply to the eye.

The rat iris also contains sensory innervations from the trigeminal ganglia (TG)[60]. In fact, one earlier study has reported a population of catecholaminergic neuronal processes coming possibly from the TG[61]. Remarkably, those processes bore some resemblance to the melanopsin-immunopositive processes currently in question, including their sinuous morphology and insensitivity to SCG-ablation[61]. Furthermore, all myelinated nerve fibers[62], as well as most neurofilament-immuopositive neuronal

processes (including some characteristically thick ones)[63], in the rat iris have been suggested to originate from the TG. We therefore looked for melanopsin expression in the rat TG by immunostaining TG cryosections with the same antibody against rat melanopsin. Intriguingly, although we did not recognize any signal in somata, we did observe immunolabeled nerve fibers that were similar to those in the iris with respect to axon diameter, myelination and TH-expression (Fig. 3-6a). The apparent lack of immunoreactivity in cell bodies may result from an efficient targeting of melanopsin proteins to axons, as RT-PCR experiments have indicated that melanopsin was expressed in the TG, presumably in somata, at least at the transcript level (Fig. 3-6b).

3.5 Melanopsin expression in mouse trigeminal ganglia

We asked if melanopsin is likewise expressed in the mouse TG. Immunohistochemistry did not reveal any obvious signal in cryosections of mouse TG (data not shown). Thus, we returned to the *Opn4-Cre;Rosa-tdTomato* mouse line for genetically-enhanced labeling. We found up to 20 tdTomato-labeled somata in each mouse TG, situated mostly in the antero-lateral region next to the mandibular (V3) branch (Fig. 3-7a), a region which was also most concentrated with melanopsin-immunopositive processes in the rats. Surprisingly, in a TG optically cleared by a modified SeeDB protocol[64], the axons of several tdTomato-labeled cells could be traced to the maxillary (V2) branch, instead of the ophthalmic (V1) branch that normally innervates the eyes (Fig. 3-7a). Consistently, and as mentioned previously, we have not seen any tdTomato-labeled neuronal processes in mouse irises (see above). Moreover, we have not been able to detect *Opn4* transcripts in mouse TG by RT-PCR (Fig. 3-7b). At

this point, we are uncertain if this could reflect some species-difference in melanopsin expression among different populations of TG neurons in mice and rats. Incidentally, we have not observed any melanopsin immunosignal in irises of Macaque monkeys (data not shown). We also do not know if melanopsin was expressed in the mouse TG only transiently during development or throughout adulthood at undetectably low level.

3.6 Discussion

We have described here some initial evidence suggesting the expression of melanopsin in extra-retinal neurons that are possibly located in the TG and extending axons to the iris. There are a number of directions that merit further investigations.

First, a more solid demonstration of melanopsin protein expression in neuronal somata of the mouse and rat TG would be necessary, as the presence of genetic labeling or RNA messages does not automatically entail protein expression, particularly throughout adulthood. There is also a slight possibility that melanopsin is expressed in glial cells that wraps the neuronal processes, instead of the processes themselves. So far, the detection of protein expression has been limited by the sensitivity of melanopsin antibody. In rat, colchicine could be used to block axonal transport and, hence, to test whether the lack of melanopsin immunoreactivity in TG somata was due to the targeting of melanopsin away from cell bodies into the axons. Mice or rats genetically engineered to report melanopsin protein expression, for example, by fusing a peptide tag or a 2A-linked fluorescent marker to melanopsin, may offer an alternative solution, although caution has to be exercised not to disrupt the proper folding and targeting of melanopsin *in vivo*.

Second, additional evidence is required for supporting a direct connection between melanopsin-immunopositive neuronal processes in the iris and those in the TG. In fact, for precisely this purpose, we have tried to inject tracer dyes into various locations in the TG or to electrolytically lesion it with stereotaxic assistance in live animals, with the hope to observe labeling/degeneration of the iridal processes. Nonetheless, because the TG was located deep at the cranial base and was fairly big in size, we have not succeeded in getting accurate and complete labelings/ablations. We have also attempted to place lipophilic dyes (e.g. DiI and Neurovue) in the TG of fixed animals, but have not yet been able to obtain satisfactory long-distance tracing to the eyes, even to the corneas where sensory supply from the TG is rich. Some technical improvements would be helpful in this case.

If melanopsin protein is indeed expressed in TG neurons that project to the iris, what function(s) may it serve? We have begun to address this question by performing electrical recordings from melanopsin-expressing processes/neurons in the iris and the TG. We are attempting to obtain: (1) sharp-electrode recordings from processes in rat irises acutely labeled by a vital myelin dye (Fluoromyelin Red, Invitrogen), and (2) whole-cell or sharp-electrode recordings from labeled neurons in acute slices of the TGs of *Opn4-Cre;Rosa-tdTomato* mice. As of now, we have not yet been able to develop a suitable preparation because of some technical difficulties, such as the thinness of iridal processes, the small number of labeled neurons per mouse TG and the toughness of the tissues, etc. Meanwhile, some clues could perhaps been learnt from tracing the central projections of melanopsin-expressing TG neurons into the trigeminal nuclei of the brainstem. The TG has been proposed to be involved in several light-dependent behaviors,

such as strong light-induced blinking[65] and lacrimation[66]. It would be exciting to see if melanopsin mediates these behaviors, in addition to the many other non-image forming visual behaviors that it is already responsible for.

Finally, with multiple histochemical and genetic-labeling methods, we have not observed any likely innervations of the iris by ipRGCs' axon collaterals. Separately, new physiological data from our laboratory have also suggested that light-triggered contraction of the iridal sphincter muscles is independent of cholinergic transmission (data from Qian Wang, not shown). It remains an interesting question as to how ipRGC's axonal processes in the CMZ[56,57] (see above) may facilitate local PLR *in vivo*.

3.7 Figures

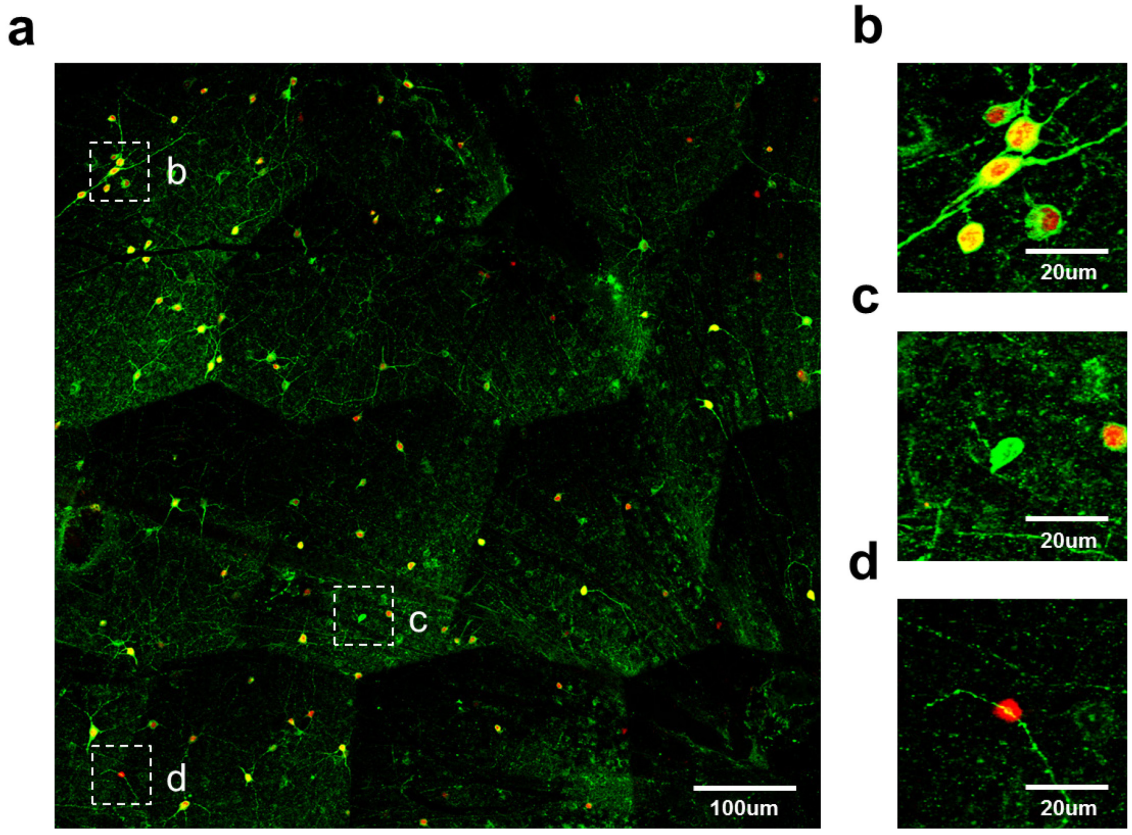

Fig. 3-1 Specificity of genetic labeling of ipRGCs in an *Opn4-Cre;Rosa-tdTomato* retina. a, Low-magnification view of an *Opn4-Cre;Rosa-tdTomato* retina immunostained for melanopsin (green). Red is fluorescence signal directly from tdTomato. **b-d,** Examples of tdTomato^{+} ipRGCs (**b**), a tdTomato^{-} ipRGC (**c**) and a tdTomato^{+} cell with no melanopsin immunosignal. This last cell may be a conventional ganglion cell or a M4- or M5-type ipRGC unable to be labeled by regular immunohistochemistry (see Chapter 3.1).

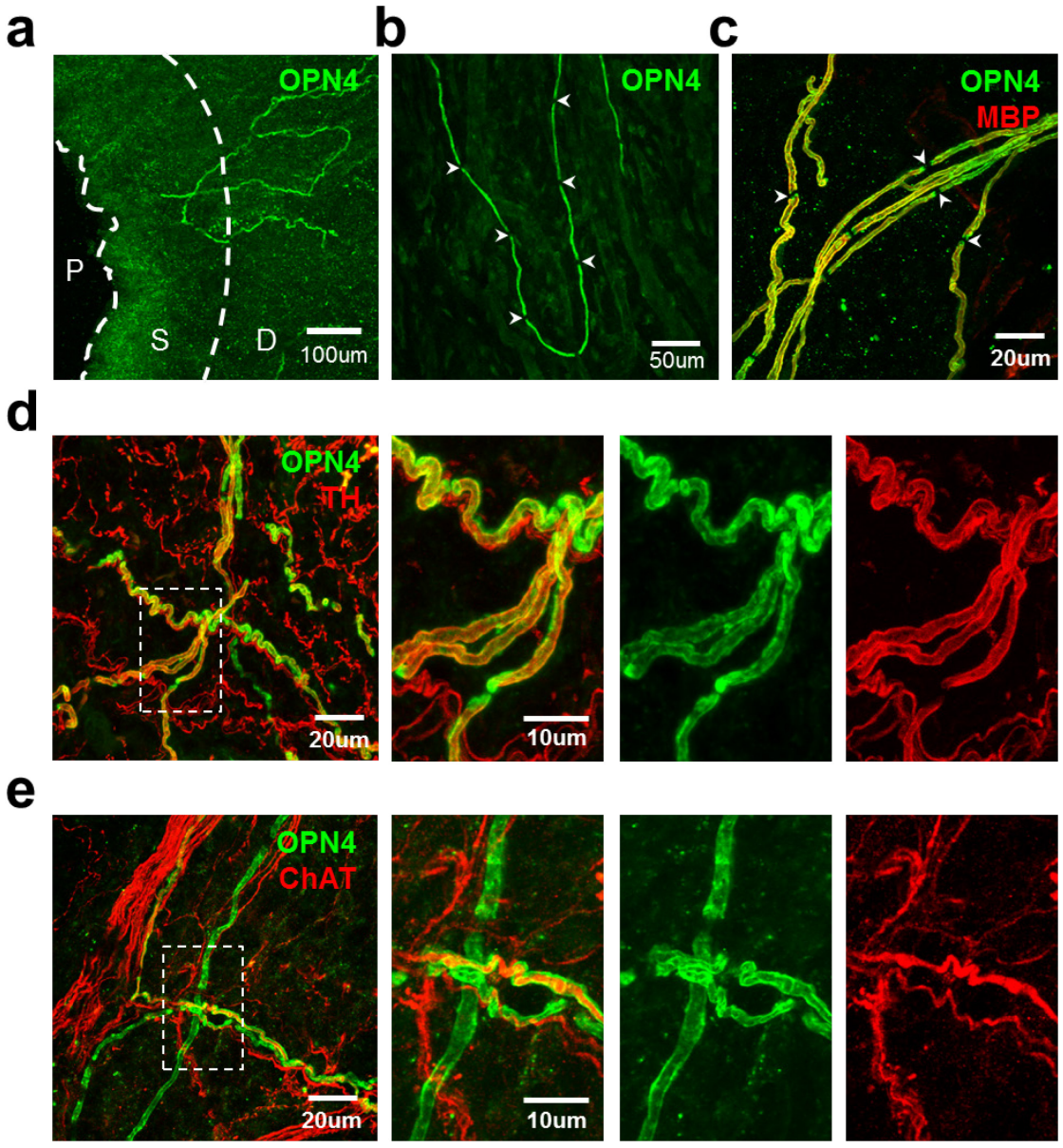
a
b
c
OPN4
OPN4
OPN4
MBP
P
S
D
100um
50um
20um
d
OPN4
TH
20um
10um
e
OPN4
ChAT
20um
10um

Fig. 3-2 Melanopsin-immunopositive processes in rat irises. a, Low-magnification view of a whole-mount rat iris immunostained for melanopsin (OPN4). The dotted lines demarcate the pupil (P) and the regions overlying the sphincter (S) and dilator (D) muscles. Note the slightly more intense immunosignal over the sphincter muscles and the immunopositive neuronal process that courses down from the top right corner. **b,** A whole-mount rabbit iris immunostained for melanopsin. Arrowheads indicate gaps in immunoreactivity along the melanopsin-immunopositive process. Image was taken from a region overlying the dilator muscles. **c,** A whole-mount rat iris immunostained for melanopsin (green) and myelin basic protein (MBP, red). Arrowheads indicate gaps in immunoreactivity in the processes. **d,** A whole-mount rat iris immunostained for melanopsin (green) and tyrosine hydroxylase (TH, red). The boxed area in the left panel is magnified in the rightmost three panels in combined or separated color channels. Note the membrane-associated expression of TH. **e,** A whole-mount rat iris immunostained for melanopsin (green) and choline acetyl-transferase (ChAT, red). The boxed area in the left panel is magnified in the rightmost three panels in combined or separated color channels. Note the cytosolic expression of ChAT.

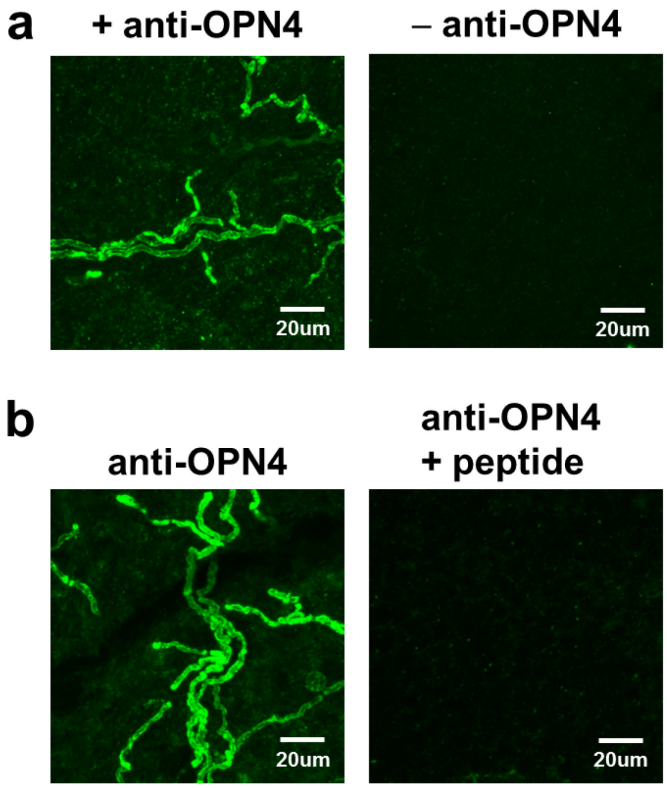

Fig. 3-3 Specificity of antibody against rat melanopsin. a, Whole-mount irises of the same rat processed for immunohistochemistry with (left) or without (right) the primary antibody against rat melanopsin. **b,** Whole-mount irises of the same rat immunostained for melanopsin with (left) or without (right) pre-incubating the primary antibody with its immunizing peptide.

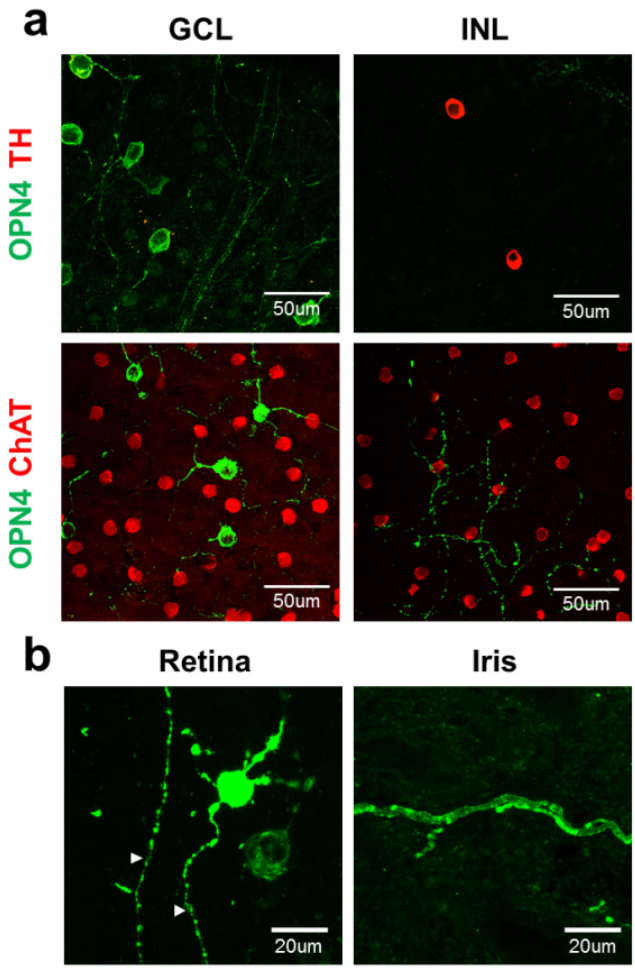

Fig. 3-4 Neurotransmitter expressions and axon caliber of rat ipRGCs. a, Flat-mount rat retinas immunostained for melanopsin (green) and TH (top row, red) or ChAT (bottom row, red). Left column are confocal images taken at the ganglion cell layer (GCL) to show ipRGCs. Images in the right column were taken at the inner nuclear layer (INL) to show TH^+ dopaminergic amacrine cells (top right) and $ChAT^+$ cholinergic amacrine cells. **b,** Flat-mount retina (left) and whole-mount iris (right) of the same rat eye immunostained for melanopsin. Note that ipRGCs' axons are thinner compared to the immunopositive processes in the iris.

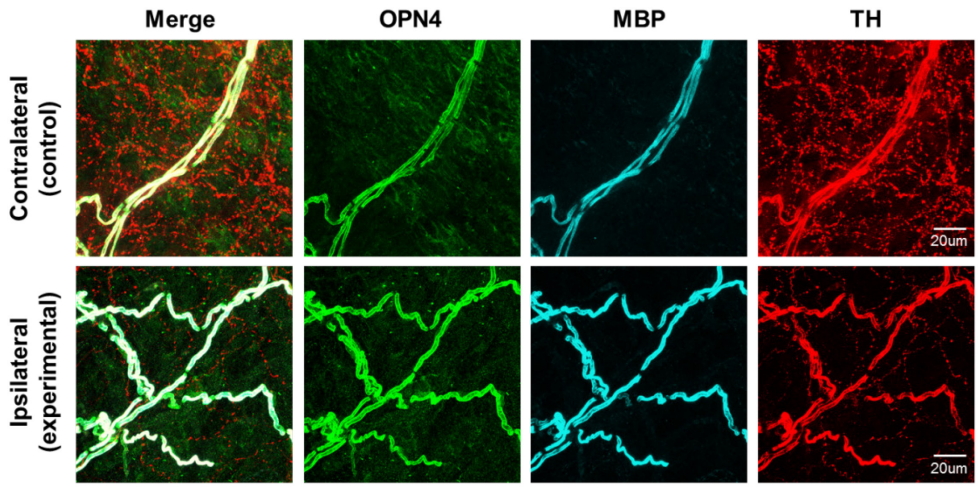

Fig. 3-5 Melanopsin-immunopositive processes in rat irises after unilateral denervation of the superior cervical ganglion (SCG). Whole-mount irises of a rat that has undergone unilateral SCG denervation, immunostained for melanopsin (green), MBP (cyan) and TH (red). Note the presence of both a thin and a thick population of TH^+ processes in the iris contralateral to the lesion (top right). The thin processes are lost but the thick, $OPN4^+$ processes are preserved in the iris ipsilateral to the lesion (bottom row).

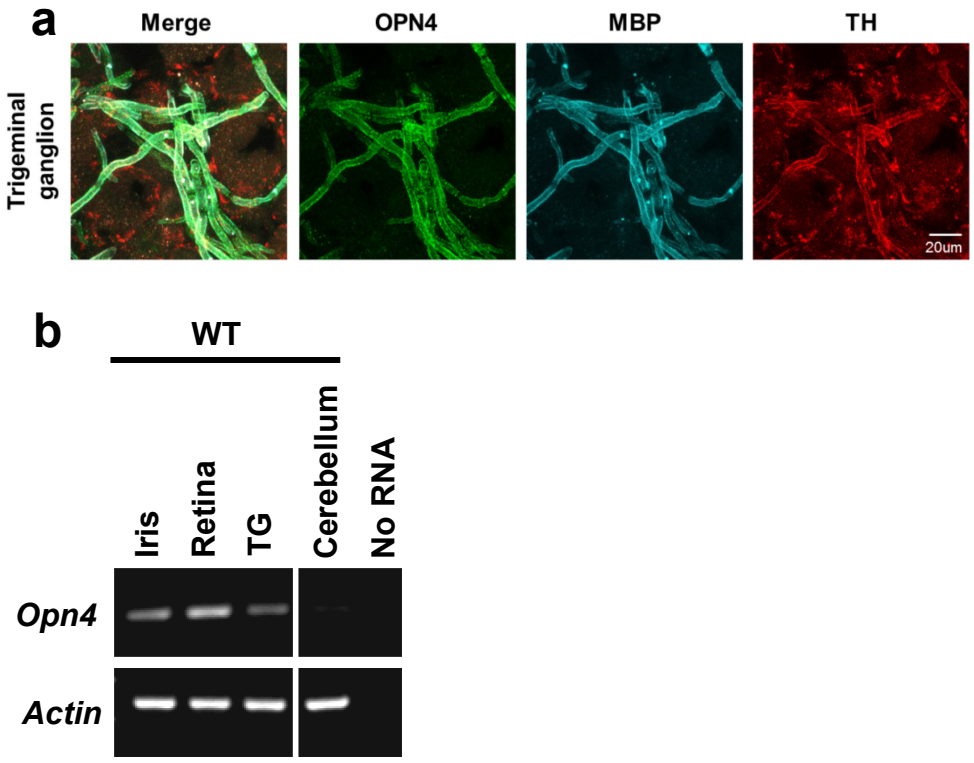

Fig. 3-6 **Melanopsin expression in rat trigeminal ganglia (TG). a,** Cryosections of rat TG immunostained for melanopsin (green), MBP (cyan) and TH (red). Image was taken from an antero-lateral region next to the mandibular branch of the TG. **b,** Detection of melanopsin transcripts in rat iris and TG by RT-PCR. Retina and cerebellum were positive and negative controls for melanopsin expression, respectively. A sample with no tissue (i.e. no RNA) but otherwise identically processed was also included as a negative control. The housekeeping gene *β-actin* was used as a positive-control for reverse-transcription.

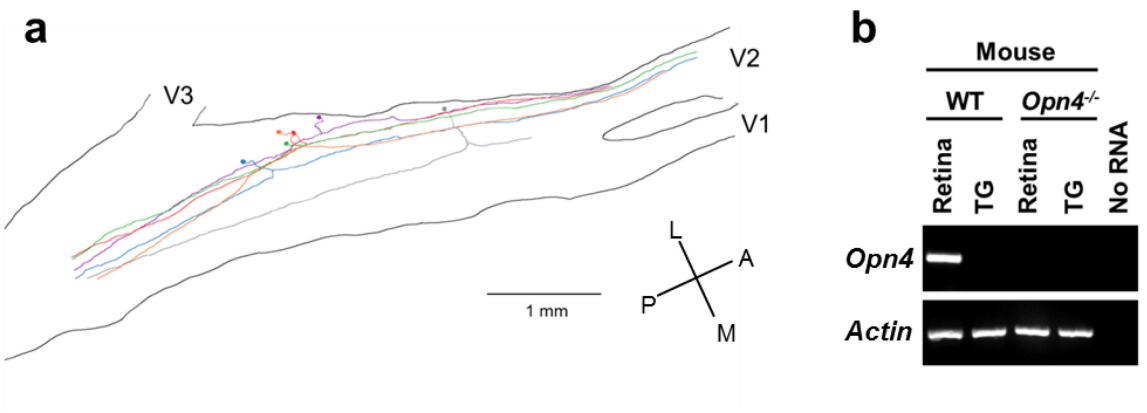

Fig. 3-7 **Melanopsin expression in mouse TG.** tdTomato-labeled neurons and their axonal projections in an optically-cleared TG of an *Opn4-Cre;Rosa-tdTomato* mouse. Note the peripheral projections of these neurons to the maxillary branch. V1: ophthalmic branch, V2: maxillary branch, V3: mandibular branch, A: anterior, P: posterior, L: lateral, M: medial. **b,** Detection of melanopsin transcripts in mouse TG by RT-PCR. Retina serves as positive control for melanopsin expression. Tissues from *Opn4*$^{-/-}$ mice were included for validating the specificity of the PCR reaction. A sample with no tissue (i.e. no RNA) but otherwise identically processed was also included as a negative control. The housekeeping gene *β-actin* was used as a positive-control for reverse-transcription.

3.8 References

1. Laurens, H. Studies on the relative physiological value of spectral lights. III. The pupillomotor effects of wave-lengths of equal energy content. *Am. J. Physiol.* **64,** 97–119 (1923).

2. Bouma, H. Size of the static pupil as a function of wavelength and luminosity of the light incident on the human eye. *Nature* **193,** 690–691 (1962).

3. McDougal, D. H. & Gamlin, P. D. The influence of intrinsically-photosensitive retinal ganglion cells on the spectral sensitivity and response dynamics of the human pupillary light reflex. *Vision Res.* **50,** 72–87 (2010).

4. Weaver, D. R. & Reppert, S. M. Definition of the developmental transition from dopaminergic to photic regulation of c-fos gene expression in the rat suprachiasmatic nucleus. *Mol. Brain Res.* **33,** 136–148 (1995).

5. Provencio, I., Wong, S., Lederman, A. B., Argamaso, S. M. & Foster, R. G. Visual and circadian responses to light in aged retinally degenerate mice. *Vision Res.* **34,** 1799–1806 (1994).

6. Foster, R. G. *et al.* Circadian photoreception in the retinally degenerate mouse (rd/rd). *J. Comp. Physiol. A* **169,** 39–50 (1991).

7. Ebihara, S. & Tsuji, K. Entrainment of the circadian activity rhythm to the light cycle: Effective light intensity for a Zeitgeber in the retinal degenerate C3H mouse and the normal C57BL mouse. *Physiol. Behav.* **24,** 523–527 (1980).

8. Freedman, M. S. *et al.* Regulation of Mammalian Circadian Behavior by Non-rod, Non-cone, Ocular Photoreceptors. *Science* **284,** 502–504 (1999).

9. Yoshimura, T. & Ebihara, S. Spectral sensitivity of photoreceptors mediating phase-shifts of circadian rhythms in retinally degenerate CBA/J (rd/rd) and normal CBA/N (+/+)mice. *J. Comp. Physiol. A.* **178,** 797–802 (1996).

10. Lucas, R. J. *et al.* Diminished pupillary light reflex at high irradiances in melanopsin-knockout mice. *Science* **299,** 245–247 (2003).

11. Semo, M. *et al.* Melanopsin retinal ganglion cells and the maintenance of circadian and pupillary responses to light in aged rodless/coneless (rd/rd cl) mice. *Eur. J. Neurosci.* **17,** 1793–1801 (2003).

12. Barnard, A. R. *et al.* Residual photosensitivity in mice lacking both rod opsin and cone photoreceptor cyclic nucleotide gated channel 3 alpha subunit. *Vis. Neurosci.* **21,** 675–683 (2004).

13. Lucas, R. J., Douglas, R. H. & Foster, R. G. Characterization of an ocular photopigment capable of driving pupillary constriction in mice. *Nat. Neurosci.* **4,** 621–626 (2001).

14. Klerman, E. B. *et al.* Photic resetting of the human circadian pacemaker in the absence of conscious vision. *J. Biol. Rhythms* **17,** 548–555 (2002).

15. Provencio, I. *et al.* A novel human opsin in the inner retina. *J. Neurosci.* **20,** 600–605 (2000).

16. Gooley, J. J., Lu, J., Chou, T. C., Scammell, T. E. & Saper, C. B. Melanopsin in cells of origin of the retinohypothalamic tract. *Nat. Neurosci.* **4,** 1165 (2001).

17. Provencio, I., Jiang, G., De Grip, W. J., Hayes, W. P. & Rollag, M. D. Melanopsin: An opsin in melanophores, brain, and eye. *Proc. Natl. Acad. Sci. U. S. A.* **95,** 340–345 (1998).

18. Berson, D. M., Dunn, F. A. & Takao, M. Phototransduction by retinal ganglion cells that set the circadian clock. *Science* **295,** 1070–1073 (2002).

19. Hattar, S., Liao, H. W., Takao, M., Berson, D. M. & Yau, K. W. Melanopsin-containing retinal ganglion cells: architecture, projections, and intrinsic photosensitivity. *Science* **295,** 1065–1070 (2002).

20. Hoshi, H., Liu, W.-L., Massey, S. C. & Mills, S. L. ON inputs to the OFF layer: bipolar cells that break the stratification rules of the retina. *J. Neurosci.* **29,** 8875–8883 (2009).

21. Kim, H. L. *et al.* Axonal synapses utilize multiple synaptic ribbons in the mammalian retina. *PLoS One* **7,** (2012).

22. Dacey, D. M. *et al.* Melanopsin-expressing ganglion cells in primate retina signal colour and irradiance and project to the LGN. *Nature* **433,** 749–754 (2005).

23. Jusuf, P. R., Lee, S. C. S., Hannibal, J. & Grünert, U. Characterization and synaptic connectivity of melanopsin-containing ganglion cells in the primate retina. *Eur. J. Neurosci.* **26,** 2906–2921 (2007).

24. Hannibal, J. *et al.* Melanopsin is expressed in PACAP-containing retinal ganglion cells of the human retinohypothalamic tract. *Investig. Ophthalmol. Vis. Sci.* **45,** 4202–4209 (2004).

25. Baver, S. B., Pickard, G. E., Sollars, P. J. & Pickard, G. E. Two types of melanopsin retinal ganglion cell differentially innervate the hypothalamic suprachiasmatic nucleus and the olivary pretectal nucleus. *Eur. J. Neurosci.* **27,** 1763–1770 (2008).

26. Dumitrescu, O. N., Pucci, F. G., Wong, K. Y. & Berson, D. M. Ectopic retinal ON bipolar cell synapses in the OFF inner plexiform layer: Contacts with dopaminergic amacrine cells and melanopsin ganglion cells. *J. Comp. Neurol.* **517,** 226–244 (2009).

27. Ecker, J. L. *et al.* Melanopsin-expressing retinal ganglion-cell photoreceptors: Cellular diversity and role in pattern vision. *Neuron* **67,** 49–60 (2010).

28. Estevez, M. E. *et al.* Form and function of the M4 cell, an intrinsically photosensitive retinal ganglion cell type contributing to geniculocortical vision. *J. Neurosci.* **32,** 13608–13620 (2012).

29. Schmidt, T. M. & Kofuji, P. Functional and morphological differences among intrinsically photosensitive retinal ganglion cells. *J. Neurosci.* **29,** 476–482 (2009).

30. Schmidt, T. M., Taniguchi, K. & Kofuji, P. Intrinsic and extrinsic light responses in melanopsin-expressing ganglion cells during mouse development. *J. Neurophysiol.* **100,** 371–384 (2008).

31. Viney, T. J. *et al.* Local retinal circuits of melanopsin-containing ganglion cells identified by transsynaptic viral tracing. *Curr. Biol.* **17,** 981–988 (2007).

32. Berson, D. M., Castrucci, A. M. & Provencio, I. Morphology and mosaics of

melanopsin-expressing retinal ganglion cell types in mice. *J. Comp. Neurol.* **518,** 2405–2422 (2010).

33. Schmidt, T. M. *et al.* A role for melanopsin in alpha retinal ganglion cells and contrast detection. *Neuron* **82,** 781–788 (2014).

34. Maloney, R. T., Yoon, J. & M., B. D. A viral method for optogenetic control of intrinsically photosensitive retinal ganglion cells. (2015).

35. Schmidt, T. M. & Kofuji, P. Structure and function of bistratified intrinsically photosensitive retinal ganglion cells in the mouse. *J. Comp. Neurol.* **519,** 1492–1504 (2011).

36. Schmidt, T. M., Chen, S. K. & Hattar, S. Intrinsically photosensitive retinal ganglion cells: Many subtypes, diverse functions. *Trends Neurosci.* **34,** 572–580 (2011).

37. Zhao, X., Stafford, B. K., Godin, A. L., King, W. M. & Wong, K. Y. Photoresponse diversity among the five types of intrinsically photosensitive retinal ganglion cells. *J. Physiol.* **592,** 1619–36 (2014).

38. Gooley, J. J., Lu, J., Fischer, D. & Saper, C. B. A broad role for melanopsin in nonvisual photoreception. *J. Neurosci.* **23,** 7093–7106 (2003).

39. Hannibal, J. & Fahrenkrug, J. Target areas innervated by PACAP-immunoreactive retinal ganglion cells. *Cell Tissue Res.* **316,** 99–113 (2004).

40. Hattar, S. *et al.* Central projections of melanopsin-expressing retinal ganglion cells in the mouse. *J. Comp. Neurol.* **497,** 326–349 (2006).

41. Panda, S. *et al.* Melanopsin is required for non-image-forming photic responses in blind mice. *Science* **301,** 525–527 (2003).

42. Zhu, Y. *et al.* Melanopsin-dependent persistence and photopotentiation of murine pupillary light responses. *Investig. Ophthalmol. Vis. Sci.* **48,** 1268–1275 (2007).

43. Ruby, N. F. *et al.* Role of melanopsin in circadian responses to light. *Science* **298,** 2211–2213 (2002).

44. Panda, S. *et al.* Melanopsin (Opn4) requirement for normal light-induced circadian phase shifting. *Science* **298,** 2213–2216 (2002).

45. Mrosovsky, N. & Hattar, S. Impaired masking responses to light in melanopsin-knockout mice. *Chronobiol. Int.* **20,** 989–999 (2003).

46. Johnson, J. *et al.* Melanopsin-dependent light avoidance in neonatal mice. *Proc. Natl. Acad. Sci. U. S. A.* **107,** 17374–17378 (2010).

47. Noseda, R. *et al.* A neural mechanism for exacerbation of headache by light. *Nat. Neurosci.* **13,** 239–245 (2010).

48. Xue, T. *et al.* Melanopsin signalling in mammalian iris and retina. *Nature* **479,** 67–73 (2011).

49. Seliger, H. H. Direct action of light in naturally pigmented muscle fibers. I. Action spectrum for contraction in eel iris sphincter. *J. Gen. Physiol.* **46,** 333–342 (1962).

50. Barr, L. & Alpern, M. Photosensitivity of the Frog Iris. *J. Gen. Physiol.* **46,** 1249–1265 (1963).

51. Kargacin, G. J. & Detwiler, P. B. Light-evoked contraction of the photosensitive iris of the frog. *J. Neurosci.* **5,** 3081–3087 (1985).

52. Tu, D. C., Batten, M. L., Palczewski, K. & Van Gelder, R. N. Nonvisual photoreception in the chick iris. *Science* **306,** 129–131 (2004).

53. Barr, L. Photomechanical coupling in the vertebrate sphincter pupillae. *Crit. Rev. Neurobiol.* **4,** 325–366 (1989).

54. Bito, L. Z. & Turansky, D. G. Photoactivation of pupillary constriction in the isolated in vitro iris of a mammal (Mesocricetus auratus). *Comp. Biochem. Physiol. A. Comp. Physiol.* **50,** 407–413 (1975).

55. Lau, K. C., So, K. F., Campbell, G. & Lieberman, A. R. Pupillary constriction in response to light in rodents, which does not depend on central neural pathways. *J. Neurol. Sci.* **113,** 70–79 (1992).

56. Semo, M., Gias, C., Ahmado, A. & Vugler, A. A role for the ciliary marginal zone in the melanopsin-dependent intrinsic pupillary light reflex. *Exp. Eye Res.* **119,** 8–18 (2014).

57. Schmidt, T. M. *et al.* A retinal projection to the iris mediates pupil constriction. (2014).

58. Kuczenski, R. T. & Mandell, a J. Regulatory properties of soluble and particulate rat brain tyrosine hydroxylase. *J. Biol. Chem.* **247,** 3114–3122 (1972).

59. Huhtala, a, Tervo, T., Huikuri, K. T. & Palkama, a. Effects of denervations on the acetylcholinesterase-containing and fluorescent nerves of the rat iris. *Acta Ophthalmol.* **54,** 85–98 (1976).

60. Olson, L. *et al.* in *Handbook of Chemical Neuroanatomy* (eds. Bjorklund, A., Hokfelt, T. & Owman, C.) 545–597 (Elsevier Science Publishers B. V., 1988).

61. Olson, L. & Seiger, A. A system of atypical catecholamine-containing nerve fibres in the rat iris present after total superior cervical ganglionectomy. *Med. Biol.* **58,** 94–100 (1980).

62. Huhtala, A. Origin of myelinated nerves in the rat iris. *Exp. Eye Res.* **22,** 259–265 (1976).

63. Seiger, A., Dahl, D., Ayer-LeLievre, C. & Björklund, H. Appearance and distribution of neurofilament immunoreactivity in iris nerves. *J. Comp. Neurol.* **223,** 457–470 (1984).

64. Ke, M.-T., Fujimoto, S. & Imai, T. SeeDB: a simple and morphology-preserving optical clearing agent for neuronal circuit reconstruction. *Nat. Neurosci.* **16,** 1154–61 (2013).

65. Dolgonos, S., Ayyala, H. & Evinger, C. Light-induced trigeminal sensitization without central visual pathways: Another mechanism for photophobia. *Investig. Ophthalmol. Vis. Sci.* **52,** 7852–7858 (2011).

66. Okamoto, K., Tashiro, A., Chang, Z. & Bereiter, D. A. Bright light activates a trigeminal nociceptive pathway. *Pain* **149,** 235–242 (2010).

Chapter 4 Neuropsin (OPN5)-mediated Photoentrainment of Local Circadian Clock in Mammalian Retina and Cornea

4.1 Introduction

As discussed briefly in Chapter 1, the evolution of circadian systems could provide survival advantages to primitive organisms. Likewise, in humans and other mammals, the circadian system casts widespread influence on many physiological processes. The subjective dawn, for example, marks the activation of the adrenocorticotropic axis, which, through the release of corticosteroids, affects multiple aspects of metabolism and immunity to prepare for awakening (see, for examples, Ref. 1, 2 for reviews). The subjective morning is met by an increase in heart rate and reduced vasodilation, with a concomitant rise in systolic blood pressure and, thus, in risk of heart attacks. Throughout the day, metabolic pathways in the liver, muscle and fat tissues are also subjected to circadian regulation. As evening approaches, our body temperature decreases and melatonin is secreted to induce sleep (see, for example, Ref. 3 for review).

The suprachiasmatic nucleus (SCN) in the anterior hypothalamus of the brain is the master circadian pacemaker that acts to synchronize bodily rhythms to external light/dark cycles (reviewed in, for examples, Ref. 4, 5). The SCN is composed primarily of γ-aminobutyric acid (GABA)-containing neurons that are organized into a dorsal "shell" and a ventral "core", with a subpopulation of the former expressing additionally vasopressin (AVP) and the latter vasoactive intestinal polypeptide (VIP). Each SCN neuron houses an autonomous molecular clock that is perpetuated by interlocked feedback mechanisms (Fig. 4-1). Briefly, in early circadian day, the transcriptional

activators CLOCK and BMAL1 stimulate the transcription of genes with Enhancer-box (E-box) elements in their promoters, which include clock-controlled genes tied directly or indirectly to various cellular processes (such as neuronal firing and neuropeptide secretion), along with the negative regulators *Period* (*Per*), *Cryptochrome* (*Cry*) and *Rev-Erbα*. As time progresses, PER and CRY proteins accumulate, assemble into a complex and translocate into the nucleus, where they suppress CLOCK/BMAL1-mediated transcriptional activation, while REV-ERBα represses the transcription of *Bmal1* and a separate set of clock-controlled genes. Together, these two arms of feedback mechanisms prevent the further build-up of CLOCK/BMAL1's target gene products. Finally, the circadian cycle returns to its start point as PER, CRY and REV-ERBα become ubiquitinated and degraded. Individually, the molecular clock residing in each SCN neuron does not appear to be reliable time-keepers – neurons in a cultured SCN explant could spontaneously gain or lose rhythmicity or go out-of-phase when they were synaptically isolated[6]. Thus, the robust rhythm of SCN as a whole, which can be tightly maintained for up to a month in culture, arises from the strong coupling among cells. Both GABA and VIP have been implicated in synchronizing SCN neurons (see, for example, Ref. 5 for review).

Our SCN clocks have an intrinsic period slightly longer than 24 hours on average (human: ~24.2 hours[7]; mouse: ~23.5 hours[8]). If left unadjusted to environmental cues (i.e., free-run), it would gradually go out-of-sync with the external light/dark cycle. Thus, the SCN needs to reset the phase of its clock at times with reference to some photic input. The SCN receives photic information from melanopsin (OPN4)-expressing, intrinsically-photosensitive retinal ganglion cells (ipRGCs, see Chapter 3), into which signals from

rods, cones and melanopsin-activation converge[9–12]. The signaling mechanism by which photic information is fed into the molecular clock has not been completely mapped out (reviewed in Ref. 13,14). Nevertheless, it is generally believed that synaptic input from ipRGCs[15] leads to the activation of a calcium-dependent kinase cascade and the consequent phosphorylation of the cyclic-AMP-responsive-element-binding (CREB) protein[16–18]. The binding of phosphorylated CREB to cAMP-responsive element (CRE)[19], plus chromatin remodeling[20], on the *Per* genes induces their expression, therefore shifting the phase of the clock.

The SCN clock is not the only clock in the body. Peripheral tissues such as the lung, the pituitary gland and fibroblasts possess similar molecular clockworks involving CLOCK, BMAL, PER and CRY as in SCN neurons (see, for example, Ref. 4 for review). Explants of these tissues also show intrinsic rhythms for days. However, unlike the sustained, high-amplitude rhythms observed in SCN explants, those in peripheral oscillators dampen quickly after a few days in culture, presumably because cells start to cycle out of synchrony. Regulation by the SCN is, therefore, necessary for keeping peripheral clocks synchronized and also well-aligned (entrained) to external light/dark cycles. SCN exerts its control on peripheral clocks through several routes: (1) by neural control through autonomic pathway that innervates the viscera, (2) by temporally-regulated release of hormones such as gluococorticoids, (3) by regulating body temperature and hence modulating the activity of temperature-sensitive transcription factors, and (4) by regulating the intake of food, which triggers clock-resetting pathways locally in peripheral tissues. Nearly all peripheral clocks are synchronized by the SCN clock.

The retina, while responsible for providing photic signals to entrain the SCN, also has itself a local clock that regulates many of its functions (reviewed in Ref. 21). At subjective night, for example, a reduction in dopamine level results in a stronger gap-junction coupling between rods and cones, which may allow the flow of rod-signals into the cone pathway to facilitate detection of dim objects[22]. The shedding of old membranous disks from the apical tips of photoreceptors' outer segments is also circadianly controlled, occurring at the beginning of day for rods[23,24]. Interestingly, the retinal clock is the only known peripheral oscillator in mammals that is directly photoentrainable independent of the SCN. Rhythms of melatonin production[25] and gene expression[26] in cultured retinas can follow external light/dark cycles. Even more surprisingly, the photoentrainment of the retinal clock does not require rods, cones nor melanopsin[27]. Thus, retinas from mice that have lost all rods and cones due to degeneration and lack melanopsin (*rd1/rd1; Opn4*$^{-/-}$) still remain synchronized to light/dark cycles both *in vivo* and *ex vivo*[27].

In collaboration with the laboratory of Russell Van Gelder at the University of Washington, we found, in work reported below, that neuropsin (OPN5) is likely the photopigment that mediates the photoentrainment of the local circadian clock in the retina, and also that in the cornea. This is the first assignment of a physiological, light-sensing function to mammalian OPN5, until now an orphan opsin.

Part of this work has been published in Buhr *et al.* (2015)[28]. Some RT-PCR experiments as well as all photoentrainment assays, electroretinogram recordings, optokinetic tests and circadian wheel-running experiments were done in Russell Van Gelder's laboratory.

4.2 Wavelength-dependence of photoentrainment of retinal rhythm

To identify the photopigment responsible for the photoentrainment of the retinal rhythm, we first examined the wavelength-dependence of the entrainment *ex vivo* in retinas of *Per2::Luciferase* mice, in which the circadian fluctuations of *PER2* protein level were reported by the activity of its fusion protein, luciferase. Pairs of retinas were cultured under 9-hr/15-hr light/dark cycles at constant temperature, with the two retinas in each pair subjected to opposite-phase entrainment (see Ref. 27 and Methods). After 4 days of such entrainment, the retinas were cultured for 4 additional days in darkness, at which time their circadian phase were determined by measuring the luciferase-dependent bioluminescence. In previous experiments of this kind with white light[27], paired retinas were entrained to opposite phases, with luminescence peaking at ~4 hours after the respective light-to-dark transition.

We repeated the experiments with monochromatic light at 370 nm, 417 nm, 475 nm, 530 nm or 628 nm. To avoid UV-elicited tissue damage, we used 370-nm light at a lower intensity (9×10^{12} photons cm^{-2} s^{-1}) than that at the other four wavelengths (9×10^{13} photons cm^{-2} s^{-1}). Stable and nearly opposite circadian phases could be attained in paired retinas exposed to 370-nm or 417-nm light/dark cycles (Fig. 4-2a). In contrast, paired retinas exposed to 475-nm light/dark cycles showed only partial entrainment, differing merely by about 6 hours in phases (Fig. 4-2a). No entrainment was achieved in paired retinas exposed to 530-nm or 628-nm light/dark cycles; they maintained phases identical to retinas kept in continuous darkness (Fig. 4-2a). In short, circadian photoentrainment *ex vivo* was most effective with UV-A and violet light.

To confirm the above spectral sensitivity, we asked if light pulses of different wavelengths would also produce varying degree of acute phase-shifts in retinal rhythms. We recorded the free-running circadian rhythms of cultured *Per2::Luciferase* retinas in continuous darkness and applied a 3-hr light pulse at 417 nm or 475 nm at selected phases of their rhythms. The resulting phase-delay or phase-advance was measured to give a phase-response curve. Consistent with the entrainment experiments, 417-nm light triggered larger phase-shifts than 475-nm light of the same intensity at all phases (Fig. 4-2b), attesting to a higher sensitivity of photoentrainment to violet light.

4.3 Photoentrainment of rhythms in *Opn1sw*$^{-/-}$, *Opn3*$^{-/-}$ and *Opn5*$^{-/-}$ retinas

The mouse S-cone pigment (OPN1SW) has a wavelength of maximal absorption (λ_{max}) of 360 nm. Although retinas with degenerated cones (adult *rd1/rd1* retinas) photoentrained normally *ex vivo*[27], some ganglion cells of these degenerated retinas have been reported to ectopically express OPN1SW[29]. We therefore tested the involvement of OPN1SW in mediating photoentrainment with the same paired-retinal-entrainment assay described above. Entrainment to white light was normal in retinas lacking OPN1SW (*Opn1sw*$^{-/-}$*;Per2::Luciferase*)[30] (Fig. 4-3).

We also tested the involvement of encephalopsin (OPN3), prompted by its expression in inner retinal neurons[31,32]. In heterologous systems, mosquito and pufferfish OPN3 homologs form functional bistable pigment with dark-state λ_{max}'s at ~500 nm and ~460 nm, respectively[33]; nonetheless, to our knowledge, there was no published absorption spectrum for mammalian OPN3. The function of mammalian OPN3 is also elusive. We generated *Opn3*$^{-/-}$ mice by homologous recombination (Fig. 4-4a and

Methods) and validated the lack of expression of *Opn3* transcripts (Fig. 4-4d). Once again, *Opn3*$^{-/-}$*;Per2::Luciferase* retinas photoentrained normally in *ex vivo* experiments, albeit having a weaker luminescence amplitude than wild-type (WT; Fig. 4-3). We are currently investigating whether this diminished amplitude is due to (1) a reduction in the absolute level of PER2 expression or a weakening of its circadian oscillations due to developmental cell loss or gene regulation, or (2) a desynchronization of rhythmic neurons.

Mouse OPN5 also constituted a functional bistable pigment when expressed heterologously, being capable of converting, upon illumination, from an inactive, 11-cis-retinal-containing state (λ_{max} = 380 nm) to a G protein-activating, all-trans-retinal-containing state (λ_{max} = 470 nm)[34,35]. OPN5 is a deep-brain photopigment in the hypothalamus of birds and has been proposed to regulate the photoperiod for reproduction[36–39]. However, little is known about the physiological function of mammalian OPN5, despite its reported expression in the retina[34,35]. We generated *Opn5*$^{tlacZ/tlacZ}$ mice (denoted *Opn5*$^{-/-}$ Line 1) by homologous recombination to simultaneously knock out *Opn5* expression and knock in a tau-lacZ cDNA into the *Opn5* gene locus for labeling purpose (Fig. 4-4b and Methods). We confirmed by RT-PCR that *Opn5* mRNA expression was undetectable in the eyes of these mice (Fig. 4-4e), and by immunohistochemistry that the expression patterns of other opsins were unaltered (Fig. 4-5). Remarkably, *Opn5*$^{-/-}$*;Per2::Luciferase* retinas completely failed to entrain in *ex vivo* experiments, having phases similar to WT retinas kept in continuous darkness (Fig. 4-3). This defect was not secondary to some global retinal dysfunction as *Opn5*$^{-/-}$*;Per2::Luciferase* mice demonstrated normal electroretinographic (ERG) light

responses in dark- and light-adapted states (Fig. 4-6a), normal optokinetic tracking reflex (Fig. 4-6b) as well as normal circadian wheel-running activities (Fig. 4-6c). To confirm the lack of photoentrainment of circadian rhythm in *Opn5*$^{-/-}$*;Per2::Luciferase* retinas, we obtained another knockout line from Dr. Richard Lang (denoted *Opn5*$^{-/-}$ Line 2), which was generated by crossing an *Opn5*$^{flox/flox}$ mouse line with a *Rosa-Flp* line and an *EIIa-Cre* line (see Methods). Retinas from transheterozygotes of *Opn5*$^{-/-}$ Lines 1 and 2 (in *Per2::Luciferase* background) also did not photoentrain in *ex vivo* experiments, although *Opn5*$^{+/-}$*;Per2::Luciferase* littermates of either *Opn5*$^{-/-}$ Line 1 or Line 2 entrained normally (Fig. 4-7).

4.4 Photoentrainment of rhythms in *Opn1sw*$^{-/-}$, *Opn3*$^{-/-}$ and *Opn5*$^{-/-}$ corneas

The mammalian cornea also shows a circadian rhythm *ex vivo*[40]. We asked if this rhythm was photoentrainable by adapting the paired-tissue-entrainment assay to *Per2::Luciferase* cornea. Indeed, the corneal rhythm could be photoentrained (Fig. 4-8), although to a phase almost opposite to that of the retinas, i.e., occurring at subjective dawn rather than subjective dusk. The reason for this phase-difference is unknown. As in the retina, photoentrainment of the corneal rhythm was unaffected by the loss of OPN1SW (*Opn1sw*$^{-/-}$*;Per2::Luciferase*) or OPN3 (*Opn3*$^{-/-}$*;Per2::Luciferase*), but was abolished by knocking out OPN5 (*Opn5*$^{-/-}$ Line 1*;Per2::Luciferase*) (Fig. 4-8). Corneas of transheterozygotes of *Opn5*$^{-/-}$ Line 1 and 2 also failed to photoentrain (Fig. 4-7). By RT-PCR, we confirmed *Opn5* mRNA expression in both fresh and cultured WT corneas.

4.5 Identity of OPN5-expressing cells

We took some initial steps to identify OPN5-expressing cells in the mouse retina and cornea.

To immunolocalize OPN5, we obtained an aliquot of a published[34] antibody against the N-terminus of mouse OPN5. By immunohistochemistry on retinal sections, we verified the reported expression of OPN5 in the majority of cells in the ganglion cell layer (GCL) as well as the inner part of the inner nuclear layer (INL) of WT retinas. No immunosignals were seen on *Opn5*$^{-/-}$ Line 1 retinal sections that were processed in parallel (Fig. 4-9a). To confirm our results, we then obtained another aliquot of the same antibody (due to the exhaustion of the initial aliquot), but from a separately purified stock. With identical immunohistochemical procedures as before, however, we observed a much weaker labeling of inner retinal neurons and also enhanced non-specific staining of, for example, photoreceptors and the outer portion of the inner nuclear layer. More importantly, these immunosignals persisted even in *Opn5*$^{-/-}$ Line 1 retinas (Fig. 4-9b). Because of this inconsistent result, we obtained another OPN5 antibody[35], generated against a different N-terminal epitope, as an alternative. This antibody has been shown to label a much-smaller population of retinal neurons in the GCL and INL. Nonetheless, with the immunohistochemical conditions specified by the provider of the antibody, we did not observe any specific immunosignal on WT and *Opn5*$^{-/-}$ Line 1 retinal sections (data not shown). Same immunohistochemical experiments have been tried with no success by using several commercial OPN5 antibodies and two other antibodies that our lab has generated via a commercial source (data not shown; see Methods). In sum, owing

to a lack of specific antibodies, we have not yet been able to reliably localize the expression of OPN5 protein.

An earlier publication[35] has reported the expression of *Opn5* mRNA in sections of immature mouse retinas by *in situ* hybridization, but the signals were not localized and they disappeared in adult retinas. We decided to further examine the transcript expression of *Opn5* by taking advantage of our *Opn5*$^{-/-}$ Line 1 (i.e., *Opn5*$^{\tau lacZ/\tau lacZ}$) mice, in which the expression of β-galactosidase (β-gal), coded by *lacZ*, should follow the activity of *Opn5* promoter. Staining with the β-gal substrate, X-gal, produced puncta of blue precipitate in about 4,800 cells per *Opn5*$^{-/-}$ retina (Fig. 4-10a). These X-gal-labeled cells were evenly spaced in the ganglion cell layer and were immunopositive for the ganglion-cell marker, Retinal Binding Protein with Multiple Splicing (RBPMS; Fig. 4-10b), suggesting that they represent a small subset of ganglion cells rather than displaced amacrine cells. A similar punctate pattern of X-gal-labeling was found in about 5,200 cells per retina of *Opn5*$^{-/-}$ Line 2 mice (Fig. 4-10c), which likewise carry a knock-in *lacZ* cDNA, but differently situated, in the *Opn5* gene locus (Fig. 4-4c). In contrast to the diffuse X-gal labeling of the somata, proximal dendrites and axons of ipRGCs in *Opn4*$^{-/-}$ retina[41], the punctate X-gal signal in *Opn5*$^{-/-}$ retinas was typically confined to the periphery of the labeled somata. Punctate X-gal labeling is not uncommon in neurons with low β-gal expression (see, for example, Ref. [42]) and is sometimes associated with the accumulation of X-gal precipitate in subcellular organelles such as the endoplasmic reticulum[43]. In the case of *Opn5*$^{-/-}$ retinas, a low β-gal expression may be a combined result of weak *Opn5*-promoter activity (supported by quantitative RT-PCR results by Xiaozhi Ren; data not shown) and low translation efficiency via the Internal Ribosome Entry Site (IRES). For

the same reason, our estimate of ~5,000 *Opn5*-expressing cells per retina could be an underestimate because neurons with extremely weak *Opn5*-promoter activity might not have been revealed by X-gal labeling, as is the case of non-M1-subtype ipRGCs, which have low OPN4 expression, in *Opn4*$^{-/-}$ retinas[44–46]. As a separate way to detect β-gal expression, we have tested a number of commercial antibodies against β-gal on *Opn5*$^{-/-}$ Line 1 retinas, but have not observed any specific immuno-labeling.

To functionally validate that retinal ganglion cells are required for retinal circadian photoentrainment, we performed *ex vivo* photoentrainment assays on *Math5*$^{-/-}$ retinas, in which over 80% of ganglion cells are absent developmentally[47]. The deletion of *Math5* has not been linked to a major loss of other retinal cell types[47], although some reductions in one amacrine-cell subtype (A2 amacrines), rod bipolar cells and Müller cells have been reported in another *Math5*$^{-/-}$ mouse line[48]. Interestingly, *Math5*$^{-/-}$ retinas still maintained robust circadian rhythmicity with normal amplitude, but were unable to photoentrain (Fig. 4-10d). In addition, *Math5*$^{-/-}$ retinas also experienced a large decrease in *Opn5* mRNA expression (Fig. 4-10e). Taking all results together, OPN5 appears to be predominantly expressed in a small subset of *Math5*-dependent retinal ganglion cells.

To get some information about the physiology of OPN5-expressing retinal neurons, we set out to characterize the morphological and molecular features of these cells for comparison with those of known retinal neuronal subtypes. Because X-gal labeling in *Opn5*$^{-/-}$ retinas appeared punctate (see above), we turned to a fluorescent substrate of β-gal [5-chloromethylfluorescein di-β-D-galactopyranoside (CMFDG)] for producing more diffuse labeling of *Opn5*-expressing cells' somata and proximal processes. CMFDG did not stain fixed retinas; moreover, its labeling on live tissues

would not persist after fixation. Furthermore, CMFDG labeling appeared to be cytotoxic, causing cell membranes to break down and the fluorescent reaction product to leak out within 10 minutes. In order to reveal the full morphology of *Opn5*-expressing neurons, we therefore relied on the injection of fixable Alexa 555/488 hydrazides to the CMFDG-labeled cells. Owing to the rapid dissipation of injected dyes from the leaky cell membranes, only 4 of 20 injected cells successfully retained enough dye to show discernable cell bodies and primary dendrites; three of these cells showed well-defined axons heading toward the optic disc, identifying them as retinal ganglion cells (Fig. 4-11). Unfortunately, the dye-leakage problem has prohibited further analyses of the cells' detailed morphologies, including the stratification of their dendritic arbors. It should also be mentioned that, based on control experiments on *Opn4*$^{-/-}$ retinas, CMFDG only labeled a selective fraction of β-gal-expressing cells (e.g., non-M1-ipRGCs in *Opn4*$^{-/-}$ retinas; data not shown), probably because it could not penetrate certain cell types. Thus, our survey of *Opn5*-expressing cells by CMFDG labeling here might be biased.

To prepare for single-cell recordings *in situ*, we have also tried to genetically label *Opn5*-expressing cells using alternative strategies. We have generated Bacterial Artificial Chromosome (BAC) transgenic *Opn5-Cre* mouse lines by inserting the Cre recombinase cDNA at the start codon of the *Opn5* gene in the BAC (work by Xiaozhi Ren). The specificity of the lines was evaluated by noting the types and numbers of retinal cells labeled after crossing the individual transgenic lines to the *Rosa-tdTomato* or *Rosa-EYFP* line. So far, we have not obtained a specific line; we observed either no labeling or labeling of diverse cell types, including horizontal, bipolar, amacrine and ganglion cells, in the 8 transgenic lines screened (Fig. 4-12). To aim for higher specificity, we made a

similar *Opn5-Cre* mouse line (with insertion of *Cre* cDNA at the start codon of the endogenous *Opn5* gene) by the conventional knock-in methodology (work by Xiaozhi Ren). The *Opn5*$^{Cre/+}$*;Rosa-tdTomato* retinas thus obtained showed labeling of typically clusters of cells with variable dendritic morphologies in the INL, and in some occasions, also a few cells in the GCL (Fig. 4-12). The number of cells labeled per retina varied from animal to animal. Besides, for unknown reasons, homozygosity in the knock-in *Opn5-Cre* allele appeared to cause embryonic lethality (out of 85 pups born, 0 was homozygous, 57 were heterozygous and 28 were WT). This phenotype could not be explained simply by the loss of *Opn5* expression because both *Opn5*$^{-/-}$ Lines 1 and 2 were vital. Owing to the above uncertainties, we are currently generating another knock-in *Opn5-Cre* mouse line with *Cre* cDNA inserted (after a sequence coding for the 2A peptide) in the middle of the *Opn5* gene, across exons 3 and 4 where the *tau-lacZ* cDNA was likewise inserted in *Opn5*$^{-/-}$ Line 1. This design would hopefully allow any gene-regulatory elements downstream of the *Opn5* promoter to also regulate the expression of *Cre*. When *Opn5*$^{Cre/+}$*;Rosa-tdTomato* mice from this line become available, we shall again examine the labeling pattern in the retina. Further validation will be done with *Opn5*$^{Cre/\tau lacZ}$ retinas, in which *Opn5*-expressing cells are expected to express both Cre and β-gal. A specific *Opn5-Cre* mouse line will be of great use for future study of OPN5's phototransduction pathway and for tracing the axonal projections of *Opn5*-expressing cells to the brain, giving clues about the visual functions that these cells may mediate.

Finally, we have not yet been able to specify the *Opn5*-expressing cells in the mouse cornea. No signal was detected by X-gal labeling, as well as immunohistochemistry with antibodies against OPN5 or β-gal, probably due to an

extremely low expression of OPN5 in the cornea. This is perhaps not surprising given the lower expression of *Opn5* mRNA in the cornea than in the retina as demonstrated by quantitative RT-PCR (Fig. 4-13).

4.6 Discussion

In the above work, we have identified a function of the mammalian orphan opsin OPN5 in mediating the photoentrainment of circadian rhythms in the retina and the cornea. Circumstantial evidence suggests that OPN5 is the photopigment underlying this entrainment. First, retinal photoentrainment is most effective with UV-A and violet light, consistent with a λ_{max} of 360 nm for OPN5 measured in heterologous systems. Second, retinas from mice with the predicted G protein-binding site of OPN5 mutated (from DRY to RDY, see Method) showed a partial defect in photoentrainment in preliminary experiments (data not shown), supporting that OPN5 acts as a signaling G protein-coupled receptor as opposed to a photoisomerase (as its close homology to the photoisomerase RGR-opsin may have suggested). The incomplete loss of function in these mutant retinas may be due to the existence in OPN5 of other G protein-activating motifs, such as NPxxY (see Chapter 1.3). OPN5 would be more firmly established as the light-sensor underlying retinal photoentrainment if one can: (1) obtain a more refined action spectrum of photoentrainment with a peak at around 360 nm, (2) demonstrate that retinas with a mutation in the chromophore-binding site of OPN5 fail to photoentrain, and/or (3) show that OPN5 is necessary for some light sensitivities at the cellular level.

OPN5 protein has been detected by immunohistochemistry in the GCL of marmoset retinas[35]. Whether OPN5 serves a similar circadian-regulation function in

primate retinas remains an open question. As for mouse OPN5, heterlogously-expressed human OPN5 has a λ_{max} of 360-380 nm[34,35]. However, transmission of UV light in the human eye[49] is much more limited than in its mouse counterpart[50], with the human lens being an effective filter against light shorter than 400 nm[49]. That said, there is still abundant blue light admitted to the retina under bright sunlight for potentially activating OPN5. A more meaningful discussion will require a better understanding of the photochemistry of OPN5, including its absorption coefficient, quantum efficiency, spectral-tuning mechanism, etc.

An interesting related aspect is the apparent bistability of OPN5. Mammalian OPN5, when heterologously-expressed, has a stable active state that is capable of reverting back to its resting state by the absorption of another photon[34,35]. Nevertheless, distinct from non-mammalian OPN5 and most of the other known bistable pigments, mammalian OPN5 does not bind all-trans retinal directly[35]. Whether these properties have any functional significance, especially *in vivo*, is currently unknown. In our retinal cultures, OPN5's photosensitivity could be sustained by chromophore provided by Müller glia[51,52]. In the intact eye, some of these chromophores, and those from the retinal pigmented epithelium, may be delivered to the cornea by interphotoreceptor retinoid-binding protein in the aqueous and vitreous humors[53] for supporting OPN5's function. What is more curious is the ability of isolated cornea to remain photoentrainable after days in culture. Without an obvious source of chromophore in the cornea, this may indirectly argue for the bistable nature of OPN5 *in vivo*.

It is surprising that all known retinal photoreceptors – rods, cones and ipRGCs – do not appear to contribute to circadian photoentrainment. As found in previous and

current work, *rd1/rd1;Opn4*$^{-/-}$ retinas photoentrained normally[27], whereas *Opn5*$^{-/-}$ retinas were non-photoentrainable even in the presence of other photoreceptors, thus demonstrating that rods, cones and ipRGCs are neither necessary nor sufficient for retinal photoentrainment. As such, the photoentrainment of the retinal clock is in effect mechanistically segregated from that of the SCN clock. What may be a selective advantage, if any, for this segregation? It is known that many aspects of rods', cones' and ipRGCs' functions (e.g., expression of their photopigments[54–57] and phototransduction components[57], electrical-coupling efficiency[22] and other response properties[58]) are themselves subject of circadian and/or acute light control. Maintaining a retinal clock independent of the functioning of these photoreceptors may help to avoid the formation of some futile regulatory cycles and to keep an objective measure of day and night. It would be of interest to see if OPN5's expression and function are indeed immune to circadian and/or light control.

The fact that signals from rods and cones failed to photoentrain *Opn5*$^{-/-}$ retinas also raises the question of how OPN5-expresing cells, which are presumably ganglion cells, could discriminate between light signals originated synaptically from the rod-cone pathways and those intrinsically from OPN5. Perhaps the most straightforward solution is that OPN5 initiates a non-electrical response, in contrast to a change in membrane conductance typically associated with signaling photopigments. Alternatively, OPN5 may still trigger an electrical response, but with temporal characteristics so different from those of a synaptically-evoked response that it could be differentially interpreted by downstream machinery. Another more remote possibility is that OPN5-expressing cells enjoy a private circuitry isolated from the rod-cone pathways. Our future goals are to map

out the phototransduction pathway downstream of OPN5 by pharmacological and genetic manipulations, as well as to study the retinal input and central output of OPN5-expressing cells by electrical recordings.

It is worth pointing out that OPN5 is unlikely to be present in every rhythmic retinal neuron and to drive cell-autonomously the photoentrainment of their rhythms. First, our X-gal labeling results suggested that OPN5 is probably expressed in only a subset of retinal ganglion cells, whereas *Per2::Luciferase* rhythm has been reported to be concentrated in the INL[59]. Secondly, the rhythm amplitude was largely unperturbed in *Math5*$^{-/-}$ retinas, but its photoentrainment was abolished and *Opn5* expression was drastically reduced. How, then, do OPN5-expressing cells communicate a phase-shift to the rhythmic neurons? Ruan et al.[59] has described the effect of applying various neurotransmitter receptor agonists to cultured *Per2::Luciferase* retinas, but found no obvious phase-shift of the free-running retinal circadian clock with agonists for melatoninergic, glutamatergic, cholinergic, GABAergic or glycinergic transmission. We are planning to re-examine the contribution of these means of neurotransmission more specifically by combining our photoentrainment assay with the application of neurotransmission inhibitors. Certainly, release of neuropeptide as the entrainment signal remains an intriguing possibility.

The OPN5-mediated corneal photosensitivity represented, to our knowledge, the first evidence for a photosensory function in the mammalian cornea. It is also one rare example of opsin-dependent, extra-retinal photoreception in mammals (see Chapter 3 for another example). Nevertheless, we caution that there is currently no indication of its physiological importance *in vivo*. In particular, the corneal clock may be photoentrained

dominantly via SCN control *in vivo*. More also need to be understood about the corneal cell types expressing OPN5 and/or showing *Per2::Luciferase* rhythm, as well as about its precise photoentrainment mechanism in comparison to that of the retina. An equally exciting, unexplored area is the role of OPN5 in other body tissues, such as the brain and certain skin cells[34,35], both in or not in relation to circadian control.

4.7 Figures

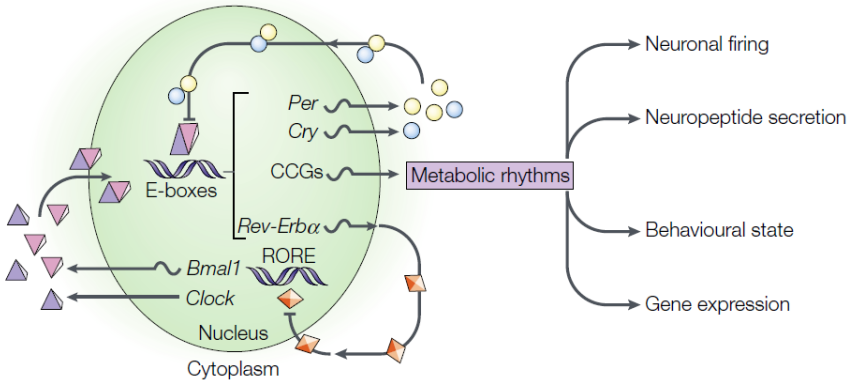

Fig. 4-1 Molecular mechanism of the mammalian circadian clock. The mammalian circadian cycle begins with E-box-mediated activation of genes including *Per*, *Cry*, *Rev-Erbα* and other clock-controlled genes (CCGs) by CLOCK (purple pyramids) and BMAL1 (pink pyramids). CCGs partake in a variety of metabolic activities and represent the output of the circadian clock. In mid- to late-circadian day, two feedback mechanisms come into operation: PER (yellow circle) and CRY (blue circle) complex inhibits CLOCK/BMAL1-activated gene expression while REV-ERBα (red diamond) represses *Bmal1* transcription. The circadian cycle is completed by the ubiquitination and degradation of PER, CRY and REV-ERBα (not shown). More descriptions are in the text. Adapted by permission from Macmillan Publishers Ltd: Nature Reviews Neuroscience (Ref. 3), copyright (2003).

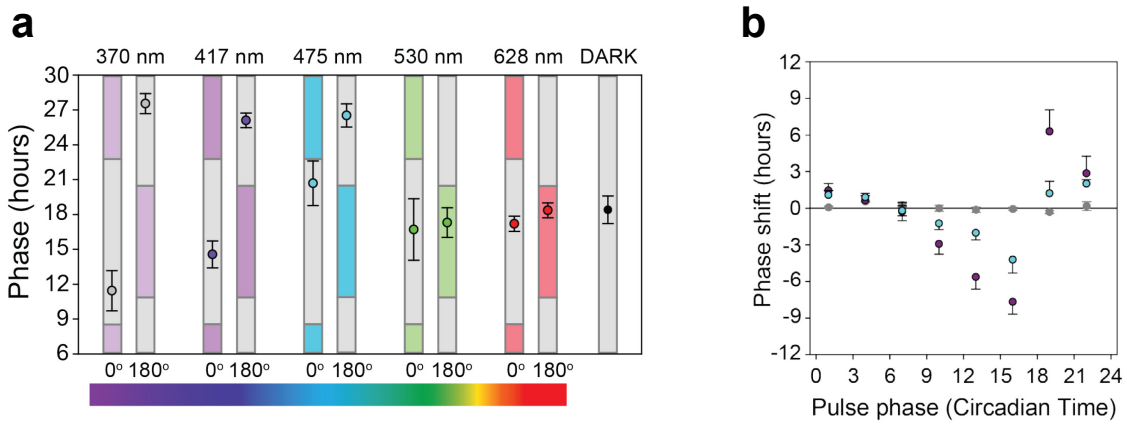

Fig. 4-2 Wavelength-dependence of photoentrainment of retinal rhythm. a, Pairs of *Per2::Luciferase* retinas were cultured for 4 days in anti-phase (0° and 180°) under 9-hr/15-hr cycles of light of different wavelengths (vertical colored bars) and darkness (vertical grey bars). Light intensity was the same at all wavelengths except for 370 nm (see Chapter 4.2 and Methods). Points indicate the mean phases (± 1 SEM) at which luciferase-dependent bioluminescence peaked on the day immediately after the light/dark exposure. Controls were retinas cultured in continuous darkness (DARK). 370 nm: n = 6 pairs, $p < 0.001$ for 1-way ANOVA and Tukey post-hoc comparisons of 0^o vs. 180^o, 0^o vs. DARK and 180^o vs. DARK; 417 nm: n = 6 pairs, $p < 0.001$ for comparisons of 0^o vs. 180^o, 0^o vs. DARK and 180^o vs. DARK; 475 nm: n = 7 pairs, p = 0.038, 0.007 and > 0.5, respectively, for comparisons of 0^o vs. 180^o, 0^o vs. DARK and 180^o vs. DARK; 530 nm and 628 nm: n = 5 pairs each, all comparisons insignificant. **b,** Phase-response curves of *Per2::Luciferase* retinas exposed to a 3-hr pulse of 417-nm (purple) or 475-nm (blue) light. Controls (grey) were not subjected to light. "Pulse phase" denotes the initial phase of the retinas at which point the stimulation was administered. Phase shifts ($n \geq 5$ for each point) are mean ± SEM. Figures modified from Ref. 28.

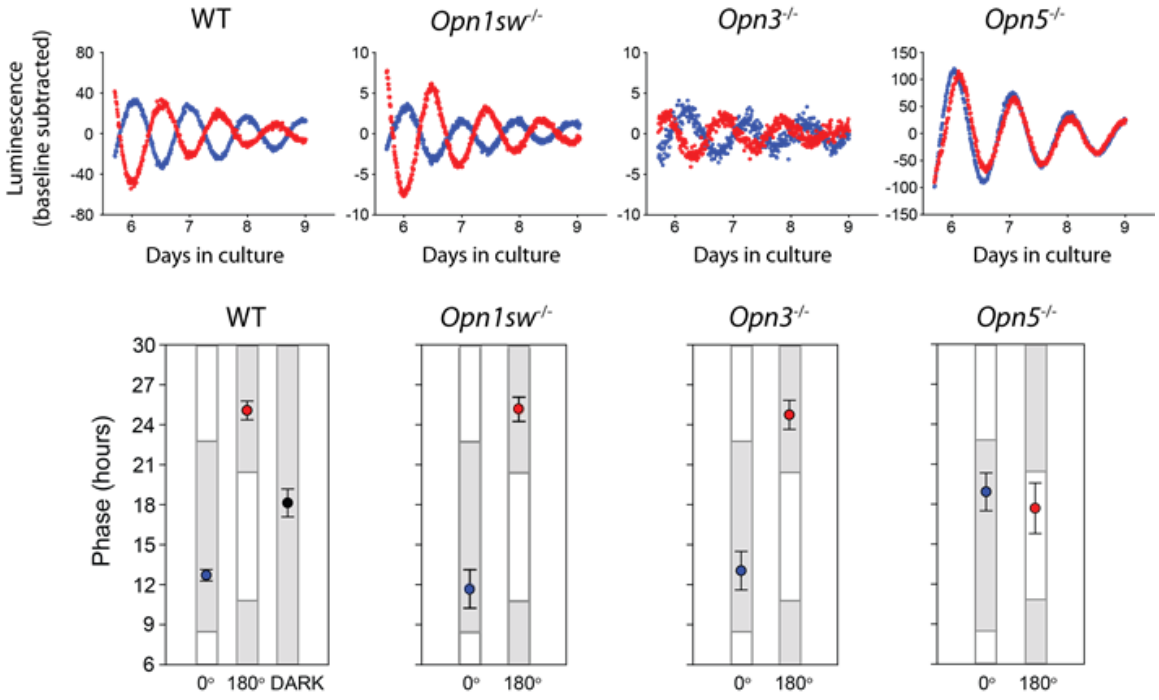

Fig. 4-3 Photoentrainment of circadian rhythms in *Opn1sw*$^{-/-}$, *Opn3*$^{-/-}$ and *Opn5*$^{-/-}$ (Line 1) retinas. Upper, bioluminescence traces recorded in the dark from a pair of wildtype (WT), *Opn1sw*$^{-/-}$, *Opn3*$^{-/-}$ or *Opn5*$^{-/-}$ (all in *Per2:: Luciferase* background) retinas after 4 days of culturing at the 0^{o} (blue) or 180^{o} (red) position of the light/dark photoentrainment apparatus (see Method). White light (5 W m^{-2}) was used in these experiments. Lower, phases of peak bioluminescence (points, mean ± SEM). Vertical bars indicate periods of darkness (grey) and light exposure (white, 5 W m^{-2}) as in Fig 4-2. Controls were retinas kept in continuous darkness (DARK). WT: n = 7 pairs; *Opn1sw*$^{-/-}$: n = 7 pairs; *Opn3* $^{-/-}$: n = 6 pairs; *Opn5* $^{-/-}$ (Line 1): n = 7 pairs. Figures modified from Ref. 28.

a *Opn3*$^{tlox/tlox}$ targeting construct

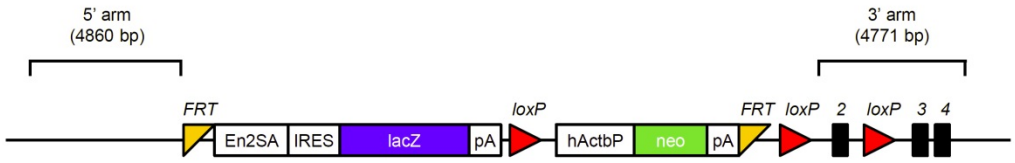

b *Opn5*$^{\tau lacZ/\tau lacZ}$ targeting construct

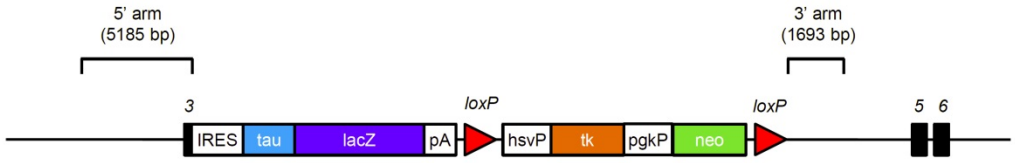

c *Opn5*$^{tlox/tlox}$ targeting construct

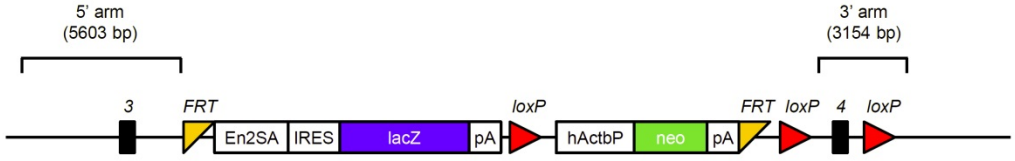

d

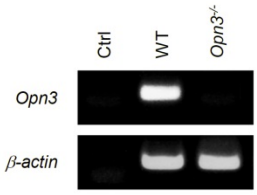

e

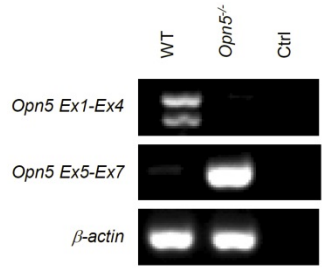

f

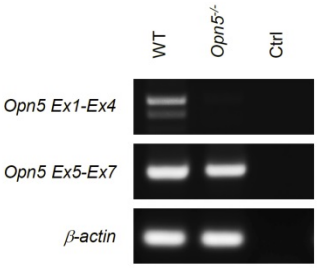

Fig. 4-4 Generation of *Opn3*$^{-/-}$ and *Opn5*$^{-/-}$ mice. a-c, Schematics of the *Opn3*$^{flox/flox}$ (**a**), *Opn5*$^{τlacZ/τlacZ}$ (**b**) and *Opn5*$^{flox/flox}$ (**c**) targeting constructs. See Methods for detailed descriptions. Dark bars: exons; En2SA: mouse *Engrailed2* intron splice acceptor; IRES: internal ribosome-entry site; lacZ: β-galactosidase cDNA; pA: SV40 polyadenylation site; hActbP: human β-actin promoter; neo: neomycin-resistance gene; tau: cDNA of microtubule-associated protein tau; hsvP: Herpes Simplex virus promoter; tk: thymidine kinase; pgkP: mouse phosphoglycerate kinase 1 promoter. **d,** RT-PCR experiment on total eye RNA to verify the absence of *Opn3* transcripts in *Opn3*$^{-/-}$ mice. The housekeeping gene *β-actin* served as a positive-control for reverse-transcription. Pure water was used as negative-control for PCR (Ctrl). **e,** RT-PCR experiment on total eye RNA to verify the absence of *Opn5* transcripts in *Opn5*$^{τlacZ/τlacZ}$ mice. Two *Opn5* isoforms could be detected with PCR spanning exon 1 to 4 (Ex1-Ex4) as previously reported (Ref); the lower band corresponds to a protein-coding isoform and the upper band to a non-coding isoform that contains an unspliced exon. A 3'-transcript of *Opn5* (exon 5 to 7, band is dim in WT) was abundant in *Opn5*$^{-/-}$ eyes, possibly being transcribed from the knocked-in *pgk* promoter (see Methods). Negative-control for PCR (Ctrl) was from RNA-extraction buffer processed identically but with no tissues. **f,** RT-PCR experiment on total eye RNA to verify the absence of *Opn5* transcripts in *Opn5*$^{-/-}$ (Line 2) mice. Two *Opn5* isoforms could be detected by PCR spanning exon 1 to 4 as in **e**. A 3'-transcript of *Opn5* (exon 5 to 7) was still present in *Opn5*$^{-/-}$ Line 2 at roughly WT level, resulting probably from the splicing of the exon 3 into exon 5 (see Methods). Control (Ctrl) was pure water. Figures adapted from Ref. 28.

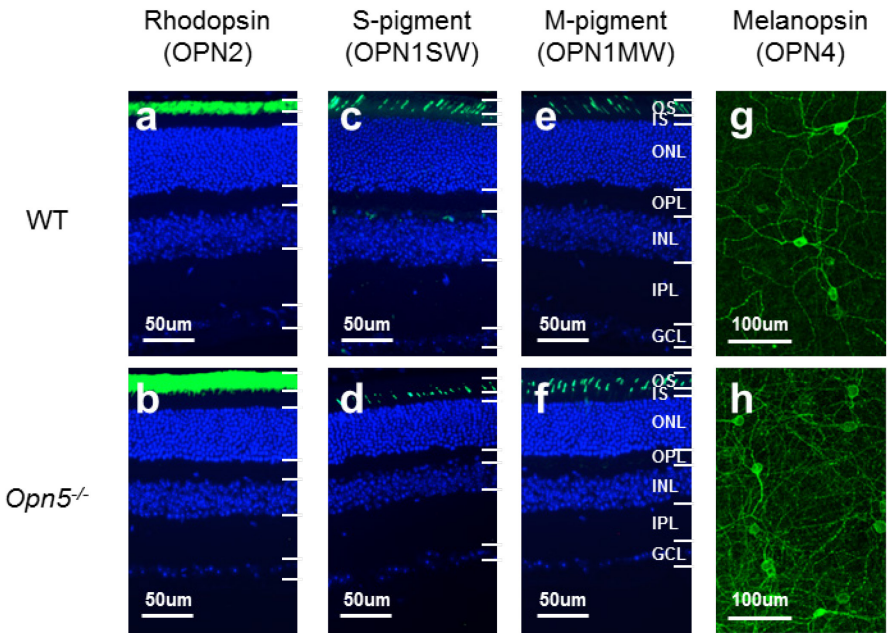

Fig. 4-5 Expressions of rod/cone opsins and melanopsin in *Opn5*$^{-/-}$ (Line 1) retinas. a-f, Retinal sections of WT and *Opn5* $^{-/-}$ (Line 1) mice immunostained (green) for rhodopsin, S-cone pigment (OPN1SW) and M-cone pigment (OPN1MW). Nuclear layers are defined by DAPI (blue) signals. OS, outer segment layer; IS, inner segment layer, ONL, outer nuclear layer; OPL, outer plexiform layer; INL, inner nuclear layer; IPL, inner plexiform layer; GCL, ganglion cell layer. We also found no ectopic expression of the above pigments in flat-mount retinas by immunohistochemistry (data not shown). **g-h,** Flat-mounts of WT and *Opn5* $^{-/-}$ (Line 1) retinas immunostained for melanopsin. Images are stacked confocal images. Figures adapted from Ref. 28.

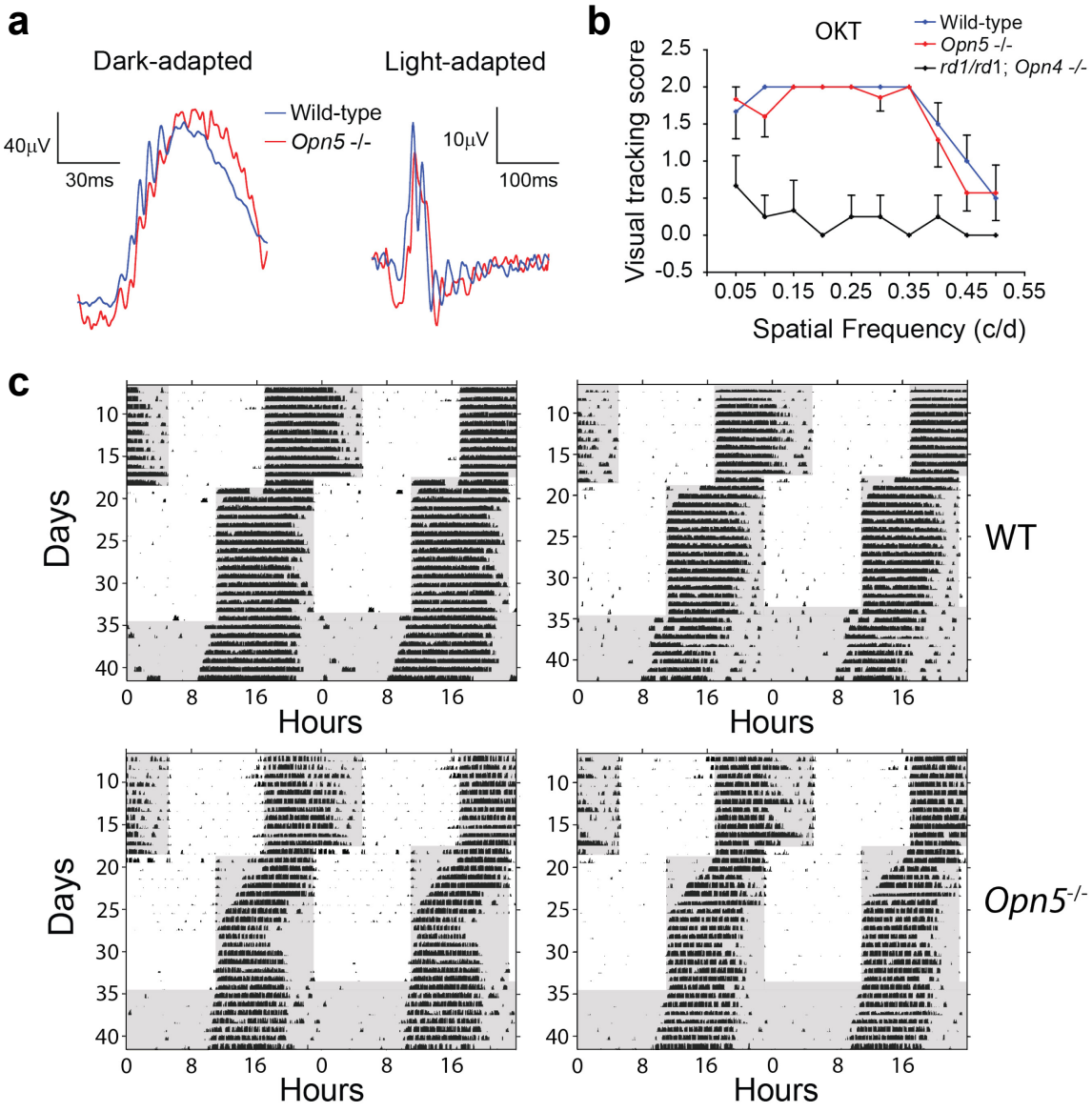
a
Dark-adapted
Light-adapted
Wild-type
Opn5 -/-
40μV
30ms
10μV
100ms
b
OKT
Wild-type
Opn5 -/-
rd1/rd1; Opn4 -/-
Visual tracking score
2.5
2.0
1.5
1.0
0.5
0.0
-0.5
0.05 0.15 0.25 0.35 0.45 0.55
Spatial Frequency (c/d)
c
Days
Hours
WT
Opn5-/-

Fig. 4-6 Electrophysiological and behavioral tests of visual functions in *Opn5*$^{-/-}$ (Line 1) mice. a, Examples of average traces from dark and light-adapted ERGs of WT (blue) and *Opn5*$^{-/-}$ (red) mice, both in *Per2::Luciferase* background. Experimental conditions are described in Methods. **b,** Optokinetic tracking reflexes of WT (blue), *Opn5*$^{-/-}$ (red) and *rd1/rd1;Opn4*$^{-/-}$ (black) mice, all in *Per2::Luciferase* background. Responses were scored based on the degree of head movements in response to the rotating gratings (See Methods). WT: n = 6; *Opn5*$^{-/-}$: n = 7; *rd1/rd1;Opn4*$^{-/-}$: n = 4. **c,** Examples of wheel-running actograms of two WT (upper) and two *Opn5*$^{-/-}$ (lower) mice, both in *Per2::Luciferase* background. Actograms are double-plotted so that each horizontal trace denotes two consecutive days, with the second day re-plotted as the first day in the trace below. Shaded areas indicate periods of darkness. Black marks are number of wheel revolutions in 5-minute bins. *Opn5*$^{-/-}$ mice photoentrained normally to a 12-hr/12-hr light/dark cycle (day 7-17), re-entrained normally (albeit more slowly) to a phase-advance in external light/dark cycles (day 19-33) and had normal free running periods (WT: 23.91 ± 0.06 hr, n = 6; *Opn5* $^{-/-}$: 23.89 ± 0.04 hr, n = 7; p = 0.762, Student's t-test) in constant darkness (day 35-41). Figures adapted from Ref. 28.

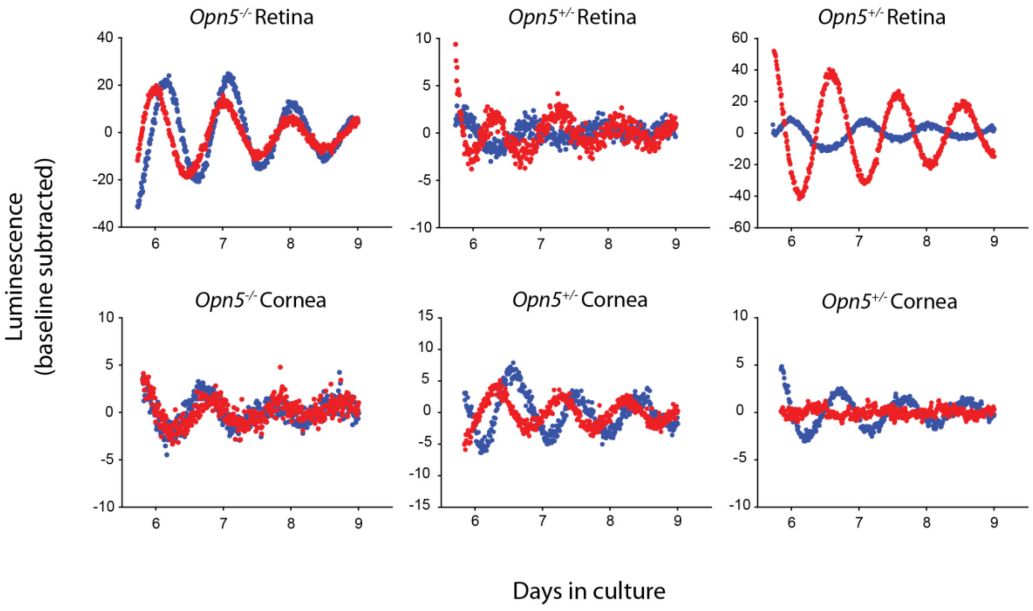

Fig. 4-7 Photoentrainment of circadian rhythms in transheterozygous *Opn5*$^{-/-}$ retinas and corneas. Upper, bioluminescence traces recorded in the dark from a pair of transheterozygous *Opn5*$^{-/-}$ (left, also see Chapter 4.4), *Opn5*$^{+/-}$ (Line 1) (middle) and *Opn5*$^{+/-}$ (Line 2) (right) retinas, all in *Per2::Luciferase* background, after 4 days of culturing at the 0^{o} (blue) or 180^{o} (red) position of the light/dark photoentrainment apparatus (see Method). White light (5 W m^{-2}) was used in these experiments. Lower, bioluminescence traces similarly recorded from corneas of the respective genotypes. Figures adapted from Ref. 28.

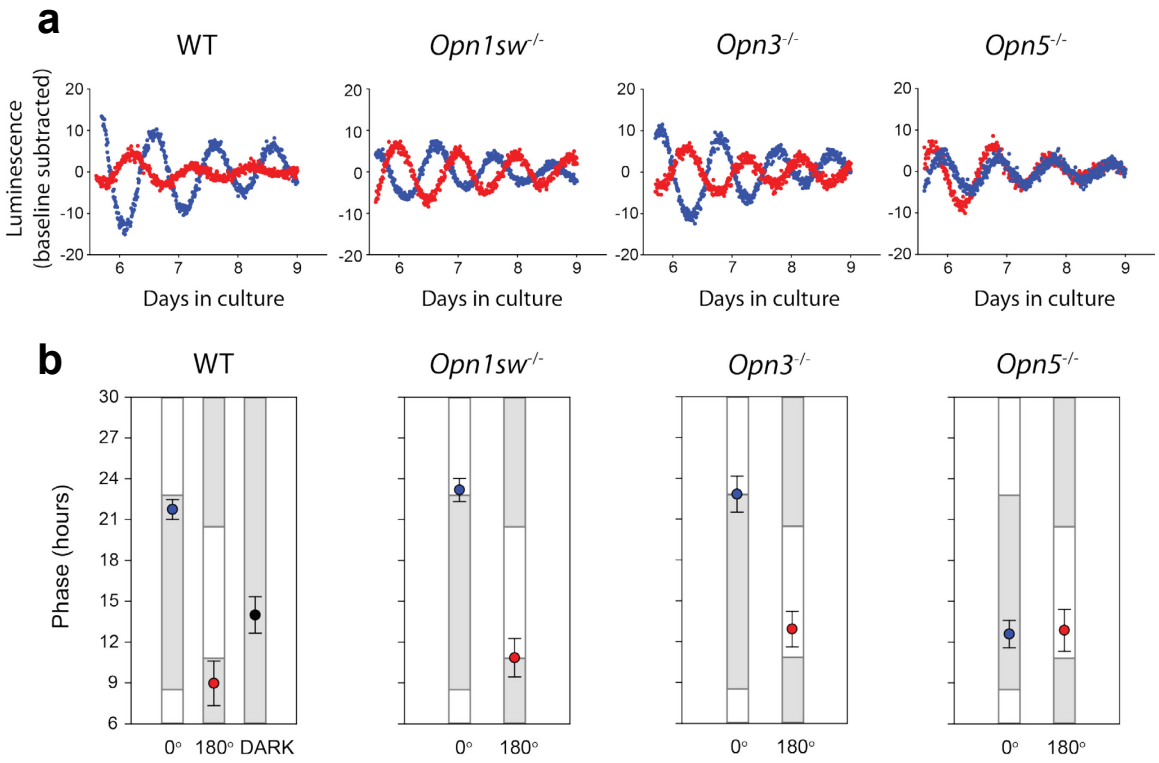

Fig. 4-8 Photoentrainment of circadian rhythms in *Opn1sw*$^{-/-}$, *Opn3*$^{-/-}$ and *Opn5*$^{-/-}$ (Line 1) corneas. a, Bioluminescence traces recorded in the dark from a pair of WT, *Opn1sw*$^{-/-}$, *Opn3*$^{-/-}$ or *Opn5*$^{-/-}$ (all in *Per2:: Luciferase* background) corneas after 4 days of culturing at the 0^{o} (blue) or 180^{o} (red) position of the light/dark photoentrainment apparatus (see Method). White light (5 W m^{-2}) was used in these experiments. **b,** Phases of peak bioluminescence (points, mean ± SEM). Vertical bars indicate periods of darkness (grey) and light exposure (white, 5 W m^{-2}) as in Fig. 4-3. Controls were corneas kept in continuous darkness (DARK). WT: n = 7 pairs; *Opn1sw*$^{-/-}$: n = 6 pairs; *Opn3*$^{-/-}$: n = 5 pairs; *Opn5*$^{-/-}$ (Line 1): n = 6 pairs. Figures adapted from Ref. 28.

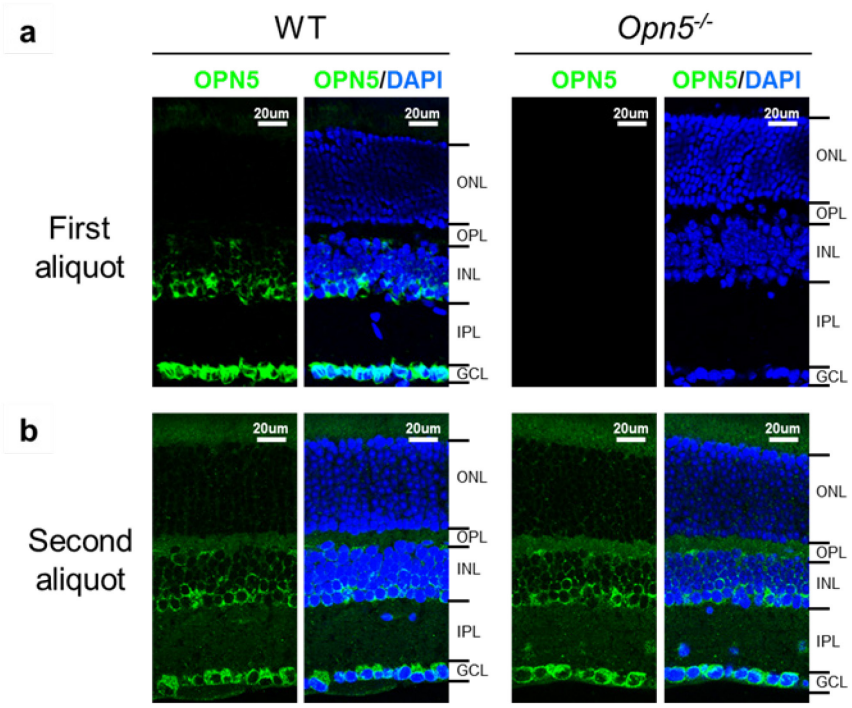

Fig. 4-9 Immunohistochemistry with an antibody against OPN5. a, Retinal cryosections of WT and *Opn5* $^{-/-}$ (Line 1) mice immunostained with an aliquot of an antibody against the N-terminus of OPN5 (Ref. 34). Nuclear layers are defined by DAPI (blue) signals. ONL, outer nuclear layer; OPL, outer plexiform layer; INL, inner nuclear layer; IPL, inner plexiform layer; GCL, ganglion cell layer. **b,** Retinal sections of WT and *Opn5* $^{-/-}$ (Line 1) mice processed identically as in **a**, but with another separately-purified aliquot of the same antibody obtained subsequent to the exhaustion of the first aliquot.

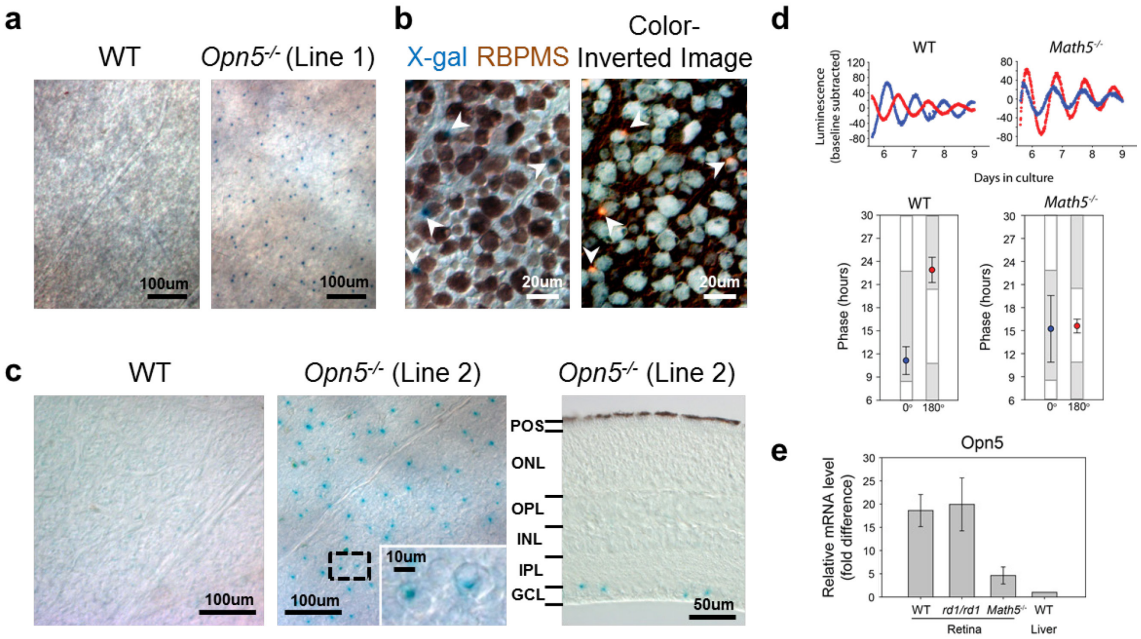
a
WT
Opn5-/- (Line 1)
100um
100um
b
X-gal RBPMS
Color-Inverted Image
20um
20um
c
WT
Opn5-/- (Line 2)
Opn5-/- (Line 2)
100um
100um
10um
POS
ONL
OPL
INL
IPL
GCL
50um
d
WT
Math5-/-
Luminescence (baseline subtracted)
Days in culture
Phase (hours)
0°
180°
e
Opn5
Relative mRNA level (fold difference)
WT
rd1/rd1
Math5-/-
WT
Retina
Liver

Fig. 4-10 Apparent *Opn5* expression in retinal ganglion cells. a, Flat-mounts of adult WT and *Opn5*$^{-/-}$ (Line 1) retinas stained with X-gal (blue puncta). **b,** WT and *Opn5*$^{-/-}$ (Line 1) retinas co-stained with X-gal (blue puncta) and an antibody against a retinal ganglion cell marker, Retinal Binding Protein with Multiple Splicing (RBPMS; brown). White arrowheads show examples of co-localization. Color-inverted and contrast-adjusted version of the images is re-produced on the right to better resolve the X-gal labeling and immunosignal. **c,** (Left and Middle) Flat-mounts of postnatal day 8 (P8) WT and *Opn5*$^{-/-}$ (Line 2) retinas stained with X-gal (blue puncta). Positive cells are enlarged in the inset. (Right) Section of a X-gal-stained P10 *Opn5*$^{-/-}$ (Line 2) retina, showing positive cells in the ganglion cell layer (GCL). No signal was detected in the inner plexiform layer (IPL), inner nuclear layer (INL), outer plexiform layer (OPL), outer nuclear layer (ONL), or photoreceptor outer segments (POS). **d,** (Top) Bioluminescence traces recorded in the dark from a pair of WT or *Math5*$^{-/-}$ (all in *Per2::Luciferase* background) retinas after 4 days of culturing at the 0^{o} (blue) or 180^{o} (red) position of the light/dark photoentrainment apparatus (see Method). White light (5 W m^{-2}) was used in these experiments. (Bottom) Phases of peak bioluminescence (points, mean ± SEM) as in Fig. 4-3. WT: n = 4 pairs; *Math5* $^{-/-}$: n = 4 pairs. **e,** Levels of *Opn5* mRNA (normalized to *Gadph* mRNA level) in WT, *rd1/rd1* or *Math5*$^{-/-}$ (all in *Per2::Luciferase* background) retinas relative to that in WT liver as quantified by the delta-delta threshold cycle ($2^{-\Delta\Delta Ct}$) method after RT-PCR. Figures adapted from Ref. 28.

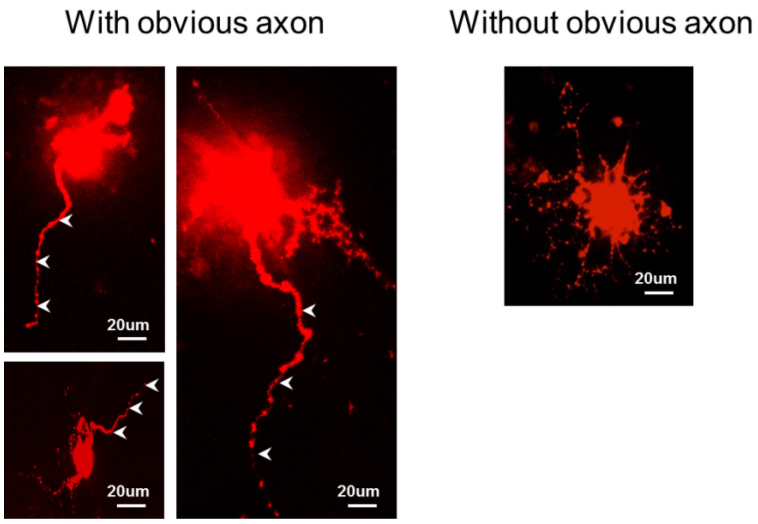

Fig. 4-11 Labeling of *Opn5*-expressing neurons by dye-injection. Neurons in *Opn5*$^{-/-}$ Line 1 retinas labeled with CMFDG (not shown) and injected with Alexa Fluor 555 hydrazide (red). Three of four cells that have retained the Alexa dye displayed obvious axons (arrowheads). Images were over-exposed to reveal the morphology of the axons. Dendritic arborizations were not revealed due to dye-leakage problem (see Chapter 4.5). Figures were stacked confocal images adapted from Ref. 28.

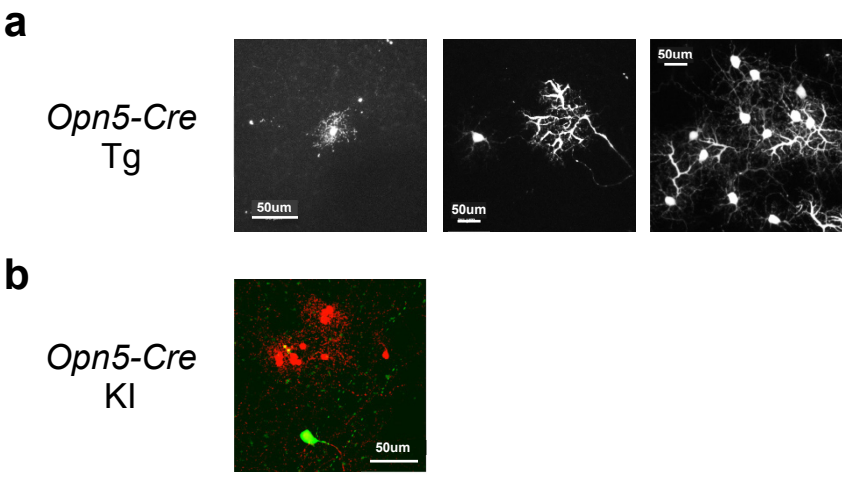

Fig. 4-12 Labeling of cells in *Opn5-Cre* mouse lines. a, Examples of cell types labeled in *Opn5-Cre*(BAC Transgenic)*;Rosa-tdTomato* retinas. Cell types were identified by dendritic and axonal morphologies. Left: bipolar cell; middle: horizontal cell; right: various cell types in the inner nuclear layer. **b,** Cluster of cells in the inner nuclear layer (red) and a ganglion cell (green) labeled in an *Opn5-Cre*(knock-in)*;Rosa-tdTomato* retinas.

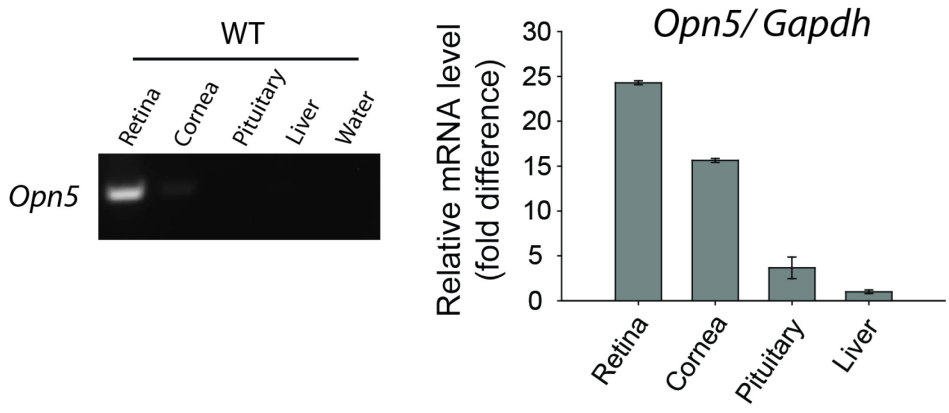

Fig. 4-13 Expression of *Opn5* in cornea. Levels of *Opn5* mRNA (normalized to *Gadph* mRNA level) in WT retina, cornea and pituitary tissues relative to that in WT liver as quantified by the delta-delta threshold cycle ($2^{-\Delta\Delta Ct}$) method after RT-PCR. All tissues: n = 3. Figures adapted from Ref. 28.

4.8 References

1. Kalsbeek, A. *et al.* Circadian rhythms in the hypothalamo-pituitary-adrenal (HPA) axis. *Mol. Cell. Endocrinol.* **349,** 20–29 (2012).

2. Nicolaides, N. C., Charmandari, E., Chrousos, G. P. & Kino, T. Circadian endocrine rhythms: The hypothalamic-pituitary-adrenal axis and its actions. *Ann. N. Y. Acad. Sci.* **1318,** 71–80 (2014).

3. Hastings, M. H., Reddy, A. B. & Maywood, E. S. A clockwork web: circadian timing in brain and periphery, in health and disease. *Nat. Rev. Neurosci.* **4,** 649–661 (2003).

4. Mohawk, J. A., Green, C. B. & Takahashi, J. S. Central and Peripheral Circadian Clocks in Mammals. *Annu. Rev. Neurosci.* **35,** 445–462 (2012).

5. Mohawk, J. A. & Takahashi, J. S. Cell autonomy and synchrony of suprachiasmatic nucleus circadian oscillators. *Trends Neurosci.* **34,** 349–358 (2011).

6. Webb, A. B., Angelo, N., Huettner, J. E. & Herzog, E. D. Intrinsic, nondeterministic circadian rhythm generation in identified mammalian neurons. *Proc. Natl. Acad. Sci. U. S. A.* **106,** 16493–16498 (2009).

7. Czeisler, C. A. *et al.* Stability, precision, and near-24-hour period of the human circadian pacemaker. *Science* **284,** 2177–2181 (1999).

8. Herzog, E. D., Takahashi, J. S. & Block, G. D. Clock controls circadian period in isolated suprachiasmatic nucleus neurons. *Nat. Neurosci.* **1,** 708–713 (1998).

9. Güler, A. D. *et al.* Melanopsin cells are the principal conduits for rod-cone input to non-image-forming vision. *Nature* **453,** 102–105 (2008).

10. Göz, D. *et al.* Targeted destruction of photosensitive retinal ganglion cells with a saporin conjugate alters the effects of light on mouse circadian rhythms. *PLoS One* **3,** (2008).

11. Hatori, M. *et al.* Inducible ablation of melanopsin-expressing retinal ganglion cells reveals their central role in non-image forming visual responses. *PLoS One* **3,** (2008).

12. Hattar, S. *et al.* Melanopsin and rod-cone photoreceptive systems account for all major accessory visual functions in mice. *Nature* **424,** 76–81 (2003).

13. Reppert, S. M. & Weaver, D. R. Coordination of circadian timing in mammals. *Nature* **418,** 935–941 (2002).

14. Meijer, J. H. & Schwartz, W. J. In search of the pathways for light-induced pacemaker resetting in the suprachiasmatic nucleus. *J. Biol. Rhythms* **18,** (2003).

15. Purrier, N., Engeland, W. C. & Kofuji, P. Mice Deficient of Glutamatergic Signaling from Intrinsically Photosensitive Retinal Ganglion Cells Exhibit Abnormal Circadian Photoentrainment. *PLoS One* **9,** e111449 (2014).

16. Ginty, D. D. *et al.* Regulation of CREB phosphorylation in the suprachiasmatic nucleus by light and a circadian clock. *Science* **260,** 238–241 (1993).

17. Ding, J. M., Faiman, L. E., Hurst, W. J., Kuriashkina, L. R. & Gillette, M. U. Resetting the biological clock: mediation of nocturnal CREB phosphorylation via light, glutamate, and nitric oxide. *J. Neurosci.* **17,** 667–675 (1997).

18. Gau, D. *et al.* Phosphorylation of CREB Ser142 regulates light-induced phase shifts of the circadian clock. *Neuron* **34,** 245–253 (2002).

19. Travnickova-Bendova, Z., Cermakian, N., Reppert, S. M. & Sassone-Corsi, P. Bimodal regulation of mPeriod promoters by CREB-dependent signaling and CLOCK/BMAL1 activity. *Proc. Natl. Acad. Sci. U. S. A.* **99,** 7728–7733 (2002).

20. Crosio, C., Cermakian, N., Allis, C. D. & Sassone-Corsi, P. Light induces chromatin modification in cells of the mammalian circadian clock. *Nat. Neurosci.* **3,** 1241–1247 (2000).

21. McMahon, D. G., Iuvone, P. M. & Tosini, G. Circadian organization of the mammalian retina: From gene regulation to physiology and diseases. *Prog. Retin. Eye Res.* **39,** 58–76 (2014).

22. Ribelayga, C., Cao, Y. & Mangel, S. C. The Circadian Clock in the Retina Controls Rod-Cone Coupling. *Neuron* **59,** 790–801 (2008).

23. LaVail, M. M. Rod outer segment disc shedding in relation to cyclic lighting. *Exp. Eye Res.* **23,** 277–280 (1976).

24. LaVail, M. M. Circadian nature of rod outer segment disc shedding in the rat. *Investig. Ophthalmol. Vis. Sci.* **19,** 407–411 (1980).

25. Tosini, G. & Menaker, M. Circadian Rhythms in Cultured Mammalian Retina. *Science* **272,** 419–421 (1996).

26. Ruan, G.-X., Zhang, D.-Q., Zhou, T., Yamazaki, S. & McMahon, D. G. Circadian organization of the mammalian retina. *Proc. Natl. Acad. Sci. U. S. A.* **103,** 9703–9708 (2006).

27. Buhr, E. D. & Van Gelder, R. N. Local photic entrainment of the retinal circadian oscillator in the absence of rods, cones, and melanopsin. *Proc. Natl. Acad. Sci. U. S. A.* **111,** 8625–30 (2014).

28. Buhr, E. D. *et al.* Neuropsin (OPN5)-mediated photoentrainment of local circadian oscillators in mammalian retina and cornea. *Proc. Natl. Acad. Sci. U. S. A.* (2015). doi:10.1073/pnas.1516259112

29. Semo, M., Vugler, A. a. & Jeffery, G. Paradoxical opsin expressing cells in the inner retina that are augmented following retinal degeneration. *Eur. J. Neurosci.* **25,** 2296–2306 (2007).

30. Greenwald, S. H., Kuchenbecker, J. A., Roberson, D. K., Neitz, M. & Neitz, J. S-opsin knockout mice with the endogenous M-opsin gene replaced by an L-opsin variant. *Vis. Neurosci.* **31,** 25–37 (2014).

31. Halford, S. *et al.* Characterization of a novel human opsin gene with wide tissue expression and identification of embedded and flanking genes on chromosome 1q43. *Genomics* **72,** 203–208 (2001).

32. Nissilä, J. *et al.* Encephalopsin (OPN3) protein abundance in the adult mouse brain. *J. Comp. Physiol. A Neuroethol. Sensory, Neural, Behav. Physiol.* **198,** 833–839 (2012).

33. Koyanagi, M., Takada, E., Nagata, T., Tsukamoto, H. & Terakita, A. Homologs of vertebrate Opn3 potentially serve as a light sensor in nonphotoreceptive tissue. *Proc. Natl. Acad. Sci. U. S. A.* **110,** 4998–5003 (2013).

34. Kojima, D. *et al.* UV-sensitive photoreceptor protein OPN5 in humans and mice. *PLoS One* **6,** (2011).

35. Yamashita, T. *et al.* Evolution of mammalian Opn5 as a specialized UV-absorbing pigment by a single amino acid mutation. *J. Biol. Chem.* **289,** 3991–4000 (2014).

36. Nakane, Y. *et al.* A mammalian neural tissue opsin (Opsin 5) is a deep brain photoreceptor in birds. *Proc. Natl. Acad. Sci. U. S. A.* **107,** 15264–15268 (2010).

37. Ohuchi, H. *et al.* A non-mammalian type opsin 5 functions dually in the photoreceptive and non-photoreceptive organs of birds. *PLoS One* **7,** e31534 (2012).

38. Stevenson, T. J. & Ball, G. F. Disruption of neuropsin mRNA expression via RNA interference facilitates the photoinduced increase in thyrotropin-stimulating subunit β in birds. *Eur. J. Neurosci.* **36,** 2859–2865 (2012).

39. Nakane, Y., Shimmura, T., Abe, H. & Yoshimura, T. Intrinsic photosensitivity of a deep brain photoreceptor. *Curr. Biol.* **24,** (2014).

40. Yoo, S.-H. *et al.* PERIOD2::LUCIFERASE real-time reporting of circadian dynamics reveals persistent circadian oscillations in mouse peripheral tissues. *Proc. Natl. Acad. Sci. U. S. A.* **101,** 5339–5346 (2004).

41. Hattar, S., Liao, H. W., Takao, M., Berson, D. M. & Yau, K. W. Melanopsin-containing retinal ganglion cells: architecture, projections, and intrinsic photosensitivity. *Science* **295,** 1065–1070 (2002).

42. Levitsky, K. L., Toledo-Aral, J. J., López-Barneo, J. & Villadiego, J. Direct confocal acquisition of fluorescence from X-gal staining on thick tissue sections. *Sci. Rep.* **3,** 2937 (2013).

43. Snyder, E. Y. *et al.* Multipotent Neural Cell-Lines Can Engraft and Participate in Development of Mouse Cerebellum. *Cell* **68,** 33–51 (1992).

44. Do, M. T. H. & Yau, K.-W. Intrinsically Photosensitive Retinal Ganglion Cells. *Physiol. Rev.* **90,** 1547–1581 (2010).

45. Sand, A., Schmidt, T. M. & Kofuji, P. Diverse types of ganglion cell photoreceptors in the mammalian retina. *Prog. Retin. Eye Res.* **31,** 287–302 (2012).

46. Bailes, H. J. & Lucas, R. J. Melanopsin and inner retinal photoreception. *Cell. Mol. Life Sci.* **67,** 99–111 (2010).

47. Wang, S. W. *et al.* Requirement for math5 in the development of retinal ganglion cells. *Genes Dev.* 24–29 (2001). doi:10.1101/gad.855301.mined

48. Brown, N. L., Patel, S., Brzezinski, J. & Glaser, T. Math5 is required for retinal ganglion cell and optic nerve formation. *Development* **128,** 2497–2508 (2001).

49. Ambach, W. *et al.* Spectral transmission of the optical media of the human eye with respect to keratitis and cataract formation. *Doc. Ophthalmol.* **88,** 165–173 (1994).

50. Henriksson, J. T., Bergmanson, J. P. G. & Walsh, J. E. Ultraviolet radiation transmittance of the mouse eye and its individual media components. *Exp. Eye Res.* **90,** 382–387 (2010).

51. Wang, J. S. & Kefalov, V. J. The Cone-specific visual cycle. *Prog. Retin. Eye Res.* **30,** 115–128 (2011).

52. Tang, P. H., Kono, M., Koutalos, Y., Ablonczy, Z. & Crouch, R. K. New insights into retinoid metabolism and cycling within the retina. *Prog. Retin. Eye Res.* **32,** 48–63 (2013).

53. Wiggert, B. *et al.* Immunochemical distribution of interphotoreceptor retinoid-binding protein in selected species. *Invest. Ophthalmol. Vis. Sci.* **27,** 1041–1049 (1986).

54. Sakamoto, K. Classical Photoreceptors Regulate Melanopsin mRNA Levels in the Rat Retina. *J. Neurosci.* **24,** 9693–9697 (2004).

55. Sakamoto, K. *et al.* Dopamine regulates melanopsin mRNA expression in intrinsically photosensitive retinal ganglion cells. *Eur. J. Neurosci.* **22,** 3129–36 (2005).

56. Hannibal, J., Georg, B., Hindersson, P. & Fahrenkrug, J. Light and darkness regulate melanopsin in the retinal ganglion cells of the albino Wistar rat. *J. Mol. Neurosci. MN* **27,** 147–155 (2005).

57. Storch, K. F. *et al.* Intrinsic Circadian Clock of the Mammalian Retina: Importance for Retinal Processing of Visual Information. *Cell* **130,** 730–741 (2007).

58. Weng, S., Wong, K. Y. & Berson, D. M. Circadian Modulation of Melanopsin-Driven Light Response in Rat Ganglion-Cell Photoreceptors. *J. Biol. Rhythms* **24,** 391–402 (2009).

59. Ruan, G. X., Allen, G. C., Yamazaki, S. & McMahon, D. G. An autonomous circadian clock in the inner mouse retina regulated by dopamine and GABA. *PLoS Biol.* **6,** 2248–2265 (2008).

Chapter 5 Methods

5.1 Animals

All animal experiments were conducted according to protocols approved by the Johns Hopkins University Institutional Animal Care and Use Committee. Animals were housed under a 12 hr/ 12 hr light/dark cycle unless specified otherwise. Table 5-1 summarizes the sources of mouse lines that were used in the current studies.

5.2 Generation of human green-cone opsin transgenic frogs

The human green-cone opsin cDNA was cloned into the pCS2+ vector under the control of the simian cytomegalovirus (sCMV) IE94 enhancer/promoter chosen to give strong expression in *Xenopus*. A pCS2+ construct carrying green fluorescent protein (GFP) was also prepared to facilitate the identification of transgenic animals. The constructs were linearized by enzyme digestion, purified and combined with permeabilized *Xenopus* sperm nuclei and egg extract in the presence of a small amount of restriction enzyme. The egg extract partially decondensed the sperm chromatin while the restriction enzyme introduced chromosomal breaks for integration of the transgenes. The concoction was then injected into unfertilized eggs collected from hormonally-primed females. The injection procedures were performed by the laboratory of Dr. Nicholas Marsh-Armstrong at Johns Hopkins University. Transgenic animals were identified by whole-body GFP expression and their genotypes were confirmed by PCR on tail DNA (Forward primer: 5'- TGG ACA GCC CCG CCC ATC TT -3'; Reverse primer: 5'- CTG

CTT TGC CAC CGC TCG GA -3'). Individual transgenic lines were established from these founder animals by breeding them with wildtype (WT) frogs.

Table 5-1 List of mouse lines

Mouse line	Description	Relevant chapter(s)	Source
Rho$^{E122Q/E122Q}$	Knock-in of a Glu-to-Gln mutation at amino acid residue 122 of rhodopsin	Ch 2	Yoshinori Shichida[1]
hOpn1lw^{+}	Transgenic expression of human red-cone opsin in rods	Ch 2	Own laboratory[2]
hOpn1mw^{+}	Transgenic expression of human green-cone opsin in rods	Ch 2	Current studies (see below)
Rho$^{REY/REY}$	Knock-in of a Glu-Arg-Tyr (ERY)-to-Arg-Glu-Tyr (REY) mutation in amino acid residues 134-136 (G-protein-binding site) of rhodopsin	Ch 2	Current studies (see below)
Gcaps$^{-/-}$	Knock-out of guanylate cyclase-activating proteins (*Gcaps*)	Ch 2	Jeannie Chen[3]
Rho$^{D190N/D190N}$	Knock-in of a Asp-to-Asn mutation at amino acid residue 190 of rhodopsin	Ch 2	Stephen Tsang[4]
Opn4-Cre	Transgenic expression of CRE recombinase under melanopsin (*Opn4*) promoter	Ch 3	Current studies (see below)
Rosa-tdTomato	Knock-in of tdTomato fluorescent protein into Rosa locus (Line Ai9: with *Neo*, more sensitive; Line Ai14: *Neo* deleted, less sensitive)	Ch 3	Jackson Laboratory
rd1/rd1	Spontaneous mutation in phosphodiesterase 6b (*Pde6b*) causing retinal degeneration	Ch 4	Jackson Laboratory
Opn1sw$^{-/-}$	Knock-out of S-cone opsin (*Opn1sw*)	Ch 4	Jay and Maureen Neitz[5]
Opn4$^{\tau lacZ/\tau lacZ}$	Knock-in of τlacZ into *Opn4* locus; also knock-out of *Opn4*	Ch 4	Own laboratory[6]
Opn5$^{\tau lacZ/\tau lacZ}$ or *Opn5*$^{-/-}$ (Line 1)	Knock-in of τlacZ into neuropsin (*Opn5*) locus; also knock-out of *Opn5*	Ch 4	Current studies[7] (see below)
Opn5$^{flox/flox}$ or *Opn5*$^{-/-}$ (Line 2)	Knock-in of loxP sites across exon 4 of *Opn5* for Cre-mediated knock-out	Ch 4	Richard Lang[7] (see below)
Opn3$^{flox/flox}$	Knock-in of loxP sites across exon 2 of encephalopsin (*Opn3*) for Cre-mediated knock-out	Ch 4	Current studies[7] (see below)
Per2::Luc	Knock-in of luciferase in fusion with PERIOD 2	Ch 4	Joseph Takahashi[8]
Opn5$^{RDY/RDY}$	Knock-in of a Asp-Arg-Tyr (DRY)-to-Arg-Asp-Tyr (RDY) mutation in amino acid residues 130-132 (G-protein-binding site) of OPN5	Ch 4	Current studies (see below)
Sox2-Cre	Transgenic expression of Cre recombinase globally in early embryos	Ch 4	Jackson Laboratory

5.3 Generation of human green-cone opsin transgenic mice

An expression cassette containing a 4.4-kb KpnI-XhoI fragment of the mouse rhodopsin promoter, the 1.1-kb human green-cone opsin cDNA with the sequence corresponding to the last ten amino acids at the C-terminus replaced by that of the last seven amino acids of rhodopsin (i.e., the 1D4 epitope TSQVAPA), as well as the polyadenylation signal from the mouse protamine gene, were assembled into the pBlueScript II KS^{+} vector by the laboratory of Dr. Jeannie Chen at University of Southern California. The cassette was released from the vector by enzyme digestion with BssHII. After purification, the DNA was injected into the pronuclei of C57BL/6J mouse embryos at the Transgenic Core Laboratory of Johns Hopkins University School of Medicine. Transgenic animals were identified by PCR on tail DNA (Forward primer: 5'-CAA AGC AGC AGA AAG AGT CTG AAT -3'; Reverse primer: 5'- CTG CGG CAG CAT CGG TAT -3'). Fourteen transgenic lines were established from these founder animals by breeding them with WT C57BL/6J mice. Three lines were eliminated because of the low rate of germ-line transmission of the transgene. The other lines were bred into $Rho^{REY/REY}$; $Gcaps^{-/-}$ background and screened for the expression of the human green-cone pigment based on the presence of large dim-flash responses (see Chapter 2.9).

5.4 Generation of $Rho^{REY/REY}$ knock-in mice

$Rho^{REY/REY}$ mice were generated by using the CRISPR/Cas system. Briefly, the CRISPR Design Tool (http://crispr.mit.edu/) was used for selecting two 20-bp target sequences close to the intended mutation site in the mouse rhodopsin gene (5'-TTGAGCGCTACGTGGTGGTC -3' and 5'- CCGATGAGCAACTTCCGCTT -3'). For

each target sequence, complementary DNA oligos were synthesized, annealed and cloned into the pX330 vector upstream of the trans-activating CRISPR RNA (tracrRNA) sequence to give a chimeric single-guide RNA (sgRNA) sequence. PCR-amplified product of this chimeric sequence was used as a template for *in vitro* transcription with the T7 Quick High Yield RNA synthesis kit (New England Biolabs). The resulting sgRNA was mixed with Cas9 mRNA (TriLink Biotechnologies) and a 166-bp synthesized oligo (5'- AGG TTA GAG CTG GAG GAC TGA CGG CTA CTA ACT GCC TTA CAG GTG AAA TCG CCC TGT GGT CCC TGG TGG TCC TGG CCA TTC GCG AGT ACG TGG TGG TCT GCA AGC CGA TGA GCA ACT TCC GCT TCG GGG AGA ATC ACG CCA TCA TGG GTG TGG TCT TCA CCT GGA T -3') for homology-directed repair. The mixture was injected into the pronuclei of *Gcaps*$^{+/-}$ embryos at the Transgenic Core Laboratory of Johns Hopkins University School of Medicine. Animals with the targeted mutation were identified by PCR on tail DNA. A set of 3 primers were used to genotype the rhodopsin allele: RhoWTFor: 5'- TGG TCC TGG CCA TTG AGC GC -3', RhoREYFor: 5'- TGG TCC TGG CCA TTC GCG AG -3' and RhoRev: 5'- CCT GGA ACC AAT CCG AGG GC -3'. The primer pair of RhoWTFor and RhoRev gave a 226-bp band for the wildtype allele whereas the pair of RhoREYFor and RhoRev gave a band of the same size for the mutant allele. Genomic PCR did not reveal any unintended mutations at off-target sites predicted by the CRISPR Design Tool. Still, the line has been crossed at least two times to *Gcaps*$^{-/-}$ mice to minimize any potential off-target effect.

5.5 Generation of *Opn4-Cre* mice

We insert the Cre recombinase cDNA, followed by the rabbit β-globin poly-A signal, immediately after the start codon of exon 1 of the mouse *Opn4* gene in a bacterial artificial chromosome (BAC) clone (BACPAC Resource Center, RP23-340N18) by bacterial homologous recombination. Successful modifications were confirmed by PCR and Southern blot. The modified BAC was linearized by enzyme digestion with AscI and SrfI, which also removed or destroyed neighboring genes in order to avoid their transgenic expression. The linearized BAC was injected into the pronuclei of B6SJLF2 embryos at the Transgenic Core Laboratory of Johns Hopkins University School of Medicine. Transgenic animals were identified by PCR on tail DNA (Forward primer: 5'-TGT GAA GGA CAG AGC CTC CT -3'; Reverse primer: 5'- CAG CCC GGA CCG ACG ATG AAG -3'). Three transgenic lines were established from these founder animals by breeding them with WT C57BL/6J mice. One of these lines showed specific expression of tdTomato in ipRGCs when crossed to the Ai14 *Rosa-tdTomato* line (Fig. 3-1) – 91% of cells showing tdTomato fluorescence were immunopositive for melanopsin and 85% of melanopsin-immunopositive cells were tdTomato-labeled (total 2342 cells from 3 animals analyzed). Because M4 and M5 subtypes of ipRGCs are known not to be stained by the melanopsin antibody (UF006) under regular conditions[9,10], some of the false-positive cells might be M4 or M5 ipRGCs. In fact, all cells labeled by *Opn4-Cre*-driven reporter (lines Ai9 and Ai14) that our laboratory has recorded so far (>150 cells) were intrinsically photosensitive. Unlike in the *Opn4-tdTomato* BAC transgenic line, where different ipRGC subtypes showed graded tdTomato intensities, labeled cells in

Opn4-Cre-driven reporter lines were equally bright, except for some large, dimmer cells that were likely M4 ipRGCs.

5.6 Generation of *Opn5*$^{\tau lacZ/\tau lacZ}$ mice [or *Opn5*$^{-/-}$ (Line 1)]

The *Opn5*$^{\tau lacZ/\tau lacZ}$ mouse line[7] was generated by homologous recombination by Hsi-Wen Rock Liao, a former student in our laboratory. A targeting construct was made to replace part of exon 3 and the entire exon 4 of the *Opn5* gene with a *tau-lacZ-floxed-neo* cassette, which was predicted to disrupt at least two transmembrane domains of the OPN5 protein (Fig. 4-4). The construct was linearized by enzyme digestion with AscI and electroporated into 129/SvJ1 embryonic stem cells at the Transgenic Core Laboratory of Johns Hopkins University School of Medicine. Successfully targeted stem-cell colonies were identified by G418-resistance and PCR on genomic DNA. They were then expanded and injected into C57BL/6J blastocytes. Chimeric mice thus derived were bred to C57BL/6J mice to obtain heterozygous animals, from which homozygous animals were produced from sibling crosses. To genotype the *Opn5* allele, a set of 3 primers were used: Opn5WTFor: 5'- TGC TTT ACC ATG CCC AGC TAA GC -3', Opn5KONeoFor: 5'- GCA GCC TCT GTT CCA CAT ACA CTT C -3', and Opn5Rev: 5'- GCC TCT CTG ACC TTA CCT TC -3'. The primer pair of Opn5WTFor and Opn5Rev gave a 182-bp band for the WT allele, whereas the pair of Opn5KONeoFor and Opn5Rev gave a 253-bp band for the *Opn5*-knockin allele. The *floxed-neo* cassette was retained in all experimental animals used in the current studies. The mouse phosphoglycerate kinase (PGK) promoter used for driving *neo* expression might have caused the upregulation of a 3' transcript of *Opn5* in these animals (see Chapter 4). To avoid this complication, we

have subsequently removed the *floxed-neo* cassette by crossing the *Opn5*$^{\tau lacZ/\tau lacZ}$ line to *Sox2-Cre* transgenic mice (Jackson Laboratory), which express Cre recombinase globally in early embryos. The genotyping protocol for the resulting animals was the same except for using Opn5KOpAFor: 5'- CCC CCT GAA CCT GAA ACA TA -3' instead of Opn5KONeoFor for the *Opn5*-knockin allele (band size: ~450 bp).

5.7 Generation of *Opn3*$^{flox/flox}$ mice

The *Opn3*$^{flox/flox}$ mouse line[7] was generated by homologous recombination by Dr. Xiaozhi Ren, a post-doctoral fellow in our laboratory. Embryonic stem cell clones (EPD0197_3_E01 in C56BL/6N background) were obtained from Knockout Mouse Project Repository and were confirmed positive by PCR for the targeted insertion of a pair of *loxP* sites across exon 2 of the *Opn3* gene, which encodes three transmembrane domains of the OPN3 protein, with also the introduction of an upstream FRT-flanked *lacZ-neo* cassette (Fig. 4-4). The clones were expanded and injected into 129/SvJ1 blastocytesto produce chimeric mice. Heterozygous, and subsequently homozygous, animals were obtained by breeding the chimeric mice with C57BL/6J mice and then performing sibling crosses. We generated an *Opn3*$^{-/-}$ mouse line by crossing the *Opn3*$^{flox/flox}$ line with a *Sox2-Cre* transgenic line. A set of 3 primers were used to genotype the *Opn3* alleles: OPN3WTFor: 5'- TGT ACC GTG GAC TGG AGA TCC AAG -3', OPN3KOFor: 5'- TTA TGG CCC ACA CCA GTG GC -3', and OPN3Rev: 5'- GTT CCC ACA CAC GAC CTG CTC -3'. The primer pair of OPN3WTFor and OPN3Rev gave a 530-bp band for the WT allele, whereas the pair of OPN3KOFor and OPN3Rev gave a 670-bp band for the Opn3-knockout allele.

5.8 Generation of *Opn5*$^{flox/flox}$ mice

The *Opn5*$^{flox/flox}$ mouse line[7] was generated by homologous recombination by the laboratory of Dr. Richard Lang at the University of Cincinnati Medical Center. Embryonic stem cell clones were obtained from International Knockout Mouse Consortium and were confirmed positive by PCR for the targeted insertion of a pair of *loxP* sites across exon 4 of the *Opn5* gene, which encodes two transmembrane domains of the OPN5 protein, with also the introduction of an upstream FRT-flanked *lacZ-neo* cassette (Fig. 4-4). The clones were expanded and injected into blastocytes to produce chimeric mice. The *Opn5*$^{flox/flox}$ line was crossed with *Rosa-FLP* mice and then with *Sox2-Cre* mice to give *Opn5*$^{-/-}$ (Line 2) mice. A set of 4 primers were used to genotype the *Opn5* alleles: F1: 5'-CAC AGT ATG TGT GAC AAC CT -3', R1: 5'-GTG GAC AGA TTA ACT GAA GC -3', F2: 5'-ACT ATC CCG ACC GCC TTA CT -3', and R2: 5'-GAA CTG ATG GCG AGC TCA GA -3'.

5.9 Generation of *Opn5*$^{RDY/RDY}$ knock-in mice

Opn5$^{RDY/RDY}$ mice were generated by using the CRISPR/Cas system as described above with the following modifications. Target sequences were 5'- GAT TAC CAT GAC TGC TGT CA -3' and 5'- GGA CCG CTA TCT GAA GAT CT -3'. The oligo for homology-directed repair was 5'- GGT TTG GCT GCC GCT GGT ATG GCT GGG CTG GAT TTT TCT TTG GCT GTG GAA GCC TGA TTA CCA TGA CTG CTG TCA GCC TGC GCG ACT ATC TGA AGA TCT GTT ATC TGT CTT ATG GTA AGC TTG AAG GTC CCT TGT TCC CTG ATA GGA AAG TTA GAT GAT CGG AGT G -3'. The mixture of sgRNA, Cas9 mRNA and repair oligo was injected into the pronuclei of

heterozygous *Per2::Luc* embryos. Animals with the targeted mutation were identified by PCR on tail DNA with the primer pair Opn5RDYFor: 5'- CAT TTT GTT GTC GTG GGT CA -3' and Opn5RDYRev: 5'- GAA GGG TTC TTG GTC ACT GAA -3'. Digestion of the PCR product with HindIII gave a 500-bp band for the wildtype allele and two bands of 384 bp and 116 bp respectively for the mutant allele. Genomic sequences at predicted off-target sites have not been checked but the mouse line has been crossed to WT C57BL/6J mice for 5 times before use.

5.10 Suction-pipette recordings

We used *Xenopus* beyond the peak of metamorphosis (stage 66; 2 – 5 cm long) and mice of 1 to 3 months old, except for the $Rho^{D190N/+};Gcaps^{-/-}$ mouse line, which we recorded at P18 to P21 for minimal photoreceptor degeneration. Animals dark-adapted overnight were euthanized and their eyes were removed under dim red light. The eyes were hemisected and the retinas were removed in Ringer (for *Xenopus*: 110 mM NaCl, 2.5 mM KCl, 1.6 mM $MgCl_2$, 1 mM $CaCl_2$, 10 mM glucose, 0.1 μg ml^{-1} bovine serum albumin and 10 mM HEPES, pH 7.8) or Locke's solution [for mouse: 112.5 mM NaCl, 3.6 mM KCl, 2.4 mM $MgCl_2$, 1.2 $CaCl_2$, 3 mM Na_2-succinate, 0.5 mM Na-glutamate, 0.02 mM EDTA, 10 mM glucose, 0.1% vitamins (Sigma-Aldrich), 0.1% amino-acid supplement (Sigma-Aldrich), 10 mM HEPES, pH 7.4 and 20 mM $NaHCO_3$ under infrared light. Retinas were stored in the respective solution, bubbled with 100% O_2 (Ringer) or 95% O_2/5% CO_2 (Locke's), at room temperature until use over not longer than 6 hours. When needed, a fraction of the retina was chopped into small pieces with a razor blade in the presence of DNase I (~20 U/ml) and was transferred to the recording

chamber perfused with bubbled Ringer at room temperature (for *Xenopus*) or Locke's solution at 37.5 ± 0.5°C (for mouse). Temperature was monitored by a thermistor situated close to the recorded cell.

Single-cell recordings were made under infrared light by drawing the outer segment of an isolated rod (for *Xenopus*), or of a rod projecting from a fragment of retina (for mouse), into a tight-fitting glass pipette containing either the Ringer solution (for *Xenopus*) or the following pipette solution (for mouse): 140 mM NaCl, 3.6 mM KCl, 2.4 mM $MgCl_2$, 1.2 mM $CaCl_2$, 0.02 mM EDTA, 10 mM glucose and 3mM HEPES, pH 7.4. For *Xenopus*, green rods were identified from red rods by their more slender outer segments and by their higher sensitivity to 420-nm over 520-nm light. In most experiments, light stimulation was 10- to 30-msec of monochromatic flashes. White flashes were used in some experiments involving $Rho^{REY/REY};Gcaps^{-/-}$ rods because of their low sensitivity; in those cases, the intensities equivalent to 500-nm light were calculated by matching the amplitudes of the dim-flash responses evoked by white light versus 500-nm light. Signals were sampled at 1 kHz through an Axopatch 200B amplifier and low-pass filtered at 20 Hz (8-pole Bessel), unless specified otherwise.

5.11 Analyses of photoresponses

Kinetic parameters of photoresponses were obtained as follows. Flash responses were typically averaged over many trials. A response was defined as a dim-flash response if its peak amplitude did not exceed 20% of the maximal response amplitude (R_{max}). The integration time (t_{int}) of a dim-flash response was given by $\int f(t)dt/f_p$, where $f(t)$ was the response waveform and f_p was the response's transient-peak amplitude. The time-to-peak

(t_{peak}) was measured as the duration between the middle of the flash and the transient peak of a dim-flash response. The time constant of response recovery (τ_{rec}) was estimated by fitting the late decay phase of a dim-flash response with the single-exponential function $f(t) = Ae^{-t/\tau}$, where $f(t)$ was the response waveform, A was a scaling constant and τ was the time constant in question. To measure the dominant time constant (τ_D), the time interval between the middle of a saturating flash and 10% recovery of the response from saturation (i.e., time-in-saturation or T_{sat}) was plotted against stimulus intensity in log scale; τ_D was given by the slope of the best-fitted line through the data points.

To determine the half-saturating flash intensity (σ), intensity-response relations were fit with the saturating exponential function $R/R_{max} = 1 - e^{-I_f/K}$, where R was the flash-response amplitude, R_{max} was the maximal response amplitude, I_f was the flash intensity (in photons μm^{-2}) and K was a constant; σ was given by $\sigma = K \ln 2$. The amplification constant (A_{amp}) was obtained by fitting the initial rising phase of a dim-flash response (normalized to the maximal response amplitude) with $R/R_{max} = \frac{1}{2}\Phi A_{amp}\left(t - t_{eff}\right)^2$, where R was the flash-response amplitude, R_{max} was the maximal response amplitude, Φ was the flash intensity (in number of photoisomerizations), t was the actual time and t_{eff} was a constant representing the effective delay time. The number of photoisomerizations (Φ) caused by a flash of intensity I_f (in photons μm^{-2}) was given by $\Phi = A_e I_f t_f$, where A_e was the effective collecting area and t_f was the duration of the flash. As stated in Eqn.4 of Chapter 2, the effective collecting area was defined by the diameter (d) and length (l) of the ROS, the quantum efficiency of rhodopsin ($Q_{isom} = 0.67$), the correction factor for light polarization (0.5 if unpolarized) as well as the axial pigment density (ρ = 0.016 μm^{-1}, Ref. 11,

confirmed by own recordings) by the equation $A_e = 2.303 \frac{\pi d^2 l}{4} Q_{isom} f \rho$. All values reported are average ± SEM, unless specified otherwise.

We estimated the amplitude of single-photon responses (a_{SPR}) by two methods. Responses of a rod to 50-100 identical dim flashes were first collected; an intensity that gave a ~50% failure rate was typically used. Assume that the number of events elicited per flash follows the Poisson distribution (which is characterized by having equal mean and variance), we have $m = \frac{\mu}{a_{SPR}} = \frac{\sigma^2}{a_{SPR}^2}$ (Eqn. 5), where m is the mean number of response per flash, μ is the mean response amplitude and σ^2 is the time-dependent ensemble variance of the dim-flash responses. The left and right side of Eqn. 5 represents the mean and variance of the underlying Poisson distribution, respectively. From Eqn. 5, the amplitude of the single-photon response could be calculated as the ensemble variance-to-mean ratio at the transient peak of the dim-flash responses (i.e., $a_{SPR} = \frac{\sigma^2}{\mu}$). Alternatively, we squared and scaled the mean of the dim-flash responses so that its initial rising phase matched that of the ensemble variance (i.e., $\sigma^2 = \frac{\mu^2}{m}$); in this case, the scaling factor would provide an estimate of m, and thus a_{SPR}.

5.12 Calculation of pigment content and half-time of a spontaneous event

For *hOpn1mw*$^+$ *Xenopus*, the expression level of the transgenic human green-cone pigment relative to the blue-cone pigment native to green rods was determined by fitting the action spectrum of a transgenic rod with a linear combination of A_2 spectral template

for the *Xenopus* blue-cone pigment (λ_{max} = 447 nm) and the transgenic green-cone pigment (λ_{max} = 579 nm). The spectral template was based on Govardovskii *et al.*[12].

For *hOpn1mw*$^{+}$*;Rho*$^{REY/REY}$*;Gcaps*$^{-/-}$ mice, the axial pigment density (ρ) of the transgenic human green-cone pigment was calculated as described in Chapter 2. A typical mouse rod outer segment is about 1.4 μm in diameter and 20 μm in length. Assuming a 3.5 mM pigment concentration[11], the number of rhodopsin molecules is about 6.5×10^7. The axial pigment density for rhodopsin is about 0.016 μm^{-1} (Ref. 11, confirmed by own recordings). Thus, the number of transgenic human green-cone pigment molecules was given by $\frac{\rho}{0.016} \times 6.5 \times 10^7$. The molecular rate constant of spontaneous activation of the green-cone pigment was calculated to be 2.6×10^{-8} sec^{-1} at 37°C from its λ_{max} of 530 nm by using Eqn. 1 and Eqn. 2 in Chapter 2, assuming $\alpha = 1$, $m = 45$ and $A = 1.88 \times 10^{-4}$ sec^{-1} as for other cone pigments. Multiplying this molecular rate constant with the number of transgenic pigment molecules gave the cellular rate constant, the reciprocal of which was taken to be the half-time of a spontaneous event.

5.13 Measurements of the rates of thermal activation

Continuous 10-min recordings were obtained from rods in complete darkness. Traces were usually low-pass filtered at 3 Hz for identifying and counting quantal events. Two criteria were imposed during identification[2]: (1) the amplitude of the event should be >30% of the single-photon response amplitude of the same cell, and (2) the integration time of the event should be within 50 – 200% of that of the average dim-flash response. The cellular rate constant of thermal activation was given by the total number of

spontaneous events divided by the total recording time from all cells. The molecular rate constant could be obtained by further dividing the measured cellular rate by the number of pigment molecules (see above).

5.14 Microspectrophotometry

Microspectrophotometric measurements were done by Dr. Rikard Frederiksen in the laboratory of Dr. Carter Cornwall. Eyes of a euthanized mouse were removed under dim red light. Under infrared illumination, the eyes were hemisected and the retinas were isolated in HEPES (10mM, pH 7.4)-buffered Ames medium (Sigma Aldrich). Each retina was divided in half, yielding altogether four pieces of tissues to be subjected to four different treatments: two pieces of retina were kept dark-adapted and were incubated for 3 hours in darkness in HEPES-buffered Ames medium containing 1% fatty-acid-free bovine serum albumin (BSA) with or without 15 μM 9-*cis* retinal; the other two pieces of retina were subjected to a 99%-bleach and then incubated in the same HEPES-buffered, BSA-supplemented Ames medium as above with or without 15 μM 9-*cis* retinal.

Bleaching was performed off-stage on a portable optical bench consisting of a tungsten/halogen lamp, a set of neutral density filters, a 500-nm interference filter and a small aperture (3250 μm). The retinal tissue was placed in Ames medium in a 35-mm petri dish under the focused circular light spot. The onset of light was controlled by a manual shutter. The bleached fraction, F, was estimated from the relation $F = 1 - e^{-IPt}$, where I was the bleaching light intensity (1.33×10^6 photons μm^{-2} s^{-1}), P was the photosensitivity (5.7×10^{-9} μm^2; Ref. [13]) of mouse rhodopsin measured *in situ* at its λ_{max}

and *t* was the duration of light exposure; the retinal tissue was typically light-exposed for 16 min to achieve a >99.9% bleach.

Preparations of 9-*cis* retinal were done in dim red light. Stock solution of 30 mM 9-*cis* retinal was prepared by dissolving a crystal of 9-*cis* retinal in ethanol. The peak absorbance (OD) of retinoid in the stock solution was measured using a conventional spectrophotometer, and its concentration was calculated as $c = (OD_{373}\ l)/\varepsilon_{373}$, where *l* was a 1-cm path length and ε_{373} = 36,100 M^{-1} cm^{-1} was the extinction coefficient of 9-*cis* retinal in ethanol. Working solutions containing 9-*cis* retinal were prepared by first adding 1 µl of stock solution to a conical vial. HEPES-buffered Ames medium containing 1% delipidated BSA was then added in multiple times in increasing amounts (9 × 5 µl, 1 × 50 µl, 2 × 450 µl, 1 × 1000 µl) until the final volume was 2 ml; the concentration of 9-*cis* retinal in the working solution was 15 µM.

After their respective treatments, the absorbance spectra of the retinal pieces were measured using a custom-built microspectrophotometer[14,15]. A retinal piece was gently flattened by forceps and a slice anchor (Warner Instruments) on a quartz cover-slip window in the bottom of a 2 mm-deep Plexiglas recording chamber with the photoreceptors facing up. The recording chamber was placed on a microscope stage located in the beam path of the microspectrophotometer. The retinal tissue was superfused at a rate of 4 ml/min with Ames medium (Sigma Aldrich) buffered with sodium bicarbonate and equilibrated 95% O_2 /5% CO_2. Temperature was maintained at 35–37°C, except where otherwise stated. Absorption spectra were obtained from a region of the retina along its edge where isolated outer segments could be visually identified; the measured area contained predominantly rod photoreceptor outer segments, as evinced by

a λ_{max} at about 500 nm. Measurements were made with the polarization of the incident beam parallel to the plane of the intracellular disks (T-polarization) over the wavelength range of 300 – 700 nm with a 2 nm resolution. The absorbance spectrum was calculated from Beers' Law $OD = \log(I_i/I_t)$, where OD is the optical density or absorbance, I_i is the light transmitted through a cell-free space adjacent to the outer segments, and I_t is the light transmitted through the tissue. Generally, 10 complete sample scans and 10 baseline scans were averaged to increase the signal-to-noise ratio.

5.15 Reverse-transcription polymerase-chain-reaction (RT-PCR)

Tissues were freshly isolated and homogenized by autoclaved pestles in Trizol reagent (Life Technologies) containing polyacryl-carrier (Molecular Research Center). RNA was extracted by phase-separation with chloroform, precipitated with isopropanol and resuspended in diethylpyrocarbonate (DEPC)-treated water (Quality Biological). To avoid any contamination from genomic DNA, the RNA solution was treated with DNase I, then precipitated and resuspended again. Reverse transcription was performed on the RNA by using the SuperScript III First-Strand Synthesis System (Life Technologies). The resulting cDNA was amplified by PCR with primer sets listed in Table 5-2 and visualized on agarose gels by electrophoresis.

5.16 Preparation of fixed tissue sections

In most cases, especially when tissue sections would be used for immunohistochemistry with a primary antibody from a host species same as the experimental species, transcardiac perfusion was performed to remove the endogenous

IgG antibodies in the bloodstream. Animals were deeply anesthetized by intraperitoneal injection of ketamine and xylazine (~100 mg/kg ketamine and 10 mg/kg xylazine for mice and rats). They were perfused with phosphate-buffered saline (PBS) until blood cleared, then with freshly-prepared 4% paraformaldehyde (PFA) before tissue-isolation. In other cases where non-specific staining of capillaries was not a concern, tissues were sometimes freshly harvested from euthanized animals.

For preparing cryosections of an eye, an isolated eyeball was post-fixed with 4% PFA for 30 minutes at 4°C. After that, the anterior chamber and the lens were removed and the remaining eyecup was post-fix for additionally 3 hours at 4°C. The eyecup was washed with PBS for 3 times (10 minutes each time) and equilibrated in 30% sucrose at 4°C for at least one day. For preparing cryosections of the trigeminal ganglia of a mouse or a rat, a perfused animal was decapitated, with its skull opened and the brain removed to expose the trigeminal ganglia. The head was then post-fixed with 4% PFA at 4°C overnight. After several washes with PBS, the head was incubated in 15% sucrose at 4°C until it sank. The procedure was repeated with 30% sucrose. Finally, the pair of trigeminal ganglia was isolated with micro-scissors while maintaining their orientations. Following equilibration in sucrose, all tissues (eyecups and trigeminal ganglia) were cryopreserved in Optimal Cutting Temperature (OCT) compound (Tissue-Tek) and sectioned at a thickness of 14-18 μm on a cryostat (Leica). Sections were stored at -80°C.

For preparing paraffin-sections of an eye, an eyeball of a perfused or acutely-euthanized animal was fixed in an alcohol-based zinc-formalin solution (Z-fix, Anatech) at room temperature overnight or at 4°C for at least one day. The eyeball was then sent to the Johns Hopkins Medical Laboratories or the laboratory of Dr. Stephen Tsang, where it

was dehydrated through a series of increasing concentrations of ethanol, embedded in paraffin and sectioned at a thickness of 5-8 μm. We typically analyzed sections obtained at the plane of the optic disc. Sections were stored at room temperature.

Table 5-2 List of RT-PCR primers

Figure(s)	Transcript	Forward primer	Reverse primer
Fig. 3-6	Rat *Opn4*	5'- ACA GGG ATG CTG GGT AAC CT -3'	5'- GGG CCT GAG TGA ACG ACA TA -3'
Fig. 3-7	Mouse *Opn4*	5'- TCT CTG TTA GCC CCA CGA CA -3'	5'- ACT GAC ATG AGG AAG TCG CTG -3'
Figs. 3-6, 3-7, 4-4	*β-actin*	5'- AAA GAG AAG CTG TGC TAT GTT G -3'	5'- CAT AGA GGT CTT TAC GGA TGT C -3'
Fig. 4-4	*Opn3*	5'- TGG CTC TAC TCC TTG GCA TGG -3'	5'- ACT GGG TTG TAC ACA GTG CTC G -3'
Fig. 4-4	*Opn5 Ex1-Ex4*	5'- GCC CCA CTA TCT TCG AGA CGA GG -3'	5'- TCC AGG GTG CAT GAG GTT CCG A -3'
Fig. 4-4	*Opn5 Ex5-Ex7*	5'- CCA TAC AGC TCT CCG TGG TG -3'	5'- TTC TCG GCC TCA GAA CAC AG -3'
Figs. 4-10, 4-13	*Opn5*	5'- AGC TTT TGG AAG GCC AGA C -3'	5'- CAG CAC AGC AGA AGA CTT CC -3'
Figs. 4-10, 4-13	*Gadph*	5'- GAC TTC AAC AGC AAC TCC CA -3'	5'- ATT GTG AGG GAG ATG CTC AGT -3'

5.17 Immunohistochemistry

For immunohistochemistry on cryosections, sections were first washed three times with 0.1% Triton X-100 in PBS (PBST-0.1%) to remove the OCT compound. Sections were then incubated with blocking buffer for 1 hour at room temperature, followed by primary antibodies in the same blocking solution at 4°C overnight. On the next day, sections were washed with PBST-0.1% and incubated with secondary antibodies in blocking solution for 1 hour at room temperature. After several final washes with PBST-0.1%, sections were mounted with mounted with anti-fade medium (Vector Laboratories) containing 4',6'-diamidino-2-phenylindole (DAPI), and cover-slipped.

For immunohistochemistry on paraffin-sections, sections were de-parffinized with xylenes (Sigma) and rehydrated through a series of decreasing concentrations of ethanol. For antibodies that require an antigen-retrieval procedure to unmask antigenic epitopes, sections were treated with citrate buffer (Sigma) for 20 min in a 98°C water bath. After cooling to room temperature, the sections were processed in the same way as for cryosections.

For immunohistochemistry on flat-mount retinas or irises, animals (except for rabbits and monkeys) were usually perfused as described above for reducing non-specific staining of blood capillaries. Perfusion also helped to dilate the pupils and thus made it easier to flatten the irises. Tissues were post-fixed with 4% PFA at room temperature for 30 minutes (all retinas and rabbit irises) or 15 minutes (mouse and rat irises). Subsequently, the tissues were washed with PBST-0.5% and incubated with blocking solution overnight at 4°C. For monkey irises, the pigmented layer was removed with forceps before blocking. Primary antibody incubation was done in the same blocking solution at 4°C for 3-5 days. After that, tissues were washed and incubated with the appropriate fluorophore-conjugated secondary antibodies in blocking solution overnight at 4°C. Finally, tissues were washed, mounted with the above DAPI-containing anti-fade medium, and cover-slipped. For immunostaining following X-gal labeling (see below), horseradish peroxidase (HRP)-conjugated secondary antibodies were used instead. Chromogenic signals were developed by using the Metal Enhanced DAB Substrate Kit (Life Technologies).

In cases where signal-enhancement was necessary, the Tyramide Signal Amplification Kit (Life Technologies) was used. The basic procedures were the same

except for the following major modifications: (1) a 3% hydrogen-peroxide-incubation step (1 hour, room temperature) was included before the regular blocking procedure to quench endogenous peroxidase activity, (2) sections were incubated with dye-labeled tyramide substrate (at 1:100 dilution in amplification buffer provided by the kit) for 5-10 minutes and then washed before being mounted.

Blocking solutions as well as primary and secondary antibodies used in the current studies are listed in Table 5-3.

Table 5-3 List of blocking solutions and antibodies for immunohistochemistry

Solution/Antibody	Source	Working conc./dilution
Blocking solutions (in PBST-0.1% or PBST-0.5%)		
Normal goat serum	Life Technologies	10%
Newborn calf serum	Life Technologies	10%
Tyramide blocking reagent*	Life Technologies	10 mg/ml
Primary antibodies (in blocking solution)		
Mouse anti-bovine rhodopsin monoclonal	Dr. Robert Molday (1D4)[16]	1:50
Rabbit anti-human OPN1MW polyclonal	Dr. Jeremy Nathans (JH492)[17]	1:10000
Rabbit anti-mouse OPN4 polyclonal	Advanced Targeting Systems (AB-N38)	1:2500
Rabbit anti-rat OPN4 polyclonal	Own laboratory[6]	1:250
Rabbit anti-rabbit OPN4 polyclonal	Dr. Stephen Massey[18]	1:1000
Mouse anti-human MBP monoclonal	Covance (SMI99)	1:500
Sheep anti-rat TH polyclonal	Millipore (AB1542)	1:500
Goat anti-human ChAT polyclonal	Millipore (AB144P)	1:100
Rabbit anti-mouse OPN1SW polyclonal	Dr. Jason Chen (based on Ref. [19])	1:500
Rabbit anti-mouse OPN1MW polyclonal	Dr. Jason Chen (based on Ref. [19])	1:500
Rabbit anti-mouse OPN5 polyclonal[#]	Dr. Yoshitaka Fukada[20]	1:100 – 1:200
Guinea pig anti-mouse OPN5 polyclonal[#]	Dr. Yoshinori Shichida[21]	1:100 – 1:2000
Rabbit anti-RBPMS polyclonal	Abcam (ab194213)	1:100
Secondary antibodies (in blocking solution)		
Alexa Fluor 488 goat anti-rabbit IgG	Life Technologies	1:500
Alexa Fluor 488 donkey anti-rabbit IgG	Life Technologies	1:500
Alexa Fluor 568 goat anti-rabbit IgG	Life Technologies	1:500
Alexa Fluor 568 goat anti-mouse IgG	Life Technologies	1:500
Alexa Fluor 647 donkey anti-mouse IgG	Life Technologies	1:500
Alexa Fluor 568 donkey anti-sheep IgG	Life Technologies	1:500
Alexa Fluor 568 donkey anti-goat IgG	Life Technologies	1:500
HRP-conjugated anti-rabbit IgG	Life Technologies	1:500

*Used with Tyramide Signal Amplification Kit or when primary antibodies from multiple host species were used for co-staining.

[#]We have not been able to obtain any specific labeling on mouse/monkey retinal cryosections by immunohistochemistry using these antibodies or other commercial OPN5 antibodies (not listed).

5.18 Optical clearing of mouse trigeminal ganglia by SeeDB

Trigeminal ganglia were isolated from mice perfused with freshly-prepared 4% PFA and post-fixed in 4% PFA overnight at 4°C. The tissues were then washed three times with PBS. The clearing procedures involve successive incubations in increasing concentrations of fructose solutions: 20% for 4 hours, 40% for 4 fours, 60% for 4 hours, 80% for 12 hours and 100% for 12 hours, all at room temperature. Unlike the original standard protocol[22], α-thioglycerol was not included in the fructose solutions because it introduced strong autofluorescence. Finally, the trigeminal ganglia were further incubated in SeeDB solution (20.25 g fructose, 5 ml distilled H_2O, 100 ul α-thioglycerol) for ~48 hours. Images were taken from tissues submerged in SeeDB solution with a confocal microscope by using a 10× objective.

5.19 Histochemical analyses

Retinal sections were deparaffinized by incubating the slides at 60°C and passing them through Xylene and then a series of ethanol solutions of decreasing concentrations for rehydration. After rinsing with tap water, the sections were stained with Gill III Haematoxylin (SL95, StatLab Medical Products) for 10 min. Extra staining solution was removed by washing with tap water. Subsequently, the sections were differentiated in acid alcohol, rinsed and blued in ammonia water. Following another rinse, the sections were stained with Eosin/Phloxine (SL104, StatLab Medical Products) for 1 min and de-stained to the appropriate intensity by passing through 95% ethanol. Finally, the slides were dehydrated through graded alcohols, cleared by Xylene and mounted with Submount (57006, StatLab Medical Products).

Thickness of the outer nuclear layer (ONL) was measured in ImageJ. The ONL was divided into 12 regions of interest with zone 1 being closest to and zone 12 farthest from the optic disk. Each zone was demarcated by the outline of the nuclei and has a fixed width of 30 μm. The ONL thickness at each zone was defined by the area of the zone divided by 30 μm.

5.20 Staining for β-galactosidase

For X-Gal staining of *Opn5*$^{-/-}$ line 1 retina, anesthetized mice were transcardially perfused with PBS, followed by freshly made X-gal fixative (0.2% glutaraldehyde and 2 mM $MgCl_2$ in PBS). Retinas were isolated and further post-fixed with X-gal fixative for 30 min at room temperature, and then rinsed three times with detergent buffer (2 mM $MgCl_2$, 0.01% Na-deoxycholate, and 0.02% Nonidet P-40 in PBS). Staining was done by incubating the retinas in detergent buffer containing 5 mM potassium ferricyanide, 5 mM potassium ferrocyanide, and 1 mg/ml X-gal; it usually took about 24 hour of incubation at room temperature to obtain reasonable staining intensities for *Opn5*$^{-/-}$ retinas. Finally, retinas were rinsed with detergent buffer and processed for imaging or immunohistochemistry as described above.

X-gal labeling of *Opn5*$^{-/-}$ (Line 2) retinas was performed by the laboratory of Dr. Richard Lang. Isolated retinas were first washed twice with PBS/0.02% Nonidet P-40, each time for 15 min, at 4°C. Afterwards, retinas were fixed with a X-gal fixative of different composition (1% formaldehyde, 0.2% glutaraldehyde, 2 mM $MgCl_2$, 5 mM EGTA, and 0.01% Nonidet P-40) for 45 min. Following two washes in the above PBS solution for 15 min each time, the retinas were allowed to incubate in X-gal staining

solution (5 mM $K_3Fe(CN)_6$, 5 mM $K_4Fe(CN)_6$, 2 mM $MgCl_2$, 0.01% Nonidet P-40, and 1 mg/ml X-gal) overnight. Stained retinas were either mounted under coverslips for direct imaging, or cryoprotected in 30% sucrose and sectioned at a thickness of 10 μm for providing a cross-sectional view.

5.21 Western blot

Western blot experiments were performed by Dr. Xiaozhi Ren, a post-doctoral fellow in our laboratory. Retinas were isolated from euthanized mice into RIPA lysis buffer (140 mM NaCl, 0.1% Na-deoxycholate, 10mM Tris-HCl, pH 8.0, 1 mM EDTA, 0.5 mM EGTA, 1% Triton X-100 and 0.1% SDS). Proteins were extracted by grinding the tissues with plastic pestles and vortexing every 5 min over a total of 30 min of incubation. Protein concentrations were determined using the bicinchoninic acid (BCA) Protein Assay Kit (Pierce). Subsequently, protein extracts (30 μg) were separated on 4%-15% or 4%-20% continuous SDS-PAGE gels (Bio-Rad) and transferred to polyvinylidene difluoride (PVDF) membrane. The membranes were blocked with 5% normal non-fat milk in TBST (500 mM NaCl, 20 mM Tris-HCl, pH 7.4, 0.1% Tween-20) for 1 hr and then incubated with different primary antibodies (Table 5-4) at 4°C overnight. After several washes with TBST (10 min each time), the blots were incubated with the appropriate HRP-conjugated secondary antibodies at room temperature for 1 hr. Finally, proteins were detected by using the Enhanced Chemiluminescence (ECL) system (Pierce). Each experiment was repeated at least three times with independent retinal samples from different groups of mice.

Table 5-4 List of antibodies for Western blot experiments

Antibody	Source	Working conc./dilution
Primary antibodies (in blocking solution)		
Mouse anti-bovine rhodopsin monoclonal	Dr. Robert Molday (1D4)[16]	1:50
Rabbit anti-human transducin polyclonal	Santa Cruz (SC-389)	1:500
Mouse anti-bovine PDE6 monoclonal	Dr. Theodore Wensel (based on Ref. [24])	1:1000
Mouse anti-bovine CNGA1 monoclonal	Dr. Robert Molday (PMc1D1)[25]	1:100
Mouse anti-bovine CNGB1 monoclonal	Dr. Robert Molday (GARP4B1)[26]	1:1000
Rabbit anti-mouse GRK1 polyclonal	Dr. Jason Chen[27]	1:1000
Rabbit anti-mouse RGS9-1 polyclonal	Dr. Jason Chen[28]	1:1000
Rabbit anti-mouse ARR1 polyclonal	Dr. Jason Chen	1:2500
Chicken anti-human GAPDH polyclonal	Millipore (AB2302)	1:1000
Secondary antibodies (in blocking solution)		
HRP-conjugated anti-rabbit IgG	Bio-Rad	1:10000
HRP-conjugated anti-mouse IgG	Bio-Rad	1:10000
HRP-conjugated anti-chicken IgG	Bio-Rad	1:10000

5.22 Photoentrainment and light pulse-induced phase-shift experiments on cultured tissues

Photoentrainment and light pulse-induced phase-shift experiments were conducted by the laboratory of Dr. Russell Van Gelder at the University of Washington, Seattle. Mice were euthanized by CO_2-asphyxiation and their retinas, corneas and pituitary glands were promptly dissected out into cold Hank's Balanced Salt Solution (HBSS, Gibco). Retinas were cultured overnightin cell-culture inserts (PICM0RG50, Millipore)in dishes containing Neurobasal A medium (Cellgro) supplemented with B-27 serum-free supplement (Life Technologies), 25 units/ml penicillin, 25 μg/ml streptomycin, and 2 mM L-glutamine at 36 °C under 5% CO_2/95% O_2. On the next day, the retinas were transferred into Dulbecco's Modified Eagle Medium (DMEM) supplemented with B-27 supplement (Life Technologies), 4.2 mM $NaHCO_3$, 10 mM HEPES (Life Technologies), 25 units/ml penicillin, 25 μg/ml streptomycin (Life Technologies), and 0.1 mM luciferin potassium salt (Biosynth) for long-term culturing. Corneal and pituitary explants were directly cultured in cell-culture inserts in dishes

containing the DMEM/luciferin medium without passing through the Neurobasal A medium. All culture dishes were sealed with vacuum grease and maintained at 36°C in CO_2-free incubators.

In a photoentrainment experiment, a pair of tissues from an animal was first subjected to opposite light/dark cycles for 4 days as previously described[29]. In specifics, the tissues were cultured in an incubator installed on its ceiling with 5 LED-sets, having peak wavelengths at 370 nm, 417 nm, 475 nm, 530 nm and 628 nm, respectively. White light was produced by switching on the 417-nm, 475-nm and 530-nm LEDs at the same time. The light/dark cycles were set up by a motor-driven solid black disk that rotated at 24 hour per revolution over the tissues. A pie-shaped transparent window was made in the disk for admitting light for 9 hours in every 24-hour cycle. The pair of tissues was cultured in separate dishes at positions antipodal to each other (designated 0^o and 180^o) beneath the disk so that they experienced anti-phasic light/dark cycles. This design ensured that the pair of tissues was cultured under the same temperature, which has been shown to affect tissue clocks. The phases of the circadian rhythm of the tissues were measured after the 4 days of photoentrainment.

Bioluminescence from cultured luciferase-expressing tissues was recorded continuously in darkness by four photomultiplier tubes in a luminometer (Lumicycle, Actimetrics). Background bioluminescence was subtracted away by de-trending the bioluminescence data with a first-order polynomial fitted to the general decline in bioluminescence. A sine wave was fitted to at least 3 days of bioluminescent oscillations to give the period and phase of a tissue clock.

In phase-shift experiments, the initial phase of a cultured tissue was first determined in darkness with the luminometer as above. The tissue was then moved to a light-proof, insulated chamber (for maintaining constant culture temperature) and transpoted to the incubator, where it received 3-hr stimulation with a light pulse of 417 nm or 475 nm (1.5×10^{15} photons cm^{-2} s^{-1}). After that, the tissue was returned to the luminometer and the phase-measurement resumed. Phase-shift was defined as the difference between the time of peak bioluminescence observed post-stimulation and that projected from the initial phase assuming no stimulation was applied.

5.23 Electroretinogram (ERG)

ERG was recorded by the laboratory of Dr. Russell Van Gelder at the University of Washington, Seattle. Mice were anesthetized by intraperitoneal injection of ketamine (110.25 mg/kg) and xylazine (11.02 mg/kg), and were placed on a water-based warming stage for protection against hypothermia. Mice used for scotopic ERGs were dark-adapted for at least 2 hours before anesthesia under dim red light. In all cases, a drop of 1% atropine sulfate was applied to one eye to dilate the pupil for light administration. A silver impregnated nylon fiber ("Dawson, Trick and Litzkow" electrode) was secured as the active lead over the cornea by a transparent contact lens. Platinum needle electrodes were placed under the skin covering the skull and the dorsal abdomen as the reference- and ground-lead, respectively. The experiment was conducted with the mouse head inside a Ganzfeld ERG System (Q450, Roland Consult, Germany), where it received light stimulations of a broad spectrum from some combinations of LEDs with peak wavelengths between 405 nm and 594 nm. For scotopic ERGs, flashes of 3 cd m^{-2} were

given at 5-second intervals in dark. For photopic ERGs, flashes were 900 cd m^{-2} white light above a background of 340 cd m^{-2} white fluorescent room light. Traces were filtered with a band-pass filter of 1-100 Hz and 20-100 Hz for scotopic and photopic ERG, respectively. Average was taken from approximately 150 trials until 60-Hz noise was reduced.

5.24 Optokinetic tracking

Optokinetic tracking experiments were done by the laboratory of Dr. Russell Van Gelder at the University of Washington, Seattle. The optokinetic tracking apparatus (Cerebral Mechanics, Canada) was installed with reflective floor and ceiling, plus computer monitors on the four sides for delivering visual stimuli. Mice were placed unrestrainedly on an elevated platform at the center of the arena and were allowed to acclimate to the environment as a uniform grey field was shown on the monitors. In one set of experiments, the monitors displayed at random: (1) high-contrast gratings of certain randomly-chosen spatial frequencies (0.05-0.5 cycles/degrees) that rotated at a constant speed in the clockwise or counter-clockwise direction, or (2) an equi-luminant grey field that served as a control. The reflexive head movements of the mice in response to the rotating stimuli were captured by an overhead video camera and were scored by an observer blind to the experimental conditions as 0 = no visual tracking, 1 = ambiguous visual tracking, or 2 = obvious visual tracking. We reported here the average score of multiple mice at a particular spatial frequency.

5.25 Behavioral wheel-running analysis

Wheel-running experiments were conducted by the laboratory of Dr. Russell Van Gelder at the University of Washington, Seattle. Mice were house individually in cages equipped with running wheels either under 12 hr/ 12 hr light/dark cycles that were provided by timer-controlled fluorescent bulbs (1 W m^{-2} white light) or in constant darkness. The activity of a mouse was recorded into a computer by a micro-switch, which was activated at every turn of the running-wheel. The numbers of wheel-revolutions in 5-minute bins were counted and plotted as black marks on a double-plotted actogram so that each horizontal trace represents two consecutive days, with the second day re-plotted as the first day on the next trace. The free-running period of a mouse in constant darkness was given by χ^2-period measurements (ClockLab software, Actimetrics).

5.26 Dye-injection into single neuron

Dye-injection experiments were done with help from Dr. Zheng Jiang, a research associate in our laboratory. To identify β-gal-positive neurons in *Opn5*$^{\tau lacZ/+}$ or *Opn5*$^{\tau lacZ/\tau lacZ}$ retinas for dye injection, freshly dissected retinas were incubated in oxygenated Ames' medium (Sigma Aldrich) containing 100 μM 5-chloromethylfluorescein di-β-D-galactopyranoside (CMFDG; Invitrogen D2920) at room temperature for 5 min. All dye-injections were done immediately after the staining procedures to minimize the leakage of the fluorescent CMFDG reaction product (see Chapter 4). A sharp electrode pulled from thick-walled borosilicate glass capillary (Harvard Apparatus GC150F-10) was filled with a small volume of 4 mM Alexa Fluor 555 and 1 mM Alexa Fluor 488 hydrazides dissolved in 1.5 M KCl at its tip, and 3 M

KCl at the back; the resistance of the electrodes was typically 50 – 150 MΩ. Under green fluorescent light, the sharp electrode was punctured into a CMFDG-labeled cell and the Alexa dyes were injected by a negative current (-500 to -1,000 pA, 3 min). Successful injection was confirmed by the retention of Alexa Fluor 555 dye in the soma and proximal dendrites. After dye injection, retinas were fixed in 4% PFA at 4 °C overnight and washed in PBS for 45 min. The injected cells were imaged by a Zeiss confocal microscope (LSM-510).

5.27 References

1. Imai, H. *et al.* Molecular Properties of Rhodopsin and Rod Function. *J. Biol. Chem.* **282,** 6677–6684 (2006).

2. Fu, Y., Kefalov, V., Luo, D.-G., Xue, T. & Yau, K.-W. Quantal noise from human red cone pigment. *Nat. Neurosci.* **11,** 565–571 (2008).

3. Mendez, A. *et al.* Role of guanylate cyclase-activating proteins (GCAPs) in setting the flash sensitivity of rod photoreceptors. *Proc. Natl. Acad. Sci. U. S. A.* **98,** 9948–53 (2001).

4. Sancho-Pelluz, J. & Tosi, J. Mice with a D190N mutation in the gene encoding rhodopsin: a model for human autosomal-dominant retinitis pigmentosa. *Mol. Med.* **18,** 549–555 (2012).

5. Greenwald, S. H., Kuchenbecker, J. A., Roberson, D. K., Neitz, M. & Neitz, J. S-opsin knockout mice with the endogenous M-opsin gene replaced by an L-opsin variant. *Vis. Neurosci.* **31,** 25–37 (2014).

6. Hattar, S., Liao, H. W., Takao, M., Berson, D. M. & Yau, K. W. Melanopsin-containing retinal ganglion cells: architecture, projections, and intrinsic photosensitivity. *Science* **295,** 1065–1070 (2002).

7. Buhr, E. D. *et al.* Neuropsin (OPN5)-mediated photoentrainment of local circadian oscillators in mammalian retina and cornea. *Proc. Natl. Acad. Sci. U. S. A.* (2015). doi:10.1073/pnas.1516259112

8. Yoo, S.-H. *et al.* PERIOD2::LUCIFERASE real-time reporting of circadian dynamics reveals persistent circadian oscillations in mouse peripheral tissues. *Proc. Natl. Acad. Sci. U. S. A.* **101,** 5339–5346 (2004).

9. Ecker, J. L. *et al.* Melanopsin-expressing retinal ganglion-cell photoreceptors: Cellular diversity and role in pattern vision. *Neuron* **67,** 49–60 (2010).

10. Estevez, M. E. *et al.* Form and function of the M4 cell, an intrinsically photosensitive retinal ganglion cell type contributing to geniculocortical vision. *J. Neurosci.* **32,** 13608–13620 (2012).

11. Harosi, F. I. Absorption Spectra and Linear Dichroism of Some Amphibian Photoreceptors. *J. Physiol.* **66,** 357–382 (1975).

12. Govardovskii, V. I., Fyhrquist, N., Reuter, T., Kuzmin, D. G. & Donner, K. In search of the visual pigment template. *Vis. Neurosci.* **17,** 509–528 (2000).

13. Woodruff, M. L., Lem, J. & Fain, G. L. Early receptor current of wild-type and transducin knockout mice: photosensitivity and light-induced Ca2+ release. *J. Physiol.* **557,** 821–8 (2004).

14. Frederiksen, R. *et al.* Low aqueous solubility of 11-cis-retinal limits the rate of pigment formation and dark adaptation in salamander rods. *J. Gen. Physiol.* **139,** 493–505 (2012).

15. Nymark, S., Frederiksen, R., Woodruff, M. L., Cornwall, M. C. & Fain, G. L. Bleaching of mouse rods: microspectrophotometry and suction-electrode recording. *J. Physiol.* **590,** 2353–2364 (2012).

16. Molday, R. S. & MacKenzie, D. Monoclonal antibodies to rhodopsin: characterization, cross-reactivity, and application as structural probes. *Biochemistry* **22,** 653–660 (1983).

17. Wang, Y. *et al.* A locus control region adjacent to the human red and green visual pigment genes. *Neuron* **9,** 429–440 (1992).

18. Kim, H. L. *et al.* Axonal synapses utilize multiple synaptic ribbons in the mammalian retina. *PLoS One* **7,** (2012).

19. Applebury, M. L. *et al.* The murine cone photoreceptor: a single cone type expresses both S and M opsins with retinal spatial patterning. *Neuron* **27,** 513–523 (2000).

20. Kojima, D. *et al.* UV-sensitive photoreceptor protein OPN5 in humans and mice. *PLoS One* **6,** (2011).

21. Yamashita, T. *et al.* Evolution of mammalian Opn5 as a specialized UV-absorbing pigment by a single amino acid mutation. *J. Biol. Chem.* **289,** 3991–4000 (2014).

22. Ke, M.-T., Fujimoto, S. & Imai, T. SeeDB: a simple and morphology-preserving optical clearing agent for neuronal circuit reconstruction. *Nat. Neurosci.* **16,** 1154–61 (2013).

23. Hicks, D. & Molday, R. S. Differential Immunogold-Dextran Labeling of Bovine and Frog Rod and Cone Cells Using Monoclonal Antibodies against Bovine Rhodopsin. *Ezp. Eye Res* **42,** 55–71 (1986).

24. Hurwitz, R. L., Bunt-Milam, A. H. & Beavo, J. A. Immunologic characterization of the photoreceptor outer segment cyclic GMP phosphodiesterase. *J. Biol. Chem.* **259,** 8612–8 (1984).

25. Cook, N. J., Molday, L. L., Reid, D., Kaupp, U. B. & Molday, R. S. The cGMP-gated Channel of Bovine. *Biochemistry* **264,** 6996–6999 (2000).

26. Poetsch, A., Molday, L. L. & Molday, R. S. The cGMP-gated channel and related glutamic acid-rich proteins interact with peripherin-2 at the rim region of rod photoreceptor disc membranes. *J. Biol. Chem.* **276,** 48009–16 (2001).

27. Chen, C.-K. *et al.* Modulation of Mouse Rod Response Decay by Rhodopsin Kinase and Recoverin. *J. Neurosci.* **32,** 15998–16006 (2012).

28. Chen, C.-K. *et al.* Slowed recovery of rod photoresponse in mice lacking the GTPase accelerating protein RGS9-1. *Nature* **403,** 557–560 (2000).

29. Buhr, E. D. & Van Gelder, R. N. Local photic entrainment of the retinal circadian oscillator in the absence of rods, cones, and melanopsin. *Proc. Natl. Acad. Sci. U. S. A.* **111,** 8625–30 (2014).

CURRICULUM VITAE FOR Ph.D. CANDIDATES

The Johns Hopkins University School of Medicine

Wendy Yue

Name (Wing Sze Wendy YUE)

December 1, 2015

Date of this version

Educational History

Ph.D. expected	2015	Program in BCMB Mentor: King-Wai Yau, Ph.D.	Johns Hopkins School of Medicine
B.Sc.	2008	Program in Biochemistry Major: Biochemistry; Minor: Mathematics	The University of Hong Kong

Other Professional Experience

Research rotation	2009	Lab of Xinzhong Dong, Johns Hopkins University
Research rotation	2009	Lab of Jeremy Nathans, Johns Hopkins University
Research rotation	2009	Lab of King-Wai Yau, Johns Hopkins University
Research project	2007-2008	Lab of Mai-Har Sham, The University of Hong Kong
Summer fellowship	2007	Lab of Mai-Har Sham, The University of Hong Kong
Summer internship	2006	Lab of Daisy Kwok Yan Shum, The University of Hong Kong

Scholarships and Fellowships

Howard Hughes Medical Institute International Student Research Fellowship 2011-2013

- An annual payment of $43, 000 (including stipend support as well as fellow's and institutional allowances) awarded to 40-50 international 3rd-4th year graduate students nominated by selected research institutions each year

HKU Faculty of Science Summer Research Fellowship 2007
HKU Foundation Entrance Scholarship 2006
Madam Poon Jing Kei Scholarship for Chemistry 2005
Lugard Scholarship 2005
St. Francis' Canossian College Past student Association Scholarship 2004
Madam Wong Yeung Yuet Sang Memorial Scholarship 2004
Lugard Scholarship 2004

Academic and Other Honors

FASEB Summer Research Conference Travel Award 2011
BCMB Graduate Program Best Fellowship Proposal in class 2009
Dean's Honors List 2008
Dr. Patrick Chow Lum Wong Memorial Prize in Biochemistry 2008
Dean's Honors List 2007
HKU Summer Research Fellowship Best Poster Presenter in Biological Sector 2007
Dean's Honors List 2006
Sir Edward Youde Memorial Prize 2004

Publications

Luo D.-G., **Yue W.W.S.**, Ala-Laurila P. and Yau K.-W. (2011) Activation of visual pigments by light and heat. *Science* 332:1307-1312. PMCID: PMC4349410.

Buhr E.D., **Yue W.W.S.**, Ren X., Jiang Z., Liao H.W., Mei X., Vemaraju S., Nguyen M.T., Reed R.R., Lang R.A., Yau K.-W., Van Gelder R.N. (2015) Neuropsin (OPN5)-mediated photoentrainment of local circadian oscillators in mammalian retina and cornea. *PNAS* 112(42):13093-13098. PMCID: PMC4620855.

Yue W.W.S., Frederiksen R., Silverman D., Ren X., Chen J., Cornwall M.C., Yau K.-W. Signal amplification by rhodopsin via G protein. (In preparation)

Yue W.W.S., Frederiksen R., Mills E.A., Marsh-Armstrong N., Chen J., Cornwall M.C., Yau K.-W. Thermal activation of cone pigments. (In preparation)

Wang Q., **Yue W.W.S.**, Jiang Z., Xue T., Kang S.H., Bergles D.E., Mikoshiba K., Offermanns S., Yau K.-W. Signalings by acetylcholine and light in mouse iris sphincter muscle. (In preparation)

Jiang Z., **Yue W.W.S.**, Sheng Y., Xue T., Do M.T.H., Yau K.-W. A novel phototransduction pathway in melanopsin-expressing intrinsically-photosensitive retinal ganglion cells. (In preparation)

Posters and abstracts

Luo D.-G., **Yue W.W.S.**, Ala-Laurila P. and Yau K.-W. (2011) Activation of visual pigments by light and heat. Biology and Chemistry of Vision Meeting, Federation of American Societies for Experimental Biology (FASEB), Carefree, AZ, June 19-24, 2011.

Luo D.-G., **Yue W.W.S.**, Ala-Laurila P. and Yau K.-W. (2013) Activation of visual pigments by light and heat. Sensory Signaling in Model Organisms, Howard Hughes Medical Institute (HHMI), Janelia Farm, Ashburn, VA, April 21-24, 2013.

Service and leadership

Volunteer, “Ask a Scientist” Forum, HHMI	2012
Tutor, Biochemical and Biophysical Principles Graduate Course, Johns Hopkins University	2010